

Alma Mater Studiorum – Università di Bologna

DOTTORATO DI RICERCA IN
SCIENZE CHIMICHE

Ciclo XXV

Settore Concorsuale di afferenza: 03/A2

Settore Scientifico disciplinare: CHIM/02

**Studies of pure rotational spectra of isolated molecules
and molecular adducts using pulsed jet Fourier
transform microwave (PJ-FTM) spectroscopy**

Presentata da: Gang Feng

Coordinatore Dottorato

Prof. Adriana Bigi

Relatore

Prof. Walther Caminati

Esame finale anno 2013

Contents

Acknowledgements.....	i
Abstract	I
Chapter 1 Introduction.....	1
1.1 Overview	1
1.2 Rotational spectroscopy	1
1.2.1 Isolated molecules.....	2
1.2.2 Molecular adducts.....	4
1.3 Motivations.....	6
References.....	7
Chapter 2 Theoretical aspect and experimental method.....	11
2.1 Angular momentum of a rigid rotor	11
2.2 Angular momentum operators and matrix elements	14
2.3 Centrifugal distortion	21
2.4 Nuclear quadrupole coupling	23
2.5 Internal rotation	29
2.6 Evaluation of molecular structure	33
2.7 Theoretical calculations.....	35
2.8 Experimental techniques	35
Reference	37
Chapter 3 Conformation and internal rotation: microwave spectroscopic studies on dimethyl sulfate	39
3.1 Introduction	39
3.2 Experimental details.....	40
3.3 Theoretical calculations.....	40
3.4 Results and analysis	42
3.4.1 Rotational spectra	42
3.4.2 Molecular structure	44
3.5 Conclusions	48
References.....	49
Chapter 4 Proton transfer in homodimers of carboxylic acids. The rotational spectrum of the dimer of acrylic acid.....	51
4.1 Introduction	51
4.2 Experimental details.....	54
4.3 Theoretical calculations.....	54
4.4 Results and discussion.....	58
4.4.1 Rotational spectra	58
4.4.2 Model calculations for proton transfer.....	61

4.5	Conclusions.....	65
	References	65
Chapter 5	Conformational equilibrium, structure, and isotopic effect in acrylic acid - formic acid bi-molecule.....	67
5.1	Introduction.....	67
5.2	Experimental details	68
5.3	<i>Ab initio</i> calculations	68
5.4	Results and discussion	71
5.4.1	Rotational spectra.....	71
5.4.2	Relative population of the two conformers in the jet.....	74
5.4.3	Dissociation energy.....	75
5.4.4	Structures and Ubbelohde effect	76
5.5	Conclusions.....	81
	References	81
Chapter 6	Conformational equilibria in adducts of alcohols with ethers: the rotational spectrum of ethylalcohol-dimethylether.....	83
6.1	Introduction.....	83
6.2	Experimental section	84
6.3	Results and discussion	85
6.3.1	<i>Ab initio</i> calculation	85
6.3.2	Rotational spectra and analysis	86
6.3.3	Conformational equilibrium.....	87
6.3.4	Structural analysis	88
6.3.5	Dissociation energy	90
6.4	Conclusions.....	91
	References	91
Chapter 7	On the weak H···halogen hydrogen bond. A rotational study of CH ₃ CHClF··H ₂ O complex	93
7.1	Introduction.....	93
7.2	Experimental section	94
7.3	Results and discussion	95
7.3.1	Theoretical calculations.....	95
7.3.2	Rotational spectra.....	96
7.3.3	Conformation and structure.....	99
7.3.4	Dissociation Energy	100
7.4	Conclusions.....	101
	References	103
Chapter 8	On the halogen bond. A rotational study of CF ₃ Cl··H ₂ O and CF ₃ Cl··NH ₃ complex	105
8.1	Introduction.....	105
8.2	Experimental section	107
8.3	Chlorotrifluoromethane/water	107
8.3.1	Theoretical calculations.....	107

8.3.2	Rotational spectra	109
8.3.3	Molecular structure	111
8.3.4	Dissociation energy.....	113
8.3.5	Conclusions.....	114
8.4	Chlorotrifluoromethane/ammonia.....	114
8.4.1	Theoretical calculations	114
8.4.2	Rotational spectra	116
8.4.3	Molecular structure and internal dynamics.....	119
8.4.4	Dissociation energy.....	121
8.4.5	Conclusion	122
	References.....	122
	Appendices.....	124
	A-Publication list	124
	B-Conferences	127

Acknowledgements

I'm indebted to many people for the enjoyable experience during my three years at Bologna. I'm very grateful to my supervisor Prof. Walther Caminati for his advice during this period of time. He introduced me into the field of microwave spectroscopy and taught me how to solve problems. He and his family are so kind and help me a lot in my daily life to let me enjoy myself staying here. I could have not completed my study and thesis without his support, and also the invitation to drinking a cup of coffee every day. Here, I express my sincere gratitude to Prof. Caminati and his family for their very kind hospitality.

The Caminati's group is an interesting place to work. It is a pleasure to express my grateful to all the members in our group. They help me a lot during my three years study and every day's life. They together make me feeling home here. They are Dr. Biagio Velino, Dr. Laura B. Favero, Prof. Sonia Melandri, Dr. Assimo Maris, Dr. Luca Evangelisti, Ms. Qian Gou, Ms. Camilla Calabrese and Mr. Lorenzo Spada.

I would like to thank my friends: they contributed to the quality of my non-academic life in Bologna. Especially thanks to Ms. Qian Gou, Mr. Wenling Qin and Ms. Sha Long, we share the apartment and have much meaningful time together.

Of course, it's impossible to finish my study without the supporting of my parents, my sisters and their families. They always provide me with freedom to make a choice of my life and support what I have chosen. I dedicate this thesis to my family.

I would like to thank MIUR (PRIN08, project KJX4SN 001) and the University of Bologna (RFO) for supporting the research work. My gratitude to the China Scholarships Council (CSC) for offering me a scholarship (file number: 2009605019) to fund my study in Bologna.

Many, many thanks to all.

Gang Feng

2013-3-11, Bologna

Abstract

Microwave spectroscopy has been the most widely used and precisely tool to obtain gas phase molecular structures. From the observed MW spectra, the rotational constants can be derived, which directly depend on the mass distribution within a given molecular systems. Thus, information obtained from the rotational spectra was routinely related to bond lengths and valence angles. However, other chemical data, such as the electronic environment of a given atom, information on the internal dynamics (obtainable from tunneling splitting on the rotational energy levels) can also be derived from the MW spectra. The combination of Fourier transform MW (FTMW) spectroscopy with supersonic-jet expansions allowed studying the rotational spectra of weakly bound molecular complexes, and thus the nature of non-covalent interaction, e.g., hydrogen bond, weak hydrogen bond, halogen bond, and van der Waals interaction can be studied. The detailed and precise chemical information obtained from MW spectroscopic studies will be helpful to understand many interesting chemical or biological problems.

This thesis focuses on studying molecular structure and internal dynamics by using pulsed jet Fourier transform microwave (PJ-FTMW) spectroscopy combined with theoretical calculations. Several kinds of interesting chemical problems are investigated by analyzing the MW spectra of the corresponding molecular systems.

First, the general aspects of rotational spectroscopy are summarized, and then the basic theory on molecular rotation and experimental method are described briefly. Theories on nuclear hyperfine structure in molecular rotational spectra arising from interactions of the molecular fields with the nuclear quadrupolar moments, internal rotation, and derivation of molecular structure are described. *ab initio* and density function theory (DFT) calculations that used in this thesis to assist the assignment of rotational spectrum are also included.

From chapter 3 to chapter 8, several molecular systems concerning different kind of general chemical problems are presented. In chapter 3, the conformation and internal motions of dimethyl sulfate are reported. The global minimum configuration of this molecule was found to the form which has a C_2 symmetry with the two methyl groups

nearly *trans* with respect to the two sulfuric oxygen atoms. The internal rotations of the two methyl groups split each rotational transition into several components line, allowing for the determination of accurate values of the V_3 barrier height to internal rotation and of the orientation of the methyl groups with respect to the principal axis system. The geometry of the molecular skeleton is fully determined

In chapter 4 and 5, the results concerning two kinds of carboxylic acid bi-molecules, formed via two strong hydrogen bonds, are presented. This kind of adduct is interesting also because a double proton transfer can easily take place, connecting either two equivalent or two non-equivalent molecular conformations. In the first case, tunneling splitting is expected which leads to the determination of the potential energy surface for the motion. The acrylic acid dimer is an example of this case: the barrier and dynamics of the proton transfer were derived from the tunneling splittings. In the second case, a conformational equilibrium is expected. As an example, in the acrylic acid – formic acid dimer, two forms of this bi-molecule have been found. Their molecular structures and the H \rightarrow D isotopic effect of the carboxylic hydrogen on the molecular structure has been quantified experimentally.

Chapter 6 concerns a medium strong hydrogen bonded molecular complex of alcohol with ether. The dimer of ethanol-dimethylether was chosen as the model system for this purpose. Both *trans* and *gauche* configuration of ethanol were preserved in the complex, giving rise to a conformational equilibrium. A switch of the conformational stability of ethanol is observed while forming the complex with dimethyl ether, with the *gauche* form becoming the global minimum. The Ubbelohde effect upon the H \rightarrow D substitution of the hydroxyl hydrogen was quantitatively observed, which corresponds to shrinkage of the O \cdots O distance of about 6 mÅ.

Chapter 7 focuses on weak halogen \cdots H hydrogen bond interaction. The nature of O-H \cdots F and C-H \cdots Cl interaction has been discussed through analyzing the rotational spectra of CH₃CHClF/H₂O. Information on molecular structure, quadrupole coupling effects of the chlorine atom, and on the internal dynamics was obtained.

In chapter 8, two molecular complexes concerning the halogen bond interaction are presented. The molecular complex of CF₃Cl with water is effectively a symmetric top and its two units are held together by an O \cdots Cl halogen bond. A N \cdots Cl halogen bond interaction plays key role in forming the complex of CF₃Cl with ammonia.

Several other molecular systems were also studied during the thesis period although they are not described in details in this thesis. For example, in 2-butyric acid, the methyl group undergoes almost free internal rotation. The rotational spectra of three conformers of trimethylmethane with different symmetry were identified. Each conformer has very complex spectra because of the internal rotation of the three methyl groups. The analysis of the internal rotation of the three methyl groups is in progress. Other kinds of non-covalent interaction such as van der Waals interaction and oxygen lone pair $\cdots\pi$ interaction were also studied through the analysis of the rotational spectra of small molecular complexes. The rotational spectrum has been assigned for one conformer of a tetramer of a relative heavy asymmetric top, the tetramer of difluoromethane.

Since all results of the studied molecular systems have been published. The experimental transition frequencies can be found in the corresponding articles.

Chapter 1 Introduction

1.1 Overview

Molecular spectroscopy, that the interaction of electromagnetic radiation with matter, is one of the most widely used and important experimental probes for studying the properties of molecular systems. For different kind of molecular process, the transition energy corresponding to absorption or emission falls in different regions of the electromagnetic spectrum. Normally, the transition energy between molecular electronic energy levels corresponds to visible and ultraviolet radiation, molecular vibrational transition energy falls in the region of infrared, while the energy involved in molecular rotation falls in the microwave region. Rotational spectroscopy or microwave (MW) spectroscopy is one of the most widely used and precise method to obtain the molecular structure in gas phase.

1.2 Rotational spectroscopy

MW spectroscopy is used to investigate the rotation of molecule. Since the energy of molecular rotation is related to the moment of inertia, which depends on the mass distribution of the given molecular system, information on molecular structure can be obtained from the rotational spectra.

Actually, the structural information is not the only information which can be obtained from the rotational spectra: chemical information on electronic environment from the nuclear quadrupole coupling which relates to the electronic field gradient at the coupling nucleus, and internal dynamics which corresponds to the tunneling splitting of the rotational transition sometime is also included in the spectrum.

Microwave spectroscopy is one of the most important experimental methods to study conformational equilibria. In 1962, Hirota already reported the first MW spectroscopic study on the conformational equilibrium between the *gauche* and *trans* forms of propyl fluoride.^[1] He found that the *gauche* conformer is more stable than the

trans one by 1.96(13) kJmol⁻¹. Since then, many conformational equilibria have been investigated by MW spectroscopy. The number of the conformers in a concerned molecular system identified by MW spectroscopy reached 15 in the case of 1-octene.^[2]

MW spectroscopy is also a precise method to study tautomeric equilibria, present in many interesting chemical and biological systems. MW spectroscopic studies already provided meaningful evidence on the Keto-enolic equilibrium. Malonaldehyde was found to adopt C_s symmetry in the enolic form with a low barrier to proton transfer.^[3] In the case of acetylacetone, a recent study shown the evidence for the C_{2v} symmetry though analyzing the totally symmetric tunneling A-state of the enolic species.^[4] Both ketonic and enolic forms can be observed in 2-hydroxypyridine,^[5] with enolic form being more stable than the ketonic form by 0.32(3) kJmol⁻¹. Similarly, the ketonic form of 4-hydroxypyrimidine is more stable than its enolic form by 2.0(9) kJmol⁻¹.^[6] This tautomeric equilibrium was also observed in 2-Mercaptopyridine.^[7]

The combination of supersonic jet expansion with Fourier transform MW (FTMW) makes the MW spectroscopy one of the most powerful method to study weakly bound molecular complexes in gas phase. Since the introducing of this method,^[8] plenty of results concerning different kind of non-covalent interaction have been reported.^[9] Details on the nature of intermolecular interactions such as hydrogen bond, weak hydrogen bond, halogen bond and van der Waals interaction have been obtained by analyzing the MW spectra of the small molecular model systems.

1.2.1 Isolated molecules

Typically small molecules with reasonable vapor pressure and dipole moment are good candidates for MW spectroscopic study. Information on the structure and conformation of many molecules has been obtained. The fine or hyperfine structure of the spectra due to internal dynamics or quadrupole coupling can also be resolved. The resulted information supplies a good understanding of the structure, dynamics and electronic environment of the coupling nucleus.

New methods to vaporize samples, such as laser ablation, electrical discharge, and pyrolysis prior to expansion allow studying of vapor-less compounds and to prepare in situ new or unstable species to be studied by MW spectroscopic.

For example, by using electrical discharge, Thaddeus *et al.* prepared in-situ the samples and then assign the rotational spectra of S_3 ,^[10] S_4 ,^[11] Si_3 ,^[12] and SiC_3 .^[13] Although the first MW spectroscopic study concerning a bio-molecule, glycine, reported in 1978,^[14] was based on heating of the sample, only a few examples^[15] were available before the laser ablation was introduced for this kind of study.^[16] Alonso and coworkers combined a laser ablation with supersonic jet FTMW spectroscopy to study several amino acids.^[17] Since now, gas phase molecular structure and shapes has been obtained for glycine^[16], isoleucine,^[18] valine,^[19] alanine,^[20] β -alanine,^[21] leucine,^[22] sarcosine,^[23] serine,^[24] cysteine,^[25] threonine,^[26] and proline.^[27] The conformational/tautomeric forms of several nucleobases have also been obtained by this technique.^[28]

With respect to amino acid, only a few examples of MW spectroscopic studies have been reported for sugars. The rotational spectrum of glycoaldehyde^[29] has been assigned first, then several “C3 sugars” were studied.^[30] In 2012, Cocinero *et al.* assigned the rotational spectra of six conformers of a C5 sugar, ribose, by applying a ultrafast UV laser vaporization.^[31]

Many transition metal complexes have also been studied, mainly by Kukolich and coworkers, by using supersonic jet FTMW spectroscopy. Details on the structure of the complexes have been obtained, which should be helpful in well understanding the reactivity of these compounds. For example, the assignment of MW spectrum of the 1, 1'-dimethylferrocene complex provides useful information on the structure and conformational preference.^[32] The rotational study on the argon-cyclopentadienyl thallium weakly bound complex allowed to evaluating the structure and the symmetry of the complex.^[33]

The pure rotational spectra of metallorganic compounds were also reported, especially by Ziury and coworkers. These compounds were prepared by the reaction of metal vapor produced by DC or AC discharge with small organic molecules or other

available metallorganic compounds. In a recent study, the methylzinc hydride molecule was prepared and identified through analyzing its rotational spectrum.^[34]

Other molecules such as radicals, ion, carbon chain compounds and even polycyclic aromatic hydrocarbons and heterocycles have also been studied by MW spectroscopy, details on these molecules can be found in the recent book chapter^[9c, 35] or articles and data base.^[36]

1.2.2 Molecular adducts

The first molecular adduct observed by MW spectroscopy is the bi-molecule of trifluoroacetic acid-formic acid ($\text{CF}_3\text{COOH-HCOOH}$) reported by Costain in 1961.^[37] In 1972, Klemperer *et al.* introduced the supersonic expansion of seeded rare gas to rotational spectroscopy to observe weakly bound molecular complex.^[8a] Later in 1979, Balle *et al.* reported the rotational spectrum of Kr-HCl observed with supersonic jet FTMW spectroscopy.^[8b] Since that time on, large number of molecular adducts have been studied by the combined supersonic jet-FTMW spectroscopy. Reviews concerning molecular complexes are available,^[9a, 9b, 35, 38-42] also that a website with the bibliography of weakly bound complexes revealed by rotational spectroscopy.^[9c] The molecular complex is formed through non-covalent interactions, thus the studies of small molecular adducts provide plenty information on the nature of several kind of non-covalent interaction.

Hydrogen bond (HB) plays very important roles in chemical and biological systems and has therefore been a contemporary research interest. "Classical" hydrogen bonds like $\text{O-H}\cdots\text{O}$, $\text{O-H}\cdots\text{N}$, $\text{O-H}\cdots\text{S}$, and $\text{N-H}\cdots\text{O}$ are characterized (for neutral species) by interactions energies in the range $15\text{-}25\text{ kJmol}^{-1}$, while other linkage like $\text{C-H}\cdots\text{O}$, $\text{C-H}\cdots\text{X}$ ($\text{X}=\text{F}, \text{Cl}$), $\text{O-H}\cdots\text{X}$ ($\text{X}=\text{F}, \text{Cl}$), $\text{CH}\cdots\text{S}$, $\text{C-H}\cdots\pi$, which have interaction energy within a few kJmol^{-1} , which are generally classified as weak hydrogen bonds (WHB) and also represent a major topic in hydrogen-bond research.^[43-50] Through MW spectroscopic studies of many hydrogen bonded molecular complexes, the nature of HB has been revealed.^[9b, 50] Due to the importance of water in everyday life and its proton donor and acceptor properties, the adducts of water with other small

molecules among the most preferred model molecules for characterizing HB. Numerous MW spectra of molecular complexes involving water have been assigned.^[9b, 51]

Halogen bond (HaB) is a non-covalent interaction similar to HB but in which the halogen atom acts as electron acceptor. In some case, HaB has been found to be competitive or preferred to HB. It plays important roles in supramolecular chemistry and in crystal engineering.^[52-58] MW spectroscopic studies of small isolated complexes formed via HaB interaction already gave interesting information on the nature of this interaction.^[39, 57-61] The FTMW spectroscopy studies of a series of $B \cdots XY$ complexes, where B is the electron donor and XY is the dihalogen molecule, have already revealed some properties of the halogen bond interaction such as bonding bridge geometry and the intermolecular stretching force and dissociation energy.^[39, 59]

Since the first observation of van der Waals complex with rotational spectroscopy,^[62, 63] a large number of the complexes of rare gas with other molecules have been investigated by MW spectroscopy, especially by supersonic jet FTMW spectroscopy. In principle, the molecular structure, stretching force and dissociation energy, and internal dynamics can be determined. By using the supersonic jet FTMW spectroscopy, all the hetero-dimer of rare gas except those involving Helium have been studied.^[64-66] The dissociation energies derived from the centrifugal distortion constants fall in range $0.3\text{-}2.0 \text{ kJmol}^{-1}$, which show that these interactions are quite weak. Although this kind of interaction is weak, the MW spectra of some mixed rare gas trimers and tetramers, that is Ne_2Ar , NeAr_2 , Ne_2Kr and Ne_2Xe , have also been assigned.^[67, 68] In small molecule-rare gas complexes, the tunneling splitting can sometimes easily be observed. The rotational assignment of the van der Waals complexes with lighter rare gas are very complicated due to the wide and irregular tunneling splitting of rotational transition into multiples. For example, the energy difference of the tunneling splitting states is $807.2(9) \text{ MHz}$ for dimethylether (DME)-Ne,^[69, 70] however, for the complexes of DME with Ar,^[71] Kr^[72] and Xe^[73] the difference is $0.9980(6)$, $0.26(5)$ and $0.105(1) \text{ MHz}$, respectively, much smaller than that of Ne involved complex.

Other interesting chemical information can also be derived from MW spectra. Endo *et al.* determined the molecular structure and the symmetry of $\text{NaCl}-(\text{H}_2\text{O})_n$ ($n=1\text{-}3$) by assigning their MW spectra. It was found that the charge distributions in NaCl are

dramatically changed after forming the complex with water and also that the $r(\text{Na-Cl})$ distance increased with the successive addition of water.^[74] MW spectroscopic studies concerning the microsolvation of small organic molecules are also available. Bauder *et al.* reported the rotational spectra of formic acid- H_2O , formic acid- $(\text{H}_2\text{O})_2$ and also (formic acid) $_2$ - H_2O .^[75] Howard *et al.* reported the rotational spectra of the complexes between one trifluoroacetic acid with up to three water molecules.^[76] Neill *et al.* assigned the rotational spectra of β -propiolactone- $(\text{H}_2\text{O})_n$ ($n=1-5$).^[77]

Molecular complexes of asymmetric molecules larger than dimers have also been investigated by MW spectroscopy. By using a chirped-pulse FTMW spectrometer, Pate and cooperators can identify three conformers of the water hexamer, that is cage, book and cyclic, in supersonic expansion.^[78] Beside the molecular structures, information on relative population of these conformers was also obtained. They could also identify the rotational spectra of water heptamer and nonamer. Actually, water is not the only asymmetric molecule whose homo oligomers have been investigated by MW spectroscopy. The rotational spectra of difluoromethane (DFM) dimer^[79], trimer^[80] and also tetramer^[81] have been assigned.

MW spectroscopy is one of the most promising methods also to study the isotopic substituted effect on molecular structure and dynamics. Isotopic substitution is generally considered not to perturb the structure of a molecular system. However, Caminati *et al.* shown that the deuteration of water produces the conformational change in the anisole-water complex.^[82] Ubbelohde effect can also be well characterized through MW spectroscopy.^[83, 84]

1.3 Motivations

This thesis concerns the study of pure rotational spectra of isolated molecules, molecular adducts seeded in supersonic expansion with FTMW spectroscopy. Plenty of chemical information including molecular structure, nuclear quadrupole coupling, internal dynamics such as internal rotation and double proton transfer are derived from the MW spectra. Studies on molecular adducts provided information concerning different kind of non-covalent interaction. These studies, together with those of other

research groups, will contribute to obtain a precise evaluation of the dynamics and energetic of relative interesting molecular systems and also that of inter-/intra-molecular non-covalent interactions.

References

- [1] E. Hirota, *J. Chem. Phys.* **1962**, *37*, 283.
- [2] G. T. Fraser, R. D. Suenram, C. L. Lugez, *J. Phys. Chem. A* **2001**, *140*, 1141.
- [3] S. L. Baughcum, Z. Smith, E. B. Wilson, R. W. Duerst, *J. Am. Chem. Soc.* **1984**, *106*, 2260.
- [4] W. Caminati, J.-U. Grabow, *J. Am. Chem. Soc.* **2006**, *128*, 854.
- [5] L. D. Hatherley, R. D. Brown, P. D. Godfrey, A. P. Pierlot, W. Caminati, D. Damiani, S. Melandri L. B. Favero, *J. Phys. Chem.* **1993**, *97*, 46.
- [6] R. Sanchez, B. M. Giuliano, S. Melandri, L. B. Favero, W. Caminati, *J. Am. Chem. Soc.* **2007**, *129*, 6287.
- [7] S. Melandri, L. Evangelisti, A. Maris, W. Caminati, B. M. Giuliano, V. Feyer, K. C. Prince, M. Coreno, *J. Am. Chem. Soc.* **2010**, *132*, 10269.
- [8] a) T. R. Dyke, B. J. Howard, W. Klemperer, *J. Chem. Phys.* **1972**, *56*, 2442.; b) T. J. Balle, E. J. Campbell, M. R. Keenan, W. H. Flygare, *J. Chem. Phys.* **1979**, *71*, 2723.
- [9] a) K. R. Leopold, G. T. Fraser, S. E. Novick, W. Klemperer, *Chem. Rev.* **1994**, *94*, 1807. b) W. Caminati and J.-U. Grabow, *Microwave Spectroscopy. Molecular Systems*, in *Frontiers of molecular Spectroscopy*, ed. J. Laane, Elsevier, Amsterdam, **2009**.
c) <http://wesleyan.edu/chem/faculty/novick/vdw.html>.
- [10] M. C. McCarthy, S. Thorwirth, C. A. Gottlieb, P. Thaddeus, *J. Am. Chem. Soc.* **2004**, *126*, 4096.
- [11] M. C. McCarthy, S. Thorwirth, C. A. Gottlieb, P. Thaddeus, *J. Chem. Phys.* **2004**, *121*, 632.
- [12] M. C. McCarthy, P. Thaddeus, *Phys. Rev. Lett.* **1997**, *90*, 213003.
- [13] a) M. C. McCarthy, A. J. Apponi, P. Thaddeus, *J. Chem. Phys.* **1999**, *110*, 10645. b) A. J. Apponi, M. C. McCarthy, C. A. Gottlieb, P. Thaddeus, *J. Chem. Phys.* **1999**, *111*, 3911. c) M. C. McCarthy, A. J. Apponi, P. Thaddeus, *J. Chem. Phys.* **1999**, *111*, 7175.
- [14] a) R. D. Brown, P. D. Godfrey, J. W. V. Storey, M. P. Bassez, *J. Chem. Soc. Chem. Comm.* **1978**, 547; b) R. D. Suenram, F. J. Lovas, *J. Mol. Spectrosc.* **1978**, *72*, 372.
- [15] a) R. D. Brown, J. G. Crofts, P. D. Godfrey, D. McNaughton, A. P. Pierlot, *J. Mol. Struct.* **1988**, *190*, 185; b) S. Melandri, W. Caminati, L. B. Favero, A. Millemaggi, P. G. Favero, *J. Mol. Struct.* **1995**, *352/353*, 253.

- [16] F. J. Lovas, Y. Kawashima, J.-U. Grabow, R. D. Suenram, G. T. Fraser, E. Hirota, *Astrophys. J.* **1995**, 455, L201.
- [17] A. Lesarri, S. Mata, J. C. López, J. L. Alonso, *Rev. Sci. Instrum.* **2003**, 74, 4799.
- [18] A. Lesarri, R. Sánchez, E. J. Cocinero, J. C. López, J. L. Alonso, *J. Am. Chem. Soc.* **2005**, 127, 12952.
- [19] A. Lesarri, E. J. Cocinero, J. C. López, J. L. Alonso, *Angew. Chem. Int. Ed.* **2004**, 43, 605.
- [20] M. E. Sanz, A. Lesarri, I. Peña, V. Vaquero, V. Cortijo, J. C. López, J. L. Alonso, *J. Am. Chem. Soc.* **2006**, 128, 3812.
- [21] S. Blanco, A. Lesarri, J. C. López, J. L. Alonso, *J. Am. Chem. Soc.* **2004**, 126, 11675.
- [22] E. J. Cocinero, A. Lesarri, J.-U. Grabow, J. C. López, J. L. Alonso, *ChemPhysChem* **2007**, 8, 599.
- [23] E. J. Cocinero, P. Villanueva, A. Lesarri, M. E. Sanz, S. Blanco, S. Mata, J. C. López, J. L. Alonso, *Chem. Phys. Lett.* **2007**, 435, 336.
- [24] S. Blanco, M. E. Sanz, J. C. López, J. L. Alonso, *Proc. Natl. Acad. Sci. USA* **2007**, 104, 20183.
- [25] M. E. Sanz, S. Blanco, J. C. López, J. L. Alonso, *Angew. Chem. Int. Ed.* **2008**, 120, 6312.
- [26] J. L. Alonso, C. Pérez, M. E. Sanz, J. C. López, S. Blanco, *Phys. Chem. Chem. Phys.* **2009**, 11, 617.
- [27] a) A. Lesarri, S. Mata, E. J. Cocinero, S. Blanco, J. C. López, J. L. Alonso, *Angew. Chem. Int. Ed.* **2002**, 41, 4673. b) S. Mata, V. Vaquero, C. Cabezas, I. Peña, C. Pérez, J. C. López, J. L. Alonso, *Phys. Chem. Chem. Phys.* **2009**, 11, 4141.
- [28] a) W. Caminati, *Angew. Chem. Int. Ed.* **2009**, 48, 9030; b) J. L. Alonso, I. Peña, J. C. López, V. Vaquero, *Angew. Chem. Int. Ed.* **2009**, 48, 1. c) V. Cortijo, M. E. Sanz, J. C. López, J. L. Alonso, *J. Phys. Chem. A* **2009**, 113, 14681.
- [29] a) K. M. Marstokk, H. Møllendal, *J. Mol. Struct.* **1970**, 5, 205; b) K. M. Marstokk, H. Møllendal, *J. Mol. Struct.* **1973**, 16, 259.
- [30] a) R. A. H. Butler, F. C. De Lucia, D. T. Petkie, H. Møllendal, A. Horn, E. Herbst, *Astrophys. J. Suppl. Ser.* **2001**, 134, 319; b) F. J. Lovas, R. D. Suenram, D. Plusquellic, H. Møllendal, *J. Mol. Spectrosc.* **2003**, 222, 263; c) G. Maccaferri, W. Caminati, P. G. Favero, *J. Chem. Soc. Faraday Trans.* **1997**, 93, 4115; d) V. V. Ilyushin, R. A. Motiyenko, F. J. Lovas, D. F. Plusquellic, *J. Mol. Spectrosc.* **2008**, 251, 129.
- [31] E. J. Cocinero, A. Lesarri, P. Écija, F. J. Basterretxea, J.-U. Grabow, J. A. Fernández, F. Castaño, *Angew. Chem. Int. Ed.* **2012**, 51, 3119.
- [32] C. Tanjaroon, K. S. Keck, S. G. Kukolich, *J. Am. Chem. Soc.* **2004**, 126, 844.
- [33] C. Tanjaroon, A. M. Daly, S. G. Kukolich, *J. Chem. Phys.* **2008**, 129, 054305.
- [34] M. A. Flory, A. J. Apponi, L. N. Zack, L. M. Ziurys, *J. Am. Chem. Soc.* **2010**, 132, 17186.

- [35] W. Caminati, Microwave Spectroscopy of Large Molecules and Molecular Complexes. In Handbook of High-resolution Spectroscopy. Ed. Martin Quack and Frédéric Merkt. John Wiley & Sons, Ltd. **2011**.
- [36] a) M.C. McCarthy, P. Thaddeus, *Chem. Soc. Rev.* **2001**, *30*, 177; b) D. McNaughton, P. D. Godfrey, R. D. Brown, S. Thorwirth, J-U. Grabow, *Astrophysical J.* **2008**, *678*, 309. c) Dr. Lovas web-site (NIST). <http://physics.nist.gov/PhysRefData/Micro/Html/contents.html>.
- [37] C. C. Costain, G. P. Srivastava, *J. Chem. Phys.* **1961**, *35*, 1903.
- [38] A. Bauder, *J. Mol. Struct.* **1997**, *408/409*, 33.
- [39] A. C. Legon, *Angew. Chem. Int. Ed.* **1999**, *38*, 2686.
- [40] Y. Xu, J. van Wijngaarden, W. Jaeger, *Int. Rev. Phys. Chem.* **2005**, *24*, 301.
- [41] E. Arunan, S. Dev, P. K. Mandal, *Appl. Spectrosc. Rev.* **2004**, *39*, 131.
- [42] S. E. Novick, K. R. Leopold, W. Klemperer. The Structure of Weakly Bound Complexes as Elucidated by Microwave and Infrared Spectroscopy, in Atomic and Molecular Clusters, Bernstein, E. R. (Ed.), p. 359 (Elsevier, Amsterdam, **1990**).
- [43] A. C. Legon, D. J. Millen, *Chem. Soc. Rev.* **1992**, *21*, 71.
- [44] G. A. Jeffrey, Introduction to hydrogen bonding, oxford University Press, Oxford, **1997**.
- [45] G. R. Desiraju, T. Steiner, The Weak Hydrogen Bond, Oxford University Press, Oxford, **1999**.
- [46] T. Steiner, *Angew. Chem. Int. Ed.* **2002**, *41*, 48.
- [47] C. L. Perrin, J. B. Nielson, *Annu. Rev. Phys. Chem.* **1997**, *48*, 511.
- [48] S. Scheiner, *Phys. Chem. Chem. Phys.* **2011**, *13*, 13860.
- [49] M. Nishio, *Phys. Chem. Chem. Phys.* **2011**, *13*, 13873.
- [50] S. Melandri, *Phys. Chem. Chem. Phys.* **2011**, *13*, 13901.
- [51] L. Evangelisti, W. Caminati, *Phys. Chem. Chem. Phys.* **2010**, *12*, 14433.
- [52] P. Politzer, P. Lane, M. C. Concha, Y. Ma, J. S. Murray, *J. Mol. Model.* **2007**, *13*, 305.
- [53] P. Politzer, J. S. Murray, Timothy Clark, *Phys. Chem. Chem. Phys.* **2010**, *12*, 7748.
- [54] P. Metrangolo, H. Neukirch, T. Pilati, G. Resnati, *Acc. Chem. Res.* **2005**, *38*, 386.
- [55] P. Metrangolo, G. Resnati, *Science* **2008**, *321*, 918.
- [56] P. Metrangolo, F. Meyer, T. Pilati, G. Resnati, G. Terraneo, *Angew. Chem. Int. Ed.* **2008**, *47*, 6114.
- [57] D. Hauchecorne, B. J. van der Veken, A. Moiana, W. Herrebout, *Chem. Phys.* **2010**, *374*, 30.
- [58] D. Hauchecorne, R. Szostak, W. A. Herrebout, B. J. van der Veken, *ChemPhysChem* **2009**, *10*, 2105.
- [59] A. C. Legon, *Phys. Chem. Chem. Phys.* **2010**, *12*, 7736.
- [60] L. Evangelisti, G. Feng, P. Écija, E. J. Cocinero, F. Castaño, W. Caminati, *Angew. Chem. Int. Ed.* **2011**, *50*, 7807.
- [61] G. Feng, L. Evangelisti, N. Gasparini, W. Caminati, *Chem. Eur. J.* **2012**, *18*, 1364.

- [62] S. E. Novick, P. Davies, S. J. Harris, W. Klemperer, *J. Chem. Phys.* **1973**, *59*, 2273.
- [63] S. G. Kucolich, J. A. Shea, *J. Chem. Phys.* **1982**, *77*, 5242.
- [64] J.-U. Grabow, A. S. Pine, G. T. Fraser, F. J. Lovas, R. D. Suenram, T. Emilsson, E. Arunan, H. S. Gutowsky, *J. Chem. Phys.* **1995**, *102*, 1181.
- [65] Y. Xu, W. Jäger, J. Djauhari, M. C. L. Gerry, *J. Chem. Phys.* **1995**, *103*, 2827.
- [66] W. Jäger, Y. Xu, M. C. L. Gerry, *J. Chem. Phys.* **1993**, *99*, 919.
- [67] Y. Xu, W. Jäger, M. C. L. Gerry, *J. Chem. Phys.* **1994**, *100*, 4171.
- [68] Y. Xu, W. Jäger, *J. Chem. Phys.* **1997**, *107*, 4788.
- [69] A. Maris, W. Caminati, *J. Chem. Phys.* **2003**, *118*, 1649.
- [70] Y. Morita, N. Ohashi, Y. Kawashima, E. Hirota, *J. Chem. Phys.* **2006**, *124*, 094301.
- [71] P. Ottaviani, A. Maris, W. Caminati, Y. Tatamitani, Y. Suzuki, T. Ogata, J. L. Alonso, *Chem. Phys. Lett.* **2002**, *361*, 341.
- [72] B. Velino, S. Melandri, W. Caminati, *J. Phys. Chem. A* **2004**, *108*, 4224.
- [73] W. Caminati, A. Millemaggi, J. L. Alonso, A. Lesarri, J. C. Lopez, S. Mata, *Chem. Phys. Lett.* **2004**, *392*, 1.
- [74] A. Mizoguchi, Y. Ohshima, Y. Endo, *J. Chem. Phys.* **2011**, *135*, 064307.
- [75] D. Priem, T. K. Ha, A. Bauder, *J. Chem. Phys.* **2000**, *113*, 169.
- [76] B. Ouyang, T. G. Starkey, B. J. Howard, *J. Phys. Chem. A* **2007**, *111*, 6165.
- [77] J. L. Neill, M. T. Muckle, B. H. Pate, 65th International Symposium on High Resolution Spectroscopy, Columbus OHIO USA, June 21-25, **2010**, Lecture TH10.
- [78] C. Pérez, M. T. Muckle, D. P. Zaleski, N. A. Seifert, B. Temelso, G. C. Shields, Z. Kisiel, B. H. Pate, *Science* **2012**, *336*, 897.
- [79] W. Caminati, S. Melandri, P. Moreschini, P. G. Favero, *Angew. Chem. Int. Ed.* **1999**, *38*, 2924.
- [80] S. Blanco, S. Melandri, P. Ottaviani, W. Caminati, *J. Am. Chem. Soc.* **2007**, *129*, 2700.
- [81] W. Caminati, unpublished result.
- [82] B. M. Giuliano, W. Caminati, *Angew. Chem. Int. Ed.* **2005**, *44*, 603.
- [83] S. Tang, I. Majerz, W. Caminati, *Phys. Chem. Chem. Phys.* **2011**, *13*, 9137.
- [84] G. Feng, Q. Gou, L. Evangelisti, Z. Xia, W. Caminati, *Phys. Chem. Chem. Phys.* **2013**, *15*, 2917.

Chapter 2 Theoretical aspect and experimental method

In this part, some fundamental theory of rotational spectroscopy that has been used to explain the relative rotational spectra measured in this thesis is described. The classical mechanics of a rotating body and the quantum mechanical properties of angular momentum for rotating tops with different type of molecular symmetry are reviewed first. Later, the centrifugal distortion is described since the real molecular system cannot be a “rigid” top. The effect of nuclear quadrupole coupling and internal rotation on the rotational spectrum are also described. Methods for evaluating molecular structure are also introduced. *ab initio* calculations and density function theory (DFT) are mentioned briefly. Finally, some details on FTMW spectrometer used for collecting the rotational spectra are given. For more details concerning the theory, one can refer to several MW books.^[1-3] For the most recent and innovative applications of microwave spectroscopy, one can refer to some book chapters^[4] and reviews.^[5]

2.1 Angular momentum of a rigid rotor

The derivation of molecular structure from the rotational spectroscopy requires the knowledge of classical mechanics of rotating bodies. Classically, the angular momentum of a rigid system is

$$\mathbf{P} = \mathbf{I}\omega \quad (2.1)$$

Where ω is the angular velocity and \mathbf{I} is the moment of inertia tensor, which is written as

$$\mathbf{I} = I_{xx}\mathbf{ii} + I_{xy}\mathbf{ij} + I_{xz}\mathbf{ik} + I_{yx}\mathbf{ji} + I_{yy}\mathbf{jj} + I_{yz}\mathbf{jk} + I_{zx}\mathbf{ki} + I_{zy}\mathbf{kj} + I_{zz}\mathbf{kk} \quad (2.2)$$

Where

$$\begin{aligned}
 I_{xx} &= \Sigma m (y^2+z^2) \\
 I_{yy} &= \Sigma m (z^2+x^2) \\
 I_{zz} &= \Sigma m (x^2+y^2) \\
 I_{xy} &= I_{yx} = -\Sigma m x y \\
 I_{zx} &= I_{xz} = -\Sigma m x z \\
 I_{yz} &= I_{zy} = -\Sigma m y z
 \end{aligned} \tag{2.3}$$

In which m is the mass of a particular particle and x, y, z are the body fixed coordinates originating at the center of mass. The summation is taken over all the particles in the body. Since the origin of the coordinate system is chosen at the center of mass, the total kinetic energy can be separated as the kinetic energy of transition motion of the center of mass and the kinetic energy of the motion relative to the center of mass. Thus the translational and rotational motions can be treated separately. It is always possible to choose the coordinate axes in which that the products of inertia vanish, leaving only the diagonal elements, called the principal moments of inertia. The principal moments are the three roots I of the equation (2.4)

$$\begin{vmatrix} I_{aa} - I & I_{ab} & I_{ac} \\ I_{ba} & I_{bb} - I & I_{bc} \\ I_{ca} & I_{cb} & I_{cc} - I \end{vmatrix} = 0 \tag{2.4}$$

Where a, b, c is the principal axes system, the components of angular momentum become

$$P_a = I_a \omega_a, P_b = I_b \omega_b, P_c = I_c \omega_c \tag{2.5}$$

The rotational kinetic energy is

$$\begin{aligned}
 E_r &= \frac{1}{2}(\omega \cdot I \cdot \omega) = \frac{1}{2}(I_{aa} \omega_a^2 + I_{bb} \omega_b^2 + I_{cc} \omega_c^2 + 2I_{ab} \omega_a \omega_b + 2I_{ac} \omega_a \omega_c + 2I_{bc} \omega_b \omega_c) \\
 &= \frac{1}{2}(P_a^2/I_a) + \frac{1}{2}(P_b^2/I_b) + \frac{1}{2}(P_c^2/I_c)
 \end{aligned} \tag{2.6}$$

When the body is subjected to a torque

$$\boldsymbol{\tau} = i \tau_x + j \tau_y + k \tau_z \tag{2.7}$$

X, Y, Z are the space fixed axes. Thus the changing of angular momentum relative to the space fixed axes is equal to the applied torque,

$$d\mathbf{P}/dt = \mathbf{i}(dP_x/dt) + \mathbf{j}(dP_y/dt) + \mathbf{k}(dP_z/dt) = \boldsymbol{\tau} \quad (2.8)$$

Obviously, the angular momentum (\mathbf{P}) is constant when no torque is applied and also the components of P_x^2, P_y^2, P_z^2 are constants. So that the square of the total angular momentum is constant

$$P^2 = P_x^2 + P_y^2 + P_z^2 = \text{constant} \quad (2.9)$$

The changing of the total angular momentum caused by a torque contains two parts: One is due to the changing of the components P_x, P_y, P_z , another is due to the rotating of the body fixed axes with angular velocities ω_x, ω_y , and ω_z . Thus

$$\mathbf{i}(dP_x/dt) + \mathbf{j}(dP_y/dt) + \mathbf{k}(dP_z/dt) + \boldsymbol{\omega} \times \mathbf{P} = \boldsymbol{\tau} \quad (2.10)$$

with components

$$\begin{aligned} (dP_x/dt) + \omega_y P_z - \omega_z P_y &= \tau_x \\ (dP_y/dt) + \omega_z P_x - \omega_x P_z &= \tau_y \\ (dP_z/dt) + \omega_x P_y - \omega_y P_x &= \tau_z \end{aligned} \quad (2.11)$$

In the principle axes system, if the body is rotating freely ($\tau = 0$), the Euler's equations of motion can be obtained as

$$\begin{aligned} (dP_a/dt) + (1/I_b - 1/I_c) P_b P_c &= 0 \\ (dP_b/dt) + (1/I_c - 1/I_a) P_c P_a &= 0 \\ (dP_c/dt) + (1/I_a - 1/I_b) P_a P_b &= 0 \end{aligned} \quad (2.12)$$

It is easy to prove that the sum of the square of the angular momentum along a, b and c axes is also constant:

$$P_a^2 + P_b^2 + P_c^2 = \text{constant} \quad (2.13)$$

Similarly, one can obtain that the rotational energy is constant:

$$E_r = \frac{1}{2}(P_a^2/I_a + P_b^2/I_b + P_c^2/I_c) = \text{constant} \quad (2.14)$$

These equations show that when no torque is applied, the square of the total angular momentum expressed in the body fixed axes and the principal axes is constant and the kinetic energy of rotation is constant.

2.2 Angular momentum operators and matrix elements

The classical angular momentum of a system of particles can be expressed as

$$\begin{aligned} \mathbf{P} &= \mathbf{i} P_X + \mathbf{j} P_Y + \mathbf{k} P_Z \\ &= \mathbf{i} (Y P_Z - Z P_Y) + \mathbf{j} (Z P_X - X P_Z) + \mathbf{k} (X P_Y - Y P_X) \end{aligned} \quad (2.15)$$

While applying the relations $X \rightarrow X$, and so on, and $P_X \rightarrow (\hbar/i) (\partial/\partial X)$, and so on, one can derive the component angular momentum operators:

$$\begin{aligned} P_X &= (\hbar/i) [Y (\partial/\partial Z) - Z (\partial/\partial Y)] \\ P_Y &= (\hbar/i) [Z (\partial/\partial X) - X (\partial/\partial Z)] \\ P_Z &= (\hbar/i) [X (\partial/\partial Y) - Y (\partial/\partial X)] \end{aligned} \quad (2.16)$$

The square of the total angular momentum P^2 commutes with its component operators

$$P^2 P_X - P_X P^2 = 0 \quad (2.17)$$

However, the component operators do not commute among themselves and the following commutation rules hold

$$P_\alpha P_\beta - P_\beta P_\alpha = i \hbar P_\gamma, \quad \alpha, \beta, \gamma = X, Y, \text{ and } Z, \text{ cyclically} \quad (2.18)$$

Also of convenience for some manipulations are the operators defined as

$$P_+ = P_X + iP_Y \quad (2.19)$$

$$P_- = P_X - iP_Y \quad (2.20)$$

The commutation rules are

$$P_+ P_- - P_- P_+ = 2 \hbar P_Z \quad (2.21)$$

$$P_Z P_+ - P_+ P_Z = \hbar P_+ \quad (2.22)$$

$$P_Z P_- - P_- P_Z = -\hbar P_- \quad (2.23)$$

Quantum mechanically, the commute operators have the common sets of eigenfunctions. Therefore P^2 and P_Z have common eigenfunctions $\psi_{J,M}$.

$$P^2 \psi_{J,M} = k_J \psi_{J,M} \quad (2.24)$$

$$P_Z \psi_{J,M} = k_M \psi_{J,M} \quad (2.25)$$

Where the k_J and k_M are the eigenvalues of P^2 and P_Z corresponding to the eigenstate described by $\psi_{J,M}$. The quantized values are $k_J = \hbar^2 J(J+1)$ and $k_M = \hbar M$, where J and M are integrals and $|M| \leq J$. Thus (2.24) and (2.25) can be expressed as

$$P^2 \psi_{J,M} = \hbar^2 J(J+1) \psi_{J,M} \quad (2.26)$$

$$P_Z \psi_{J,M} = \hbar M \psi_{J,M} \quad (2.27)$$

With $J = 0, 1, 2, 3, \dots$ and $M = J, J-1, J-2, \dots, -J$

The Hamiltonian operator is obtained from the classical Hamiltonian when the momenta are replaced by their conjugate operators. When no torques is applied, the classical Hamiltonian of the rigid rotor consists of only kinetic energy which can be expressed in terms of the components of angular momentum in the principal axes. To find the corresponding Hamiltonian operator, one simply substitutes for the P 's the conjugate angular momentum operator. In the principal axes, a, b, c , this operator is

$$H_r = \frac{1}{2}(P_a^2/I_a + P_b^2/I_b + P_c^2/I_c) \quad (2.28)$$

Where $P_a, P_b,$ and P_c are the angular momentum components as shown in (2.16).

The eigenvalues of the Hamiltonian operators represent the quantized energies from the determined microwave spectra. For a rigid spherical top rotor, the three principal moments of inertia are equal, $I_a = I_b = I_c = I$. The Hamiltonian operator H_r of (2.28) becomes

$$H_r = \frac{1}{2}I (P_a^2 + P_b^2 + P_c^2) = P^2/2I \quad (2.29)$$

The Hamiltonian commutes with P^2 , the eigenvalues of H_r which corresponding to the quantized energy values are

$$E_r = (J, M|H_r|J, M) = \frac{1}{2}I (J, M|P^2|J, M) = \frac{\hbar^2}{2I} J(J+1) \quad (2.30)$$

For a symmetric top rotor, one of the principal axes of inertia must lie along the molecular symmetry axis. The principal moments of inertia which have their axes perpendicular to this axis are equal. If a -axis lies along the symmetry axis ($I_a < I_b = I_c$), the molecule is a prolate symmetric top. If c lies along the symmetric axis ($I_a = I_b < I_c$), the molecule is an oblate top. The Hamiltonian commutes with P_z and P_Z as well as P^2 and is therefore diagonal in the J, K, M representation. With the a -axis chosen along the symmetry axis ($I_b = I_c$) and with $P^2 = P_a^2 + P_b^2 + P_c^2$, the Hamiltonian can be expressed as

$$H_r = P^2/2I_b + (1/2I_a - 1/2I_b) P_a^2 \quad (2.31)$$

Eigenvalues for the angular momentum operators P^2 , P_z , and P_Z for the symmetric top rotor are

$$(J, K, M|P^2|J, K, M) = \hbar^2 J(J+1) \quad (2.32)$$

$$(J, K, M|P_z|J, K, M) = \hbar K \quad (2.33)$$

$$(J, K, M|P_Z|J, K, M) = \hbar M \quad (2.34)$$

Where $J = 0, 1, 2, 3, \dots$, $K = 0, \pm 1, \pm 2, \pm 3, \dots, \pm J$, $M = 0, \pm 1, \pm 2, \pm 3, \dots, \pm J$

In the field free rotor, the rotational energies do not depend on M . The quantized rotational energies of the rigid prolate symmetric top are

$$E_{J,K} = (J, K|H_r|J, K) = \frac{1}{2}I_b (J, K|P^2|J, K) + \frac{1}{2}(1/I_a - 1/I_b) (J, K|P_a^2|J, K)$$

$$= (h^2/8\pi^2 I_b) J(J+1) + (h^2/8\pi^2) (1/I_a - 1/I_b) K^2 \quad (2.35)$$

With the designation $A = h^2/(8\pi^2 I_a)$ and $B = h^2/(8\pi^2 I_b)$, $E_{J,K}$ can be written as

$$E_{J,K} = h [B J(J+1) + (A-B) K^2] \quad (2.36)$$

In a true symmetric top, any permanent dipole moment must lie along the symmetry axis. All matrix elements of this dipole moment resolved along a space-fixed axis vanish except those between states corresponding to $J \rightarrow J$ or $J \pm 1$, $K \rightarrow K$. The selection rules for the field free rotor are

$$\Delta J = 0, \pm 1 \quad \Delta K = 0 \quad (2.37)$$

For absorption transition, the selection rule is $J \rightarrow J+1$, $K \rightarrow K$. Applying these rules to (2.36) gives the formula for the absorption frequencies for the rigid symmetric top

$$\nu = 2 B (J+1) \quad (2.38)$$

However, as what will be described in the following text, centrifugal distortion separates the lines corresponding to different $|K|$ by small frequency differences which are usually sufficient to make these lines resolvable in the microwave region.

The Hamiltonian operator for the asymmetric-top rotor for which $I_a \neq I_b \neq I_c$, does not commute with the operator P_a or with the other component operators P_b or P_c . The resulting matrix will not be diagonal, and the elements will not represent eigenvalues of H_r .

The general procedure used to give the energy levels and wave functions for the asymmetric rotor is to assume that the wave functions can be expanded in terms of an orthogonal set of functions (a natural basis would be the symmetric-top functions) and to set up the secular equations for the unknown coefficients and energies. The resulting secular determinant can be broken down into a number of subdeterminants, the order of which increases with J . The solution of these subdeterminants yields the required energy levels and expansion coefficients. The King's double subscript system is the

most descriptive and useful designation of the asymmetric top energy levels. This system is best understood by a comparison of the prolate and oblate symmetric tops limitation.

In the conventional order, $I_a < I_b < I_c$, when $I_b \rightarrow I_c$, the prolate symmetric top is approached; and when $I_a \rightarrow I_b$, the oblate symmetric top is approached. The behavior of the asymmetric rotor can be described in terms of the parameter

$$\kappa = (2B-A-C)/(A-C) \quad (2.39)$$

The limiting values for κ are -1 and +1, corresponding to the prolate and oblate symmetric tops, respectively. Thus the energy levels can be note as $J_{K_1 K_2}$, in which the first subscript, K_1 , represents the κ value of the limiting prolate top with which the asymmetric-top level connects as κ approaches -1. The second subscript, K_2 , represents the κ value of the limiting oblate top with which the particular level connects as κ approaches 1.

The quantum mechanical Hamiltonian describing the rotation of a rigid asymmetric rotor is then

$$H_r = A P_a^2 + B P_b^2 + C P_c^2 \quad (2.40)$$

The calculation of the energy levels is facilitated by rearrangement of (2.40) as suggested by Ray

$$H_r = \frac{1}{2}(A+C) P^2 + \frac{1}{2}(A-C) H(\kappa) \quad (2.41)$$

$$H(\kappa) = P_a^2 + \kappa P_b^2 - P_c^2 \quad (2.42)$$

Unlike the symmetric rotor Hamiltonian, this Hamiltonian is such that the Schrodinger equation cannot be solved directly. Thus a closed general expression for the asymmetric rotor wave functions is not possible. However, they may be represented by a linear combination of symmetric rotor functions

$$\psi_{J\tau M} = \sum_{J,K,M} a_{J,K,M} \psi_{J,K,M} \quad (2.43)$$

Where the a_{JKM} 's are numerical constants and

$$\psi_{JKM} = \Theta_{JKM} e^{iK\phi} e^{iM\chi} \quad (2.44)$$

$$\Theta_{JKM} = N_{JKM} (\sin(\theta/2))^{|K-M|} (\cos(\theta/2))^{|K+M|} F(\sin^2(\theta/2)) \quad (2.45)$$

Where θ , ϕ , χ are the Euler's angles, $F(\sin^2(\theta/2))$ is a hypergeometric series and N_{JKM} is a normalizing factor determined by the condition $N_{JKM}^2 \int \psi_{JKM} \psi_{JKM}^* d\tau = 1$.

By solving the secular determinant, the total rotational energy for a particular level can be expressed as

$$E = \frac{1}{2}(A+C) J(J+1) + \frac{1}{2}(A-C) E(\kappa) \quad (2.46)$$

The nonvanishing matrix elements of $E(\kappa)$ are

$$E_{K,K} = (J, K, M | H(\kappa) | J, K, M) = F [J(J+1) - K^2] + G K^2 \quad (2.47)$$

$$E_{K,K\pm 2} = (J, K, M | H(\kappa) | J, K\pm 2, M) = H [f(J, K\pm 1)]^{1/2} \quad (2.48)$$

With the fact that

$$E_{K,K} = E_{-K,-K}, E_{K,K+2} = E_{K+2,K} = E_{-K,-K-2} = E_{-K-2,-K} \quad (2.49)$$

The constants F , G , and H depend on the particular way in which the a , b , and c axes are identified with the axes x , y , and z , which are summarized in **Table 2.1**. The I^f and III^l type representation are sufficient to handle conveniently most asymmetric tops.

Table 2.1 Identification of a , b , c with x , y , z and the coefficients for the matrix elements of $E(\kappa)$

	I^r	II^r	III^r	I^l	II^l	III^l
x	b	c	a	c	a	b
y	c	a	b	b	c	a
z	a	b	c	a	b	c
F	$1/2(\kappa-1)$	0	$1/2(\kappa+1)$	$1/2(\kappa-1)$	0	$1/2(\kappa+1)$
G	1	κ	-1	1	κ	-1
H	$-1/2(\kappa+1)$	1	$1/2(\kappa-1)$	$1/2(\kappa+1)$	-1	$-1/2(\kappa-1)$

Like a symmetric top, the allowed changes in J for the dipole absorption of radiation results from the non-vanishing property of the dipole matrix elements $\int A J_\tau \mu A' J'_\tau$, when $J' = J$ or $J' = J \pm 1$, are:

$$\Delta J = 0, \pm 1 \quad (2.50)$$

In addition to the selection rules for J , there are also restrictions on the changes that can occur in the pseudo-quantum numbers, which result from the symmetry properties of the ellipsoid of the inertia.

The component of the electric moment along a space fixed axis F can be described as

$$\mu_F = \sum_g \cos(Fg) \mu_g \quad F = X, Y, Z; g = a, b, c \quad (2.51)$$

where μ_g are the molecular dipole moment components resolved along the principal axes of inertia. The $\cos(Fg)$ are the cosine of angles between the nonrotating F and rotating g axes, which are commonly indicated by the symbol Φ_{Fg} . The dipole matrix element for the case where the electric moment lies only along one of the principal axis, the a -axis is

$$(J, K-1, K1 | \mu_F | J', K'-1, K'1) = \mu_a (J, K-1, K1 | \cos(Fa) \mu_F | J', K'-1, K'1) \quad (2.52)$$

If this integral is not to vanish, it must be unchanged for any operation that carries the system into a configuration indistinguishable from the original, or the integrand $(J, K-1, K1 | \cos(Fa) \mu_F | J', K'-1, K'1)$ transforms according to the totally symmetric representation A . The symmetry of interest is not the molecular symmetry but the symmetry of the inertia ellipsoid, which for the asymmetric rotor is characterized by the Four-group operations, as reported in **Table 2.2**. If the integrand is to belong to species A , then for each symmetry operation of G either each term of the integrand is even, or one term is even and the other two are odd. Under the Four-group operations, the direction cosines have B symmetries. For a rotation of 180° about a -axis (C_2^a), the $\cos(Fg)$ does not change, but it does change sign for a rotation about b or c -axis since the angle changes from Fa to $\pi - Fa$. Therefore it transforms according to the $B_a(eo)$ representation. Likewise, $\cos(Fb)$ does not change sign for C_2^b symmetric operation but

changes sign for C_2^a and C_2^c operation and transforms as the species $B_b(oo)$. $\cos(Fc)$ transforms as the species $B_c(oe)$.

For the case under consideration ($\mu_a \neq 0$, $\mu_b = \mu_c = 0$), the direction cosine transforms as B_a , if the integrand has symmetry A , the functions A^*J_τ and AJ_τ must be of symmetry A and B_a , or of symmetry B_b and B_c . The allowed transitions are then $A \leftrightarrow B_a$, and $B_b \leftrightarrow B_c$. Similarly, the selection rules for electric dipole components along the b and c -axes can be established, which are summarized in **Table 2.3**.

Table 2.2 Character table of the Four group $G(a, b, c)$

Symmetric species	E	C_2^a	C_2^b	C_2^c
A	1	1	1	1
B_a	1	1	-1	-1
B_b	1	-1	1	-1
B_c	1	-1	-1	1

Table 2.3 Selection rules in terms of the evenness or oddness of $K-1$, $K1$ subscripts

Dipole component	Permitted transitions
$\mu_a \neq 0$	$ee \leftrightarrow eo, oe \leftrightarrow oo$
$\mu_b \neq 0$	$ee \leftrightarrow oo, oe \leftrightarrow eo$
$\mu_c \neq 0$	$ee \leftrightarrow oe, eo \leftrightarrow oo$

2.3 Centrifugal distortion

The real molecule can not be a rigid rotor. While rotating, the bond distances and angles will vary because of the centrifugal force, which gives rise to a centrifugal distortion. The rotating molecule will no longer be in its equilibrium configuration but in a distorted configuration. These effects are usually large for light molecules because of the small moments of inertia. Due to the effect of this distortion, the moments of inertia can not be considered as constant and the value of which dependent on the rotational state. Consequently, the rotational spectrum can not be just treated as a rigid rotor characterized by a sequence of equilibrium moments of inertia. Because of the precise

of microwave measurements, the centrifugal distortion effect can be observed even for low-lying levels with relatively small rotational energies.

Interestingly, the study of centrifugal also provides very accurate ground state spectroscopic constants, which allows one to predict unmeasured transition frequencies precisely, and the distortion constants themselves provide direct information on the vibrational potential function and fundamental information for elucidation of interatomic forces and bonding.

Centrifugal distortion effects only represent a small part of the rotational energy which is accounted for mainly by the rigid rotor term. Therefore in many cases this effect can be treated as a perturbation to the rigid rotor Hamiltonian.

$$H = H_r + H_d \quad (2.53)$$

$$H_r = A P_a^2 + B P_b^2 + C P_c^2 \quad (2.54)$$

$$H_d = \hbar^4/4 \sum_{\alpha,\beta,\gamma,\delta} \tau_{\alpha,\beta,\gamma,\delta} P_\alpha P_\beta P_\gamma P_\delta \quad (2.55)$$

Here the angular momentum has unit of \hbar , and $\alpha, \beta, \gamma, \delta = x, y, z$. A rigorous treatment of the problem indicates that the rotation and distortion constants in the foregoing Hamiltonian must be regarded as effective constants and thus dependent on the vibrational state. The effects of centrifugal distortion on the rotational spectra will depend on both the constants $\tau_{\alpha,\beta,\gamma,\delta}$ and the angular momentum operators. A simple closed-form expression for the effect of these operators, like that obtained for a symmetric rotor, cannot be obtained for an asymmetric rotor. However, the distortion effects for a large number of asymmetric rotors may be treated to a good approximation by first-order perturbation theory. The first order perturbation treatment involves averaging the perturbing operator H_d over the asymmetric rigid rotor wave functions. In the second order perturbation treatment of the term H_d , it's possible to transform the Hamiltonian H_r to an effective form H_{eff} which is diagonal in the vibrational quantum numbers transforming the Hamiltonian terms into the fourth degree in angular momentum P called quartic centrifugal distortion term.

By a second order treatment to an asymmetric top, the quartic centrifugal distortion coefficients $\tau_{\alpha\beta\gamma\delta}$ can be reduced to five independent as discussed in details in Watson's

review.^[6] For the *A*- and *S*-reduction, the reduced quartic centrifugal distortion Hamiltonian have the following forms

$$H_d^{(A)} = -A_J P^4 - A_{JK} P^2 P_z^2 - A_K P_z^4 - 2\delta_J P^2 (P_x^2 - P_y^2) - \delta_K [P_z^2 (P_x^2 - P_y^2) + (P_x^2 - P_y^2) P_z^2] \quad (2.56)$$

$$H_d^{(S)} = -D_J P^4 - D_{JK} P^2 P_z^2 - D_K P_z^4 + d_1 P^2 (P_+^2 + P_-^2) + d_2 (P_+^4 + P_-^4) \quad (2.57)$$

A least square fitting of the observed frequencies is carried out to obtain the rotational and centrifugal distortion constants. Particularly, the differences between the observed frequency and the calculated rigid rotor frequency are taken as the distortion effect.

2.4 Nuclear quadrupole coupling

The interaction of the electric or magnetic of the molecular field with the nuclear moments may result the nuclear hyperfine structure in rotational spectra. The most important of these interactions is that of the molecular field gradient with the electric quadrupole of the nuclei. This information provides a measure of the molecular field gradients from which information on the electronic structure and chemical bonds can be obtained. However, this interaction is only possible for isotopes with nuclear spin larger than 1/2 ($I > 1/2$), because isotopes with nuclear spins equal to 0 or 1/2 have spherically symmetric and have no quadrupole moments.

In a external field free molecule, the nuclear spin I is coupled to the molecular rotational angular momentum J to form a resultant F , as shown in the vector model in **Figure 2.1**. The total angular momentum of the molecule is thus represented by F rather than J . The new angular momentum quantum numbers are

$$F = J+I, J+I-1, J+I-2, \dots, |J-I| \quad (2.58)$$

$$\text{And } M_F = F, F-1, F-2, \dots, -F \quad (2.59)$$

The eigenvalues of the square of the total angular momentum and its components along an axis space thus are

$$(F, M_F|F^2|F, M_F) = F(F+1) \quad (2.60)$$

$$(F, M_F|F_z|F, M_F) = M_F \quad (2.61)$$

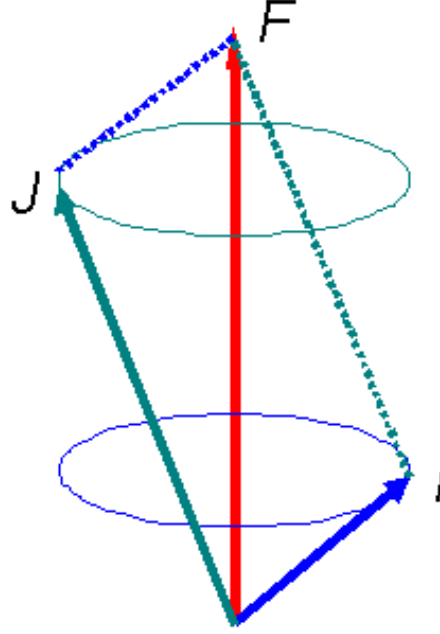


Figure 2.1 Vector diagram of coupling of the nuclear spin I with molecular rotational momentum J .

While subtraction and addition of $1/6\nabla^2V \int \rho_n R_n^2 d\tau_n$ to the classical quadrupole interaction, the interaction energy has the form

$$E_Q = 1/6[(\partial^2V/\partial X^2)_0 \int (3X_n^2 - R_n^2) \rho_n d\tau_n + (\partial^2V/\partial Y^2)_0 \int (3Y_n^2 - R_n^2) \rho_n d\tau_n + (\partial^2V/\partial Z^2)_0 \int (3Z_n^2 - R_n^2) \rho_n d\tau_n + 6(\partial^2V/\partial X \partial Y)_0 \int X_n Y_n \rho_n d\tau_n + 6(\partial^2V/\partial X \partial Z)_0 \int X_n Z_n \rho_n d\tau_n + 6(\partial^2V/\partial Y \partial Z)_0 \int Y_n Z_n \rho_n d\tau_n] + 1/6[(\partial^2V/\partial X^2)_0 + (\partial^2V/\partial Y^2)_0 + (\partial^2V/\partial Z^2)_0] \int R_n^2 \rho_n d\tau_n \quad (2.62)$$

Because the Laplace's equation $\nabla^2V = 0$ holds over the nuclear volume, the expression can be written as the scalar product of two symmetric dyadics

$$E_Q = -1/6\mathbf{Q}:\nabla\mathbf{E} = 1/6\sum_{i,j=X,Y,Z}Q_{ij}V_{ij} \quad (2.63)$$

Where $V_{ij} = -\nabla E_{ij}$ and the $\nabla\mathbf{E}$ is the gradient of the electric field of the extra nuclear charges

$$\nabla E = \mathbf{e}_X (\partial E / \partial X) + \mathbf{e}_Y (\partial E / \partial Y) + \mathbf{e}_Z (\partial E / \partial Z) \quad (2.64)$$

And \mathbf{Q} is the quadrupole moment dyadic

$$\mathbf{Q} = \int \rho_n [(3 \mathbf{R}_n \mathbf{R}_n - I R_n^2)] d\tau_n \quad (2.65)$$

Here \mathbf{R}_n represents the vector locating points of the nuclear volume in the space-fixed X, Y, Z system. $I = \mathbf{e}_X \mathbf{e}_X + \mathbf{e}_Y \mathbf{e}_Y + \mathbf{e}_Z \mathbf{e}_Z$ is the unit dyadic and $\mathbf{e}_X, \mathbf{e}_Y,$ and \mathbf{e}_Z are unit vectors along $X, Y,$ and Z .

The potential V at the nucleus arises from all the various extra nuclear charges of the molecule, however only the extra nuclear electrons need to be considered, and can be expressed as

$$V = \sum_k e (1/R_e)_k \quad (2.66)$$

Where $(1/R_e)_k$ represents the distance from the k th electron to the nucleus and where the summation is taken over all electrons contributing to V . For simplicity, one can only consider one component of the tensor. Since

$$(\partial^2 / \partial X^2) (1/R) = (\partial^2 / \partial X^2) (X^2 + Y^2 + Z^2)^{-1/2} = (3X^2 - R^2)/R^5 \quad (2.67)$$

Thus

$$\begin{aligned} V_{XX} &= (\partial^2 V / \partial X^2)_0 = e \sum_k \langle (1 - R_e^3)_k \rangle \langle [3 (X_e / R_e)^2 - 1]_k \rangle \\ &= e \sum_k \langle (1 - R_e^3)_k \rangle \langle (3 \cos^2 \theta_X - 1)_k \rangle \end{aligned} \quad (2.68)$$

Where θ_X is the angle between R_e and the X -axis fixed in space. The average is taken over the electronic orbitals and over the vibrational and rotational states of the molecule. $\langle (1/R_e^3)_k \rangle$ is independent of the rotation and in a particular vibrational state may be treated as a constant. Equation (2.68) can be written as

$$V_{XX} = \sum_k C_k \langle [3 (X_e / R_e)^2 - 1]_k \rangle \quad (2.69)$$

Because the orbitals of all the electrons are fixed in the molecule and rotate with the molecular frame about the axis of \mathbf{J} , the angular dependence of their averaged sum will be the same as that of \mathbf{J} , and their resultant field gradient will resolve along space-fixed axes in the same proportions as the components of \mathbf{J} ; the rapid rotation about \mathbf{J} will effectively average out the components of the field gradient perpendicular to \mathbf{J} and make \mathbf{J} an axis of symmetry for the gradient.

$$(V_{XX})_{op} = C [(3J_X^2/J^2) - 1] \quad (2.70)$$

Where C is proportionality constant to be evaluated, which depends on the electronic distribution in the whole molecule but primarily in the atom of the particular coupling nucleus. Since the eigenvalues of J^2 are $J(J+1)$, thus (2.70) can be written as

$$(V_{XX})_{op} = C/[J(J+1)] [3J_X^2 - J(J+1)] \quad (2.71)$$

The expressions for V_{YY} and V_{ZZ} are similar. While the operators for the cross product terms must be summarized. For example,

$$V_{XY} = \sum_k C_k \langle (3 X_e Y_e / R_e)_k \rangle \quad (2.72)$$

The conjugate operator is

$$(V_{XY})_{op} = C/[J(J+1)] [(3(J_X J_Y + J_Y J_X)/2)] \quad (2.73)$$

From the ZZ component, one can define q_J , which has the form

$$q_J = (J, J | V_{ZZ} | J, J) = C/[J(J+1)] [3J^2 - J(J+1)] \quad (2.74)$$

and

$$C = (J+1)/(2J-1) q_J \quad (2.75)$$

Hence

$$(V_{ZZ})_{op} = [q_J/J(2J-1)] [3J_Z^2 - J(J+1)] \quad (2.76)$$

The nuclear quadrupole operator can be expressed as

$$(Q_{ij})_{op} = C_n [(3(I_i I_j + I_j I_i)/2 - \delta_{ij} I^2)] \quad (2.77)$$

Where C_n is the proportionality constant evaluated by definition of Q as the value for maximum resolution along a space fixed axis, that is, when $M_I = I$. Thus

$$eQ \equiv (I, I|Q_{zz}|I, I) = C_n (I, I|3I_z^2 - I(I+1)|I, I) = C_n [3I^2 - I(I+1)] \quad (2.78)$$

$$\text{with } C_n = eQ/[I(2I-1)] \quad (2.79)$$

and

$$(Q_{ij})_{op} = [eQ/I(2I-1)][3(I_i I_j + I_j I_i)/2 - \delta_{ij} I^2] \quad (2.80)$$

Thus the obtained Hamiltonian operator for the quadrupole interaction is

$$H_Q = eq_J Q/[6J(2J-1)I(2I-1)] \sum_{i,j=x,y,z} [3(I_i I_j + I_j I_i)/2 - \delta_{ij} I^2] [3(J_i J_j + J_j J_i)/2 - \delta_{ij} J^2] \quad (2.81)$$

By applying the commute rules between the components of I with those of J , (2.81) becomes

$$H_Q = [eQq_J/2J(2J-1)I(2I-1)] [3(\mathbf{I} \cdot \mathbf{J})^2 + 3/2\mathbf{I} \cdot \mathbf{J} - I^2 J^2] \quad (2.82)$$

Thus the interaction energy is

$$E_Q = [eQq_J/2J(2J-1)I(2I-1)] [3C(C+1)/4 - J(J+1)I(I+1)] \quad (2.83)$$

Where

$$C = F(F+1) - J(J+1) - I(I+1) \quad (2.84)$$

$$q_J = q_{aa} (J, i, M_J=J|\Phi_{Za}^2|J, i, M_J=J) + q_{bb} (J, i, M_J=J|\Phi_{Zb}^2|J, i, M_J=J) + q_{cc} (J, i, M_J=J|\Phi_{Zc}^2|J, i, M_J=J) \quad (2.85)$$

where q_{aa} , q_{bb} , and q_{cc} are the molecular field gradients at the coupling nucleus with reference to the inertial axes. For brevity, the coupling constant eQq is often designated by χ . With this designation the general expression for the quadrupole coupling energy is

$$E_Q = \sum_{g=a,b,c} \chi_{gg} \langle J, i, M_J=J | \Phi_{Zg}^2 | J, i, M_J=J \rangle Y(J, I, F) \quad (2.86)$$

$$Y(J, I, F) = [3C(C+1)/4 - J(J+1)I(I+1)] / [2J(2J-1)I(2I-1)] \quad (2.87)$$

Selection rules for hyperfine transitions in rotational absorption spectra are

$$J \rightarrow J+1, F \rightarrow F, F \rightarrow F\pm 1, I \rightarrow I$$

The rotational frequencies perturbed by quadrupole coupling are

$$\nu = \nu_0 - eQq [Y(J+1, I, F') - Y(J, I, F)] \quad (2.88)$$

For a symmetric top rotor with one single coupling nucleus on the symmetry axis- z , (2.85) becomes

$$q_J = q(J, K, M_J=J) (3\Phi_{zz}^2 - 1) / 2 | J, K, M_J=J \rangle = [q_J / (2J+3)] [3K^2 / J(J+1) - 1] \quad (2.89)$$

the resulting quadrupole energy is

$$E_Q = eQq [3K^2 / J(J+1) - 1] Y(J, I, F) \quad (2.90)$$

With $eQq = eQ_k \langle (\partial^2 V / \partial z^2) \rangle = \chi$ is the coupling constant with reference to the molecular axis of symmetry. Selection rules are $\Delta J = \pm 1$; $\Delta K = 0$; $\Delta F = 0, \pm 1$, $\Delta I = 0$.

In the asymmetric top, the quadrupole energy is

$$E_Q = \sum_{g=a,b,c} q_{gg} \langle J_g^2 \rangle [(2J+3)/J] Y(J, I, F) \quad (2.91)$$

$$\text{Where } \langle J_g^2 \rangle = \langle J, K_{-1}, K_1 | J_g^2 | J, K_{-1}, K_1 \rangle \quad (2.92)$$

$$\langle J_a^2 \rangle = \frac{1}{2}[J(J+1) + E(\kappa) - (\kappa+1)] (\partial E(\kappa)/\partial \kappa) \quad (2.93)$$

$$\langle J_b^2 \rangle = \partial E(\kappa)/\partial \kappa \quad (2.94)$$

$$\langle J_c^2 \rangle = \frac{1}{2}[J(J+1) - E(\kappa) + (\kappa-1)] (\partial E(\kappa)/\partial \kappa) \quad (2.95)$$

Which lead to an expression for the quadrupole energy in the form

$$E_Q = [1/J(J+1)] \{ \chi_{aa} [J(J+1) + E(\kappa) - (\kappa+1)] (\partial E(\kappa)/\partial \kappa) + 2\chi_{bb} (\partial E(\kappa)/\partial \kappa) + \chi_{cc} [J(J+1) - E(\kappa) + (\kappa-1)] (\partial E(\kappa)/\partial \kappa) \} Y(J, I, F) \quad (2.96)$$

In which $E(\kappa)$ is the reduced energy of the asymmetric rotor and κ is the Ray's asymmetry parameter.

Selection rules $\Delta F = 0, \pm 1$; $\Delta I = 0$ apply with those given for J_{K-1K1} for an asymmetric rotor.

2.5 Internal rotation

For molecules consist of two groups connected by a single bond, the groups can rotate with respect to one another around the single bond. Since the work of Kemp and Pitzer^[7] on estimating the barrier to internal rotation of methyl group in ethane, many examples proved that rotation about single bonds is restricted although the barrier are not large enough to permit chemical isolation. Microwave spectroscopy is an effective method to study the problem of hindered internal rotation. The barrier to internal rotation can be obtained with an accuracy of better than 5%. Moreover, structural parameters and equilibrium configuration of the methyl group can also be obtained.

The internal rotation of two parts of a molecule can be described by the torsional angle α . The potential energy to internal rotation, varying as a function of α , is required to be a periodic function in α which repeats itself N times in the interval $\alpha=0$ to $\alpha=2\pi$. N is the number of equivalent configurations, which depends on the symmetry of the molecule.

The potential energy with period $2\pi/N$ can be expressed as

$$V(\alpha) = a_0 + \sum_{k=1}^{\infty} a_k \cos(kN\alpha) \quad (2.97)$$

$$\text{Where } a_0 = - \sum_{k=1}^{\infty} a_k \quad (2.98)$$

$V(\alpha)$ is zero at $\alpha = 0, \pm 2\pi/N, \pm 4\pi/N$, and so on. For a N -fold symmetry system, this potential function can also be written as

$$V(\alpha) = \frac{1}{2}V_N (1 - \cos N\alpha) + \frac{1}{2}V_{2N} (1 - \cos 2N\alpha) + \dots \quad (2.99)$$

For molecules having a threefold barrier, e.g. methyl group, usually only the first term of the cosine is retained, the potential function is

$$V(\alpha) = \frac{1}{2}V_3 (1 - \cos 3\alpha) \quad (2.100)$$

With this potential energy, the torsional one dimensional Schrödinger can be written as

$$-F [d^2(U(\alpha))/d\alpha^2] + [1/2V_3 (1 - \cos 3\alpha)] U(\alpha) = E U(\alpha) \quad (2.101)$$

Where $F = \hbar^2/2I_r$ with I_r the reduced moment of inertia for relative motion of the two groups. Solution of this equation yields the torsional eigenvalues E and eigenfunctions $U(\alpha)$.

For a very small barrier so that $V_3 \rightarrow 0$, which means the group undergoing a free rotation, (2.101) reduces to

$$d^2(U(\alpha))/d\alpha^2 + (1/F) E U(\alpha) = 0 \quad (2.102)$$

$$\text{The solution is } U(\alpha) = A e^{im\alpha} = A (\cos m\alpha + i \sin m\alpha) \quad (2.103)$$

With A an appropriate normalization factor and with the energy given by

$$E = F m^2 \quad (2.104)$$

While the boundary condition is applied, m is required to take on the values $m = 0, \pm 1, \pm 2, \pm 3, \dots$ and A has the value $(1/2)^{1/2}\pi$.

The wave functions of (2.103) are also eigenfunctions of the angular momentum operator $p = -i\hbar(\partial/\partial\alpha)$, the eigenvalues of p being $m\hbar$. For the state m the two possible values of p , namely $|m|\hbar$ and $-|m|\hbar$ correspond to the two possible directions of internal rotation.

In the case of $V_3 \rightarrow \infty$, the internal motion will be restricted to small torsional oscillations about the minima of the barrier. The cosine function in (2.100) can be written as

$$\cos 3\alpha = 1 - (9/2)\alpha^2 + (27/8)\alpha^4 + \dots \quad (2.105)$$

$$V(\alpha) = (9/4)V_3\alpha^2 - (27/16)V_3\alpha^4 + \dots \quad (2.106)$$

For a harmonic approximation, only the first term of the expansion is retained, thus the torsional wave equation becomes

$$F [d^2(U(\alpha))/d\alpha^2] - (9/4)V_3\alpha^2 = E U(\alpha) \quad (2.107)$$

The solutions are

$$E = 3 (V_3 F)^{1/2} (v + 1) \quad (2.108)$$

With $v = 0, 1, 2, 3, \dots$

The frequency of torsional oscillation is $\nu = (3/2\pi) (V_3/2I_r)^{1/2}$, which related to the barrier. This relationship provides the basis for determining the barrier by infrared or microwave intensity studies. In the case of an infinite barrier, each torsional state ν is threefold degenerate since the internal motion is torsional oscillation in any one of the three equivalent potential well. For a finite barrier, the quantum mechanical tunneling effect leads to a splitting of this threefold degeneracy level ν into two levels, a nondegenerate level A and a doubly degenerate level designated as level E .

Two approaches have been used to treat the problem of internal rotation. One is the principal axis method (PAM) introduced by Wilson^[8] and Crawford,^[9] which used the principle axis of the whole molecule as the coordinate system. The internal axis method (IAM) used a coordinate system in which the symmetry axis of the top is chosen as one of the coordinate axes. The other two axes are fixed with respect to the framework and their orientation may be judiciously chosen.^[10]

The PAM uses the x, y, z coordinate system rigidly attached to the framework, which coincides with the principle axes of the entire molecule. The kinetic energy of an asymmetric molecule contains three parts, first part is the energy of the over all rotation of the molecule, second part is the energy of internal rotation of the top and the third part is the interaction between internal and external rotation, which in all can be written as

$$T = \frac{1}{2} \sum_g I_g \omega_g^2 + \frac{1}{2} I_\alpha \dot{\alpha}^2 + I_\alpha \dot{\alpha} \sum_g \lambda_g \omega_g \quad g = x, y, z \quad (2.109)$$

Where I_g are the principal moments of inertia of the entire molecule, I_α is the moment of inertia of the top around its symmetric axis, ω_g are the angular velocity of the framework along the principal axis, $\dot{\alpha}$ is the angular velocity of the top relative to the framework, and λ_g are the direction cosine between the symmetry axis of the top and the principal axes of the entire molecule.

The kinetic energy can also be expressed as a function of angular momentum

$$T = \frac{1}{2} \sum_g P_g^2 / I_g + \frac{1}{2} (p - \mathcal{P})^2 / r I_\alpha \quad (2.110)$$

With definitions

$$\begin{aligned} \mathcal{P} &= \sum_g \rho_g P_g, \quad \rho_g = \lambda_g I_\alpha / I_g \\ r &= 1 - \sum_g \lambda_g^2 I_\alpha / I_g \\ P_g &= \partial T / \partial \omega_g = I_g \omega_g + \lambda_g I_\alpha \dot{\alpha} \\ p &= \partial T / \partial \dot{\alpha} = I_\alpha \dot{\alpha} + I_\alpha \sum_g \lambda_g \omega_g \end{aligned} \quad (2.111)$$

Where rI_α is the reduced moment of inertia for internal rotation of the two rigid parts of the molecule, P_g is the total angular momentum of the molecule and p is the total angular momentum of the internal rotor.

Thus the Hamiltonian operator of the overall rotation and internal rotation can be written as

$$H = H_R + H_T + H_{RT} \quad (2.112)$$

With

$$H_R = H_r + F P^2 \quad (2.113)$$

$$H_T = F p^2 + \frac{1}{2} V_3 (1 - \cos 3\alpha) \quad (2.114)$$

$$H_{RT} = -2F P p \quad (2.115)$$

Where $V(\alpha)$ has the form of (2.106), H_r is the rigid rotor Hamiltonian and $F = \hbar^2 r I_\alpha / 2$ is the reduced rotational constant for internal rotation.

In the case of two tops internal rotation system, the Hamiltonian should include the term of top-top interaction, which can be written as

$$H = H_R + H_T + H_{RT} + H_{TT} \quad (2.116)$$

2.6 Evaluation of molecular structure

The structural information from microwave spectroscopy is contained in the principal moments of inertia which derived from the rotational constants, A , B , C . Two types of experimental structure will be discussed in the molecular systems.

r_0 , the effective structure for the ground vibrational state could be calculated from the experimental rotational constants. A least squares fitting procedure has been used to evaluate the r_0 of the studied molecular systems. Several structural parameters could be chosen to fit the differences between experimental and theoretical values of rotational

constants. The procedure of the fitting is based on the linearization of the following equation

$$B_i = B_i^0 + \sum_j (dB_i/dp_j) \Delta p_j \quad (2.117)$$

Where B_i is the i th experimental rotational constant, B_i^0 is the i th rotational constant calculated from the initial assumed structure and p_i is the structural parameter chose for fitting, (dB_i/dp_i) is the changing of B_i^0 with respect to a small changing of p_i while all other structural parameters were kept constant. This procedure is repeated until the convergence has been achieved. However, normally the set of experimental data are not enough to determine the molecular structure completely. Only several bond lengths, valence angles, or valence dihedral angles can be evaluated from the structure fitting and thus only partial r_0 structure can be obtained. For non-covalent interaction bonded molecular complexes, this procedure is adoptable to determine the intermolecular bond length and angles while keeping the geometry of molecular moieties constants.

r_s , the substitution structure, is derived from the isotopic substitutions. Kraitchman^[11] method is applied to calculate the position of an atom in a molecule utilizing the changes of moments of inertia resulting from a single isotopic substitution of the atom. The molecule is assumed rigid so that the bond distances and angles are unchanged due to isotopic substitution. The I_x, I_y, I_z and I'_x, I'_y, I'_z are the moments of inertia along the principal axes for the parent and isotopically substituted molecule. The coordinates are measured from the center of mass principal axis system of the parent molecule. The mass of the isotopic atom can be denoted by $m+\Delta m$, with m the original mass of the atom. The moment of inertia in the parent center of mass principal axis system can be expressed as

$$I'_{xx} = I_x + \Delta m (y^2 + z^2) - (\Delta m y)^2 / (M + \Delta m) - (\Delta m z)^2 / (M + \Delta m) = I_x + \mu (y^2 + z^2) \quad (2.118)$$

Similarly, that

$$I'_{yy} = I_y + \mu (z^2 + x^2) \quad (2.119)$$

$$I'_{zz} = I_z + \mu (x^2 + y^2) \quad (2.120)$$

Where the μ is the reduced mass for the isotopic substitution, $\mu = M \Delta m / (M + \Delta m)$ with M is the total mass of the parent molecule. The I_x, I_y, I_z and I'_x, I'_y, I'_z can be determined experimentally, thus the coordinates $x, y,$ and z of the isotopic substituted atom can be obtained.

2.7 Theoretical calculations

Ab initio and density functional theory (DFT) are used to assist the assignment of the rotational spectra. Geometry optimizations are used to predict the molecular equilibrium structure and conformational preferences from the potential energy surface (PES). The resulting information on rotational constants, dipole moment components, relative stabilized energies and quadrupole coupling constants are helpful indications for searching for rotational spectra and conformational assignment. Since the studied molecular system is not large, high level calculations like MP2/6-311++G(d, p) level theory can be chosen. Frequency calculations are used to calculate the zero point energy and force constants. For molecular complexes, a counterpoise correction^[12] is used to remove the well known basis set superposition error (BSSE). All theoretical calculations are performed with Gaussian03 program package.^[13]

2.8 Experimental techniques

The rotational spectra were measured on Bologna's pulsed-jet molecular beam Fourier transform microwave spectrometer.^[14] The spectrometer has a coaxially oriented beam resonator arrangement (COBRA) and a Fabry-Pérot type resonator.^[15] The spectrometer covers the range 6-18 GHz, follows the guidelines given by Stahl and Grabow^[16-18] and most of the details are taken from the Valladolid spectrometer,^[19] and now operated with the FTMW++ set of programs.^[20] The mirrors are in aluminum with a curvature radius of 60 cm and with 35 cm diameter. The vacuum chamber was built by HVP (Parma, Italy), which is a stainless steel cylinder with a diameter of 40 cm and length of 85 cm. The chamber is evacuated with a 8000 s⁻¹ diffusion pump operated by a block of two Leybold mechanical pumps (D65B and Ruvac WAU 251, rotary and

booster pumps, respectively). The solenoid valve (General Valve, Series 9) is used to generate the supersonic expansion (nozzle diameter 0.5 mm). The frequencies were determined after Fourier transformation of the 8 k data points time domain signal, recorded with 100 ns sample interval. The pulsed nozzle valve is mounted near the centre of one of the mirrors in such a way that the supersonic beam propagates parallel to the resonator axis. In this set-up, all lines appear as enhanced Doppler doublets. The line position is the arithmetic mean of both Doppler components. The estimated accuracy of the frequency measurements is better than 3 kHz, resolution is better than 7 kHz.

It is well known that the supersonic expansion of molecular systems seeded in rare gas is rich in molecules of low rotational temperature. It's stated that normally rotational temperature about 1 K can be reached. Thus supersonic expansion provides significantly sensitivity advantage for transitions originating from low energy rotational levels in the vibrational states. This expansion can be generated by using an electromagnetic valve and provide a sample of high number density. The COBRA can significantly increase the resolution and sensitivity than the orientation that molecular beam is perpendicular to microwave pulsed excitation.

Typically, ~1 percent sample seeded in rare gas at a total pressure in range of 1-3 bars is expanded into a high evacuated resonator chamber. The process is a rapid adiabatic expansion rather than effusive, which cool the molecular systems to very low vibrational temperature and generate molecules traveling along radial path without collision. Thus the transition lines are very narrow and the broadening of transitions is only due to that natural line width, which corresponds to a very high resolution.

The interaction of microwave radiation and the molecular beam results in rotational coherence. The molecular signal power is relative to the fraction of the total energy stored by the field within the resonator volume. Due to the coaxially of the jet expansion and the microwave radiation, the amplitude of the molecular signal is approximated by

$$S_{ab}(t) \propto s' \exp(i (\omega_{ab}-k v_{\infty}) t+\theta_{ab}''')+s'' \exp(i (\omega_{ab}+k v_{\infty}) t+\theta_{ab}''') \quad (2.121)$$

Where ω_{ab} is the angular resonance frequency and $k = \omega/c$ is the wavenumber of the radiation. The Doppler doublet consisting of frequency components at $\nu_{ab} (1 - v_{\infty}/c)$ and $\nu_{ab} (1 + v_{\infty}/c)$ is observed in the frequency domain. The molecular resonance frequency is then recovered as the arithmetic mean of the components separated by $\Delta\nu_{ab} = 2\nu_{ab}v_{\infty}/c$. The line width of the individual components is on the order of 1.5 kHz; at an appreciable S/N ratio, a frequency accuracy of 150 Hz, is achieved for unblended lines. The sensitivity allows for the routine observation of mono-deuterated asymmetric-top molecules in natural abundance.

Reference

- [1] W. Gordy and L. R. Cook, "Microwave Molecular Spectra", 3rd Edition, in Weissberger, A. (ED.), *Techniques of Chemistry*, vol. XVIII, John Wiley & Sons Inc., New York, **1984**.
- [2] C. H. Townes and A. L. Schawlow, "Microwave Spectroscopy", McGraw-Hill, New York, **1955**.
- [3] D. A. McQuarrie, J. D. Simon, *Physical Chemistry: A Molecular Approach*.
- [4] See Ref. 9b and 35 in chapter 1.
- [5] See Ref. 50 in chapter 1.
- [6] J. K. G Watson in "vibrational Spectra and Structure", volume 6. Elsevier, Amsterdam **1977**.
- [7] J. D. Kemp, K. S. Pitzer, *J. Chem. Phys.* **1936**, 4,749.; *J. Am. Chem. Soc.* **1937**, 59, 276.
- [8] E. B. Wilson, Jr., *Chem. Rev.* **1940**, 27, 17.
- [9] B. L. Crawford, *J. Chem. Phys.* **1940**, 8, 273.
- [10] a) H. H. Nielsen, *Phys. Rev.* **1932**, 40, 445. b) J. S. Kohler, D. M. Dennison, *Phys. Rev.* **1940**, 57, 106.
- [11] J. Kraitchman, *Am. J. Phys.* **1953**, 21, 17 .
- [12] S. F. Boys, F. Bernardi, *Mol. Phys.* **1970**, 19, 553.
- [13] M. J. Frisch, G. W. Trucks, H. B. Schlegel, G. E. Scuseria, M. A. Robb, J. R. Cheeseman, J. A. Montgomery, Jr., T. Vreven, K. N. Kudin, J. C. Burant, J. M. Millam, S. S. Iyengar, J. Tomasi, V. Barone, B. Mennucci, M. Cossi, G. Scalmani, N. Rega, G. A. Petersson, H. Nakatsuji, M. Hada, M. Ehara, K. Toyota, R. Fukuda, J. Hasegawa, M. Ishida, T. Nakajima, Y. Honda, O. Kitao, H. Nakai, M. Klene, X. Li, J. E. Knox, H. P. Hratchian, J. B. Cross, C. Adamo, J. Jaramillo, R. Gomperts, R. E. Stratmann, O. Yazyev, A. J. Austin, R. Cammi, C. Pomelli, J. W. Ochterski, P. Y. Ayala, K. Morokuma, G. A. Voth, P. Salvador, J. J. Dannenberg, V. G. Zakrzewski, S. Dapprich, A. D. Daniels, M. C. Strain, O. Farkas, D. K. Malick, A. D. Rabuck, K. Raghavachari, J. B. Foresman, J. V. Ortiz, Q. Cui, A. G. Baboul, S. Clifford, J. Cioslowski, B. B. Stefanov, G. Liu, A. Liashenko, P.

Piskorz, I. Komaromi, R. L. Martin, D. J. Fox, T. Keith, M. A. Al-Laham, C. Y. Peng, A. Nanayakkara, M. Challacombe, P. M. W. Gill, B. Johnson, W. Chen, M. W. Wong, C. Gonzalez and J. A. Pople, Gaussian 03, Revision B.01, Gaussian, Inc., Pittsburgh PA, **2003**.

[14] See Ref. 73 in chapter 1.

[15] T. J. Balle, W. H. Flygare, *Rev. Sci. Instrum.* **1981**, 52, 33.

[16] J.-U. Grabow, W. Stahl, *Z. Naturforsch.* **1990**, 45a, 1043.

[17] a)see ref. 73 in chapter 1. b) J.-U. Grabow, W. Stahl, H. Dreizler, *Rev. Sci. Instrum.* **1996**, 67, 4072.

[18] J.-U. Grabow, Ph.D Thesis, Kiel University, Germany, **1992**.

[19] J. L. Alonso, F. J. Lorenzo, J. C. Lopez, A. Lesarri, S. Mata, H. Dreizler, *Chem. Phys.* **1997**, 218, 267.

[20] J.-U. Grabow, Habilitationsschrift, Universität Hannover, Hannover, **2004**. <http://www.pci.uni-hannover.de/Blgpca/spectroscopy/ftmwi>.

Chapter 3 Conformation and internal rotation: microwave spectroscopic studies on dimethyl sulfate

3.1 Introduction

Dimethyl sulfate (DMS) is widely used as a methylating reagent to convert compounds such as amines, phenols, and thiols to the corresponding methyl derivatives. It is also used in the manufacture of methyl esters, ethers, and amines in dyes, drugs, perfumes, pesticides, phenol derivatives, and other organic chemicals. As a solvent, it is important for the separation of mineral oils and for the analysis of auto fluids and as a component of polyurethane based adhesives. Formerly, dimethyl sulfate was used as a war gas.^[1, 2] However, despite its essential use in fundamental chemistry, only little spectroscopic information is available. This lack of spectroscopic data on DMS is probably related to the following reasons: (a) DMS is highly toxic to human and reasonably a human carcinogen; (b) although stable at room temperature, the compound rapidly hydrolyzes in water; (c) when heated, it produces toxic fumes including sulfur oxides and sulfuric acid; (d) until some years ago, the theoretical computations of compounds containing sulfur and oxygen atoms were expensive. As a result, the peculiarity of the sulfur-to-oxygen linkages is not yet completely explored. The structure of DMS has been the subject of just one electron diffraction (ED) study^[3] and two FT-IR investigations.^[4, 5] However, the composition of the conformational mixture is still controversial. Brunvoll *et al.*^[3] interpreted the ED diffraction curve of DMS as a mixture of the C_2 and C_{2v} rotamers; later, Fausto *et al.*^[4, 5] suggested the coexistence of a C_2 symmetry conformer with a less stable C_1 symmetry species; the latter one quickly converts to the C_2 one in matrix isolation.^[5]

DMS could also represent a system to investigate the anomeric effect^[6], similarly to dimethoxymethane.^[7, 8] The anomeric effect generally involves the donation of electron density from a lone pair on one oxygen atom to the adjacent carbon-oxygen bond. Such interaction, believed to be the result of $n-s^*$ overlap, reaches its maximum value when the -O-S-O-C torsional angle is at 90° and is excluded in case of a planar arrangement. Moreover, the MW study would allow observing the effect of the electron

pair repulsion on the structure and on the V_3 barrier of the methyl groups. For this reasons, the molecular properties of DMS, both theoretically and by rotational spectroscopy, were studied.

3.2 Experimental details

A commercial sample of DMS bought from Aldrich was used without further purification. The spectra of the isotopic ^{13}C -, ^{18}O - and ^{34}S -containing species were measured in natural abundance.

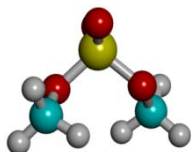
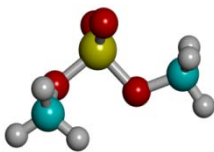
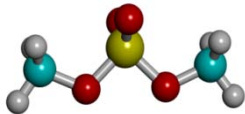
The carrier gas Helium was passed over the DMS at room temperature, at a backing pressure of about 0.2 MPa, and expanded through the pulsed valve into the Fabry–Perot cavity to generate the supersonic expansion.

3.3 Theoretical calculations

In order to obtain the structural and energetic properties of the plausible conformations of DMS, *ab initio* calculations were first performed before searching for the rotational spectra. The computational methods were selected to provide their equilibrium geometries, the rotational constants, the dipole moment components along the principal axes and the relative energies. The nature of all stationary points was verified by subsequent harmonic frequency calculation and also quartic centrifugal distortion constants were calculated from the harmonic force field. All *ab initio* quantum chemical calculations were performed at MP2/6-311++G(d, p) level using the GAUSSIAN03 software package.^[12] Three energy minima, with C_2 , C_1 and C_{2v} symmetry, respectively, were shown in **Table 3.1**. Zero point corrected energy has been also calculated. All the obtained parameters are collected in **Table 3.1**. The relatively small energy difference between the first two conformers appears as promising for the observation of both species. This is supported by the experimental observation of the two stable conformers in previous works.^[5] However, conformational relaxation within supersonic expansions has been often observed when the barriers connecting minima

are of the order of $2kT$.^[13] The potential curve for the interconversion between the predicted conformers is additionally calculated to investigate the possibility of conformational relaxation. The potential energy pathway describing the internal rotation around the S1-O5 bond (corresponding to the O4-S1-O5-C10 dihedral angle, see **Figure 3.1** for labeling), which interconverts conformers C_2 and C_1 , was calculated *ab initio* and is plotted in **Figure 3.2**. The *ab initio* scan was carried out in steps of 5° over the full range of the O4-S1-O5-C10 dihedral angle of the main chain frame. While the dihedral angle was kept fixed at every step, all other geometric parameters were re-optimized for each point along the path. The potential energy function proved that a conformational relaxation is plausible according to the relatively low barrier (ca. 340 cm^{-1}).

Table 3.1 Ab initio spectroscopic parameters of the three most stable conformers of DMS, obtained at MP2/6-311++G(d, p) level of theory.

	C_2	C_1	C_{2v}
			
$A, B, C/\text{MHz}$	3029.2, 2251.6, 1809.6	3297.8, 2079.2, 1754.8	4442.1, 1717.3, 1673.3
$\mu_a, \mu_b, \mu_c/\text{D}$	0.0, 4.2, 0.0	-0.06, -3.8, -0.09	0.0, -1.1, 0.0
$D_J, D_{JK}, D_K/\text{kHz}$	1.11, 7.43, -4.99,	0.43, -0.72, 1.47,	0.13, 0.70, 2.13,
$d_1, d_2/\text{kHz}$	-0.46, 0.002	-0.03, 0.10	-0.002, 0.01
$\Delta E, \Delta E_0/\text{cm}^{-1}$	0 ^a , 0 ^b	297, 290	1267, 1254
V_3/cm^{-1}	447		

^a Absolute energy: $-777.467111 E_h$, ^b Absolute energy: $-777.370024 E_h$

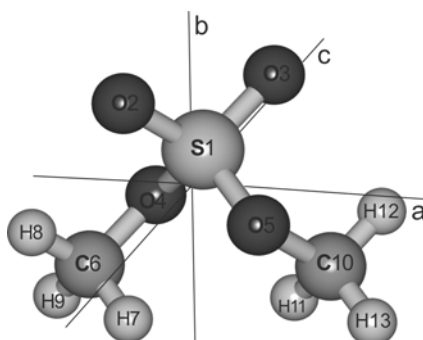


Figure 3.1 Shape and atom numbering of the C_2 form of dimethyl sulfate.

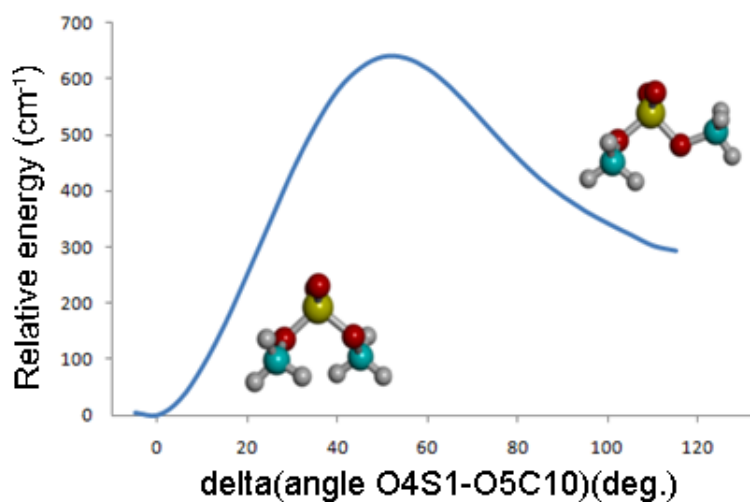


Figure 3.2 Potential energy function (MP2/6-311++G(d, p)) for the interconversion between the C_2 (most stable) and C_1 forms of the dimethyl sulfate.

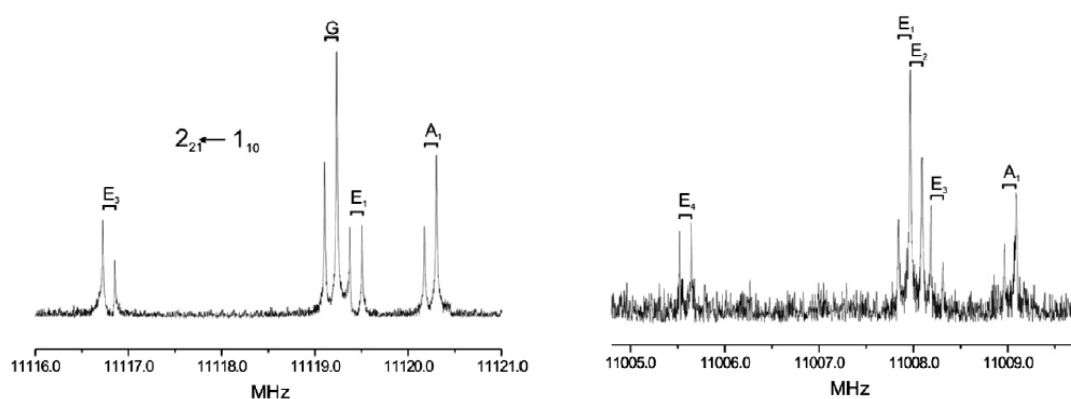


Figure 3.3 The internal rotation quartet (left) or quintet (right) patterns of the $2_{2,1} \leftarrow 1_{1,0}$ transition for normal and mono- ^{13}C species of dimethyl sulfate (see text), respectively.

3.4 Results and analysis

3.4.1 Rotational spectra

The results of the theoretical calculations (see **Table 3.1**) and previously experimental measurements consistently predicted the C_2 form to be more stable, so that the initial survey scans targeted this conformation. Due to its symmetry only μ_b -type dipole moment component is non-zero so the assignment of the rotational transitions

initiated where the lowest $J\mu_b$ transition, $2_{1,2} \leftarrow 1_{0,1}$, was predicted. After the observation of this line, many more transition, with J up to 7, were assigned and measured. No lines due to μ_a and μ_c dipole moment components have been observed and this is in agreement with the expected symmetry. All transitions appear as quartets, according to the effect expected for the hindered internal rotation of two equivalent methyl groups. The pattern is shown in **Figure 3.3**–left for the $2_{2,1} \leftarrow 1_{1,0}$ transition. The experimental measurements for the C_2 parent specie were immediately extended to other mono-substituted species in natural abundance, after a preliminary structure adjustment. The mono-substituted species DMS (^{13}C) or DMS (^{18}O) have a reduced symmetry. As a consequence, their rotational transitions are split into five components labeled, according to the values of the torsional symmetry numbers σ_1 and σ_2 , as 00, 01, 10, 11 and 12 (or 00, 01, 10, 11 and 1–1 within the scheme of program XIAM^[14], described below). Such a quintet is shown in **Figure 3.3**–right for the $2_{2,1} \leftarrow 1_{1,0}$ transition. In the parent specie, with equivalent rotors, the components 01 and 10 are degenerate. Also notations based on the symmetry classification of the torsional wavefunctions have been used. The rotational–torsional energy levels of the normal DMS and monosubstituted DMS (^{34}S) relate to the molecular symmetry (MS) group $G36$, and their torsional wavefunctions are symmetry classified as A , G , E_1 and E_3 . Due to the modified molecular symmetry, the roto-torsional energy levels of the others singly substituted species relate to MS group $G18$ and their torsional wavefunctions are symmetry classified as A , E_1 , E_2 , E_4 and E_3 .^[15–17] The intensities of the lines of the mono-substituted species DMS (^{13}C) or DMS (^{18}O) were about 2% and 0.4% that of the normal species, showing that the carbon and oxygen atoms in the molecule constitute pairs of equivalent atoms, according to the C_2 symmetry. Also the rotational spectrum of DMS (^{34}S) was assigned and its transitions have ca. 4.3% intensity of those of the parent species. The complex rotational spectra of molecules with two methyl rotors have been analyzed in the past with different model Hamiltonians^[14,18,19] and recently comparisons among the various methods have been made.^[20–23] In the present case all components lines of each isotopologues were fitted with two different methods, both referred to Watson’s A reduction and I' representation.^[24] The first fit was done using XIAM program (based on the combined axis method, CAM^[14]), whereas the second fit was performed using ERHAM program, which fits an effective rotational Hamiltonian.^[18] Both programs allow fitting all kind of component lines simultaneously. The results are reported in **Tables 3.2** and **3.3** for the XIAM and ERHAM fits, respectively. It is interesting to note that both program determine the

angles ($\angle(a, i)$, $\angle(b, i)$, $\angle(c, i)$) that the internal rotation axis i of the methyl tops forms with the principal axis of inertia (a, b, c); the values obtained with the two methods are in a good agreement. However, ERHAM requires some expertise in choosing the best set of parameters to be fitted, because the internal rotation is treated by a Fourier expansion and the resulting numerical values are not easily interpretable. It is established that the ERHAM method reproduces high frequency rotational spectra with extremely accuracy,^[21, 25] while XIAM supply parameters with a clear physical meaning. The XIAM experimental value of V_3 (395.5 cm^{-1}) is in good agreement with 447 cm^{-1} calculated at the MP2/6-311++G(d, p) level. ERHAM does not provide directly the value of V_3 . However, the internal rotational parameters were used together with its tunneling energy parameters in the Meyer's flexible model described earlier^[26] to determine the leading terms of the torsion potential function. The V_3 term of the potential energy function, 394.5 cm^{-1} for the parent species, agrees with the experimental value obtained with the XIAM program. The missing of experimental signals for the C_1 species confirms the conformational relaxation predicted in the *ab initio* calculations section.

3.4.2 Molecular structure

To obtain the molecular structure, the absolute atomic substitution coordinates for the heavy atom skeleton were calculated first by using the Kraitchman equations and uncertainties estimated according to Constain's rule ($\delta z = K/|z|$, $K = 0.15 \text{ \AA}$).^[27,28] Both r_s and theoretical (in principle r_e) structures are reported in **Table 3.4**.

The sign of the r_s atomic coordinates was inferred by the comparison with the theoretical values. O2, O4 and C6 are equal by symmetry to O3, O5 and C10, respectively. The S1 atom lies in the b -axis and it is very close to the a - and c -axes, yielding unphysical imaginary coordinates upon isotopic substitution. Additionally, an effective structure was calculated by a least-squares fit of the 15 rotational constants to a set of 8 structural parameters (three bond lengths, three valence angles and 2 dihedral angles) defining the positions of the heavy atoms in the molecule.^[29] The others parameters were fixed to the *ab initio* structure reported in **Table 3.5**. The effective structure satisfactorily reproduces the A , B and C rotational constants for

Table 3.2. Experimental spectroscopic constants of the observed isotopologues of DMS (*A*-reduction, *F* representation) obtained with the Xiam program.

	Parent	³⁴ S	¹³ C	¹⁸ O-CH ₃	¹⁸ O=S	
<i>A</i> /MHz	3090.2959(3) ^a	3081.350(3)	3064.567(1)	3058.424(2)	3006.396(1)	
<i>B</i> /MHz	2317.9391(2)	2317.9951(5)	2278.8418(7)	2287.212(1)	2286.2842(5)	
<i>C</i> /MHz	1848.8522(2)	1845.6380(3)	1814.8471(4)	1834.1250(5)	1822.5994(5)	
<i>A</i> _{<i>j</i>} /kHz	1.183(7)	1.15(2)	1.15(1)	1.12(3)	1.14(2)	
<i>A</i> _{<i>JK</i>} /kHz	-5.238(4)	-4.6(3)	-4.8(3)	-4.6(4)	-5.0(2)	
<i>A</i> _{<i>K</i>} /kHz	7.535(5)	7.3(2)	7.1(3)	6.8(5)	7.0(2)	
<i>δ</i> _{<i>j</i>} /kHz	0.4876(5)	[0.4876] ^b	[0.4876] ^b	[0.4876] ^b	[0.4876] ^b	
<i>δ</i> _{<i>K</i>} /kHz	-0.105(3)	[-0.105] ^b	[-0.105] ^b	[-0.105] ^b	[-0.105] ^b	
			¹³ C	¹² C	¹⁸ O	¹⁶ O
<i>V</i> ₃ /kJmol ⁻¹	4.731(6)	4.732(1)	4.740(5)	4.733(5)	4.740(5)	4.799(1)
<i>I</i> _{<i>a</i>} /uÅ ²	3.233(4)	[3.233] ^b	[3.233] ^b	[3.233] ^b	[3.233] ^b	[3.233] ^b
∠(<i>a</i> , <i>i</i>)/deg	46.396(9)	46.38(3)	44.5(2)	132.0(1)	46.7(2)	46.03(5)
∠(<i>b</i> , <i>i</i>)/deg	57.25(1)	57.28(5)	59.6(3)	55.6(3)	57.0(4)	55.9(1)
∠(<i>c</i> , <i>i</i>)/deg	61.29(1)	61.32(5)	61.1(3)	118.8(3)	61.2(4)	61.8(1)
<i>N</i> ^c	131	31	36	30	30	37
<i>σ</i> ^d /kHz	1.7	2.0	2.0	3.4	3.4	2.0

^aError in parentheses in units of the last digit. ^bFixed to the value of the parent species. ^cNumber of lines in the fit. ^dRoot-mean-square deviation of the fit.

Table 3.3. Experimental spectroscopic constants of the observed isotopologues of DMS (A-reduction, I' representation) obtained with the Erham program.

	Parent	^{34}S			^{13}C			$^{18}\text{O-CH}_3$			$^{18}\text{O-S}$		
A/MHz	3090.2958(1) ^a	3081.3468(2)	3064.5668(7)	3058.423(1)	3006.3960(5)								
B/MHz	2317.9282(1)	2317.9853(2)	2278.8311(6)	2287.202(1)	2286.2740(3)								
C/MHz	1848.8632(1)	1845.6491(1)	1814.8578(4)	1834.1353(6)	1822.6097(4)								
A_J/kHz	1.187(5)	[1.187] ^b	1.16(2)	1.16(4)	1.14(1)								
A_{JK}/kHz	-5.238(3)	[-5.238] ^b	-4.8(3)	-4.9(5)	-4.9(1)								
A_K/kHz	7.532(4)	[7.532] ^b	7.1(3)	7.1(5)	6.9(2)								
δ_J/kHz	0.4867(4)	[0.4867] ^b	[0.4867] ^b	[0.4867] ^b	[0.486] ^b								
δ_K/kHz	-0.104(2)	[-0.104] ^b	[-0.104] ^b	[-0.104] ^b	[-0.104] ^b								
			^{13}C	^{12}C	$\text{CH}_3\text{-}^{18}\text{O}$	$\text{CH}_3\text{-}^{16}\text{O}$	$\text{CH}_3\text{-}^{18}\text{O}$	$\text{CH}_3\text{-}^{16}\text{O}$	Top closes to ^{18}O	^{18}O	Top closes to ^{16}O		
qq^c			01	10	01	10	01	10	01	01	10		
$\varepsilon_{\text{qd}}/\text{MHz}^d$	-102.5(1)	-102.8(2)	-102.6(3)	-102.8(2)	-100.1(7)	-103.9(7)	-100.6(4)	-103.9(7)	-100.6(4)	-100.6(4)	-104.1(3)		
B_{020}/kHz^e	-0.72(14)	[-0.72] ^b	[-0.72] ^b	[-0.72] ^b	[-0.72] ^b	[-0.72] ^b	[-0.72] ^b	[-0.72] ^b	[-0.72] ^b	[-0.72] ^b	[-0.72] ^b		
$I_a/\text{u}\text{\AA}^2$	3.228(3)	3.220(6)	3.220(8)	3.1219(8)	3.22(2)	3.122(2)	3.22(2)	3.122(2)	3.31(2)	3.31(2)	3.15(1)		
$\angle(a, i)/\text{deg}$	46.410(2)	46.43(2)	44.5(2)	131.9(1)	47.3(3)	133.4(2)	47.3(3)	133.4(2)	46.74(6)	46.74(6)	134.9(1)		
$\angle(b, i)/\text{deg}$	57.224(2)	57.20(2)	59.5(3)	55.47(8)	55.9(4)	58.53(8)	55.9(4)	58.53(8)	56.4(1)	56.4(1)	58.12(5)		
$\angle(c, i)/\text{deg}$	61.237(1)	61.25(1)	61.0(1)	118.84(8)	61.6(2)	120.3(2)	61.6(2)	120.3(2)	61.73(5)	61.73(5)	118.1(1)		
N^f	131	31	36	36	30	30	30	30	37	37	37		
σ^g/kHz	1.8	2.7	1.7	1.7	1.4	1.4	1.4	1.4	1.9	1.9	1.9		

^aError in parentheses in units of the last digit. ^bFixed to the value of the parent species. ^cLabels used to identify the localized state to which a tunneling parameter is related. ^dEnergy tunneling parameter. ^eRotational constant tunnelling parameter $[A-(B+C)/2]_{\text{qd}}$. ^fNumber of lines in the fit. ^gRoot-mean-square

Table 3.4 Substitution and *ab-initio* coordinates of the DMS skeleton.

	S		O2		O4		C6	
	r_s	Calc.	r_s	Calc.	r_s	Calc.	r_s	Calc.
$ a /\text{\AA}$	0.03299*i	0.000	0.752(2)	-0.756	0.922(2)	-0.926	1.9149(8)	-1.919
$ b /\text{\AA}$	0.493(3) ^a	-0.499	1.172(1)	-1.174	0.498(3)	0.497	1.216(1)	1.214
$ c /\text{\AA}$	0.04057*i	0.000	0.990(2)	0.989	0.796(2)	-0.795	0.06604*i	-0.025

^a Error in parenthesis in the units of the last digit.

Table 3.5 MP2/6-311++G(d, p) calculated molecular structure of DMS.

Bond lengths/\AA		Valence angles/°		Dihedral angles/°	
O2S1	1.403				
O3S1	1.403	O3S1O2	123.9		
O4S1	1.592	O4S1O2	109.6	O4S1O2O3	-124.9
O5S1	1.592	O5S1O3	109.6	O5S1O3O2	-124.9
C6O4	1.446	C6O4S1	115.9	C6O4S1O5	71.8
H7C6	1.092	H7C6O4	110.3	H7C6O4S1	-57.0
H8C6	1.090	H8C6O4	110.1	H8C6O4H7	122.0
H9C6	1.088	H9C6O4	104.6	H9C6O4H7	-118.8
C10O5	1.446	C10O5S1	115.9	C10O5S1O4	71.8
H11C10	1.092	H11C10O5	110.3	H11C10O5S1	-57.0
H12C10	1.090	H12C10O5	110.1	H12C10O5H11	122.0
H13C10	1.088	H13C10O5	104.6	H13C10O5H11	-118.8

all isotopologues within 100 kHz. The substitution (r_s), effective (r_0) and equilibrium (r_e) structure are compared in **Table 3.6**. The consistency among the three structures is relatively good despite their different operational definitions. The fact that only μ_b -type transitions were observed confirms that the molecule does have C_2 symmetry. Its C_2 symmetry form, which is the less elongated one, is favored, similarly to dimethoxymethane, by the anomeric effect [see Refs. 6-8]. The relative stability of the three conformers C_2 , C_1 and C_{2v} is confirmed by NBO analyses.^[30] The hyperconjugative interactions have been calculated into the E_2 (stabilization energies). A decrease in the value of the GAE (generalized anomeric effect) in going from the C_2 to the C_{2v} and to the C_1 conformer according to the following values was found: $E_2(C_2)$

= 1227.3 kJmol⁻¹, $E_2(C_{2v}) = 1225.7$ kJmol⁻¹ and $E_2(C_1) = 1221.9$ kJmol⁻¹, respectively. This is an evidence of the anomeric stabilization in agreement with the experimental observation. The distance along the series C_2 , C_1 and C_{2v} between the methoxy oxygen lone electron pairs of the two methoxy oxygen atoms decreases along the series C_2 , C_1 and C_{2v} (2.534, 2.514 and 2.499 Å in the r_e structure). In the C_1 and C_{2v} conformers the methyl groups close to the S=O bonds hinder the opening of the O-S-O angle. Other non bonding parameters of interest are the weak hydrogen bond lengths C-H...O (between the methyl hydrogens and both S-O and S=O type oxygen atoms). As in DMM, such a kind of distance is in the range 2.5-2.7 Å, typical of this weak interaction.^[31] The increase of the stability, due to the shortening of the distance from DMS to DMM, is reflected in the increasing of the methyl group V_3 barriers. In fact these interactions and their relatively influences modify the shape of the potential energy function of the hindered motions.^[22,32]

Table 3.6 Experimental (r_s and r_0) and theoretical (r_e , MP2/6-311++G(d, p)) structural parameters of DMS (C_2 symmetry).

	Bond distances/Å			Valence and dihedral angles/°			
	r_s^a	r_0	r_e	r_s^a	r_0	r_e	
S1O2	1.417(2)	1.416(2)	1.436	O2S1O3	122.8(3)	123.1(3)	123.9
S1O4	1.570(3)	1.575(3)	1.612	O4S1O2	110.2(3)	109.9(1)	109.6
O4C6	1.461(2)	1.447(3)	1.446	C6O4S1	115.7(3)	116.6(2)	115.9
C6H8			1.090	O4S1O5	101.7(2)	101.6 ^b	101.3
C6H7			1.093	O4S1O2O3	124.5	124.7(2)	125.0
C6H9			1.088	C6O4S1O5	71.8	72.1(3)	72.8
O4H11		2.692 ^b	2.716	C6O4S1O2	39.2	38.9 ^b	37.9

^a Calculated by fixing to zero the $|a|$ and $|c|$ values of S and the $|c|$ values of C6 and C10. ^b Derived parameters.

3.5 Conclusions

The rotational spectra of the most stable (C_2) conformer of DMS and of all the heavy atoms isotopologues have been assigned. It has then been possible to determine

the experimental structure of the heavy atoms skeleton. Information on the internal dynamics of the two methyl groups was also obtained. The analysis of the spectra has been performed following two different approaches, which led to very similar spectroscopic and structural values, by using XIAM and ERHAM programs. The failure in observing other forms can be due to their higher energies and conformational relaxation process upon supersonic expansion,^[13] in accord with the potential energy curve shown in **Figure 3.2**. The anomeric effect and the C-H \cdots O interactions seem to play an important role in stabilizing the observed conformer.

References

- [1] Du Pont, Dimethyl Sulfate Properties, Uses, Storage and Handling, E.I. Du Pont de Nemours & Co. Inc., Wilmington, Delaware, **1981**, p. 24.
- [2] National Institute for Occupational Safety and Health (NIOSH), Information Profiles on Potential Occupational Hazards. I. Single Chemicals I. Dimethyl Sulfate, NIOSH, Rockville, MD, **1979**, p. 9.
- [3] J. Brunvoll, O. Exner, I. Hargittai, *J. Mol. Struct.* **1981**, 73, 99.
- [4] A. B. Remizov, A. I. Fishman, I. S. Pominov, *Spectrochim. Acta* **1979**, 35A, 909.
- [5] A. Borha, A. Gomez-Zavaglia, P. N. N. L. Simoes, R. Fausto, *Spectrochim. Acta A* **2005**, 61, 1461.
- [6] Anomeric effect, see for example: N. L. Allinger, *Molecular Structure: Understanding Steric and Electronic Effects from Molecular Mechanics*, Wiley, Hoboken, New Jersey, **2010**.
- [7] L. B. Favero, W. Caminati, B. Velino, *Phys. Chem. Chem. Phys.* **2003**, 5, 4776.
- [8] R. J. Gillespie, E. A. Robinson, G. Pilme, *Chem. Eur. J.* **2010**, 16, 3663.
- [9] See Ref. 15 in chapter 2.
- [10] See Ref. 16 in chapter 2.
- [11] See Ref. 73 in chapter 1.
- [12] See Ref. 13 in chapter 2.
- [13] See for example: R. S. Ruoff, T. D. Klots, T. Emilson, H. S. Gutowski, *J. Chem. Phys.* **1990**, 93, 3142.
- [14] H. Hartwig, H. Dreizler, *Z. Naturforsch.* **1996**, 51a, 923.

- [15] H. C. Longuet-Higgins, *Mol. Phys.* **1963**, *6*, 445.
- [16] P. R. Bunker, P. Jensen, in: *Molecular Symmetry and Spectroscopy*, 2nd ed., NRC Research Press, Ottawa, **1998**, p. 515.
- [17] M. Schnell, J.-U. Grabow, H. Hartwig, N. Heineking, M. Meyer, W. Stahl, W. Caminati, *J. Mol. Spectrosc.* **2005**, *229*, 1.
- [18] P. J. Groner, *Chem. Phys.* **1997**, *107*, 4483.
- [19] I. Kleiner, *J. Mol. Spectrosc.* **2010**, *260*, 1.
- [20] D. Gerhard, A. Hellweg, I. Merke, W. Stahl, M. Baudelet, D. Petitprez, G. Włodarczyk, *J. Mol. Spectrosc.* **2003**, *220*, 234.
- [21] Z. Kisiel, L. Pszczołkowski, E. Białkowska-Jaworska, S. B. Charnley, *J. Mol. Spectrosc.* **2007**, *241*, 220.
- [22] B. Ouyang, B. J. Howard, *Phys. Chem. Chem. Phys.* **2009**, *11*, 366.
- [23] L. Evangelisti, L. B. Favero, A. Maris, S. Melandri, A. Vega-Toribio, A. Lesarri, W. Caminati, *J. Mol. Spectrosc.* **2010**, *259*, 65.
- [24] See Ref. 6 in chapter 2.
- [25] P. Groner, S. Albert, E. Herbst, F. C. De Lucia, F. J. Lovas, B. J. Drouin, J. C. Pearson, *Astrophys. J. Suppl. Ser.* **2002**, *142*, 145.
- [26] R. Meyer, *J. Mol. Spectrosc.* **1979**, *76*, 266.
- [27] See Ref. 11 in chapter 2.
- [28] C. C. Constain, *Trans. Am. Crystallogr. Assoc.* **1966**, *2*, 157.
- [29] Z. Kisiel, *J. Mol. Spectrosc.* **2003**, *218*, 58.
- [30] E. D. Glendenning, A. E. Reed, J. E. Carpenter, F. Weinhold, Link 607 to Gaussian03 (Ref. [12]): NBO Version 3.1.
- [31] G. A. Jeffrey, *An Introduction to Hydrogen Bonding*, Oxford University Press, Oxford, **1997**.
- [32] L. B. Favero, L. Evangelisti, A. Maris, A. Vega-Toribio, A. Lesarri, W. Caminati, *J. Phys. Chem. A* **2011**, *115*, 9493.

Chapter 4 Proton transfer in homodimers of carboxylic acids. The rotational spectrum of the dimer of acrylic acid

4.1 Introduction

Pairs of carboxyl groups bind cooperatively together, since both units act as proton donor and acceptor, forming a large eight-membered ring containing two hydrogen bonds. Such a kind of hydrogen bonding is the strongest one found within neutral species, with the monomers held together by more than 60 kJmol^{-1} . Gilli suggested explaining such a “strong” interaction in terms of a resonance assisted hydrogen bond model.^[1]

Another interesting feature of these bi-molecules is that the concerted double transfer of the protons corresponds to a motion with a double minimum potential (**Figure 4.1**), which can generate tunneling doubling within spectroscopic studies, useful to determine the barrier to the proton transfer.

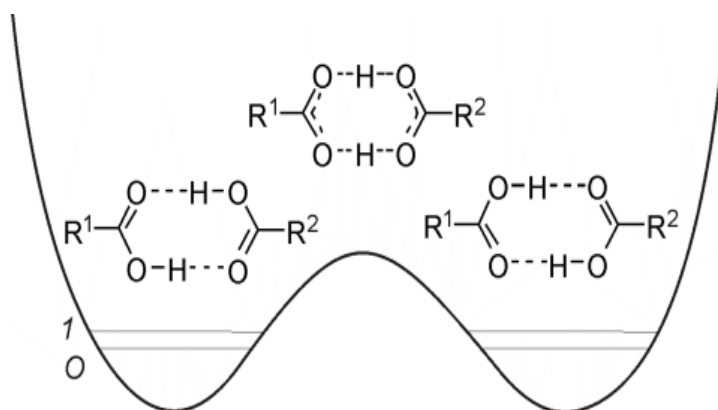


Figure 4.1 Proton tunneling and potential energy function to the proton transfer in carboxylic acid bi-molecules.

At a first sight, homodimers do not possess a dipole moment, so that they cannot be studied by microwave spectroscopy (MW).

However, admirable spectroscopic results have been obtained so far on the homodimers of carboxylic acids with other high resolution techniques. Among them, a rotationally resolved laser-induced fluorescence (LIF) investigation of the dimer of benzoic acid^[2] allowed for the tunnelling effects to be measured.

LIF generally requires a chromophore, so that the homodimers of simpler carboxylic acids have been investigated with other high-resolution methods such as femtosecond degenerate four-wave mixing and Raman spectroscopy.

These methods supplied information, such as tunnelling splittings in the ground and vibrationally excited states, on formic acid^[3-9] and acetic acid^[10] homo-dimers.

This kind of complex has been investigated also by MW spectroscopy. Carboxylic acid dimers were early observed with low resolution MW spectroscopic methods by Costain in 1961^[11] and Bellot and Wilson in 1975.^[12] Then Bauder and coworkers provided detailed supersonic-jet FTMW analyses for some carboxylic acid bi-molecules: the structures of $\text{CF}_3\text{COOH}\cdots\text{HCOOH}$ and $\text{CF}_3\text{COOH}\cdots\text{CH}_3\text{COOH}$ have been determined through the analyses of the rotational spectra of several isotopologues.^[13] For the latter complex, also the V_3 barrier to internal rotation of the methyl group was determined. Antolinez *et al.* reported the MW spectrum of the trifluoroacetic acid-cyclopropanecarboxylic acid bi-molecule.^[14] In none of these cases, doubling of the rotational transitions attributable to a double proton transfer tunnelling is observed. The proton transfer would have required, indeed, a simultaneous internal rotation of the heavy CF_3 top to reach an equivalent potential energy minimum. The resulting small reduced constants of the motion quench the tunneling effects.

Only recently, doubling related to the proton transfer have been observed on the FTMW spectrum of the formic acid-propionic acid dimer,^[15] but it was soon realized that the spectral assignment was wrong. Precise proton tunneling data have been reported one year later, following a broad band FTMW investigation.^[16]

In 2011, Howard and collaborators published the results of their investigation on the formic acid-acetic acid bi-molecule.^[17] There, the double proton transfer motion is coupled – in order to reach an equivalent minimum - with a 60° internal rotation of the methyl group. The problem is similar to that encountered in the case of proton transfer in methylmalonaldehyde.^[18] Howard conducted a superb analysis of the two dimensional problem, but its complexity made it difficult to obtain from the determined splittings a precise and unique value of the barrier to the proton transfer.

In case of dimers without additional motion with respect to the coupled proton transfer, it would be more direct to estimate the potential energy surface.

In their paper, Howard and collaborators claim that “only hetero dimers can be studied by microwave spectroscopy”.^[17] Actually, there are at least three cases in which homo-dimers of carboxylic acids can give a rotational spectrum: (i) homodimers with a dipole moment induced by asymmetric isotopic substitution, as observed so far only for monomers, such as in the case of benzene-*d*1;^[19] (ii) homodimers of homochiral carboxylic acids; (iii) homodimers of different conformers of the same carboxylic acid.

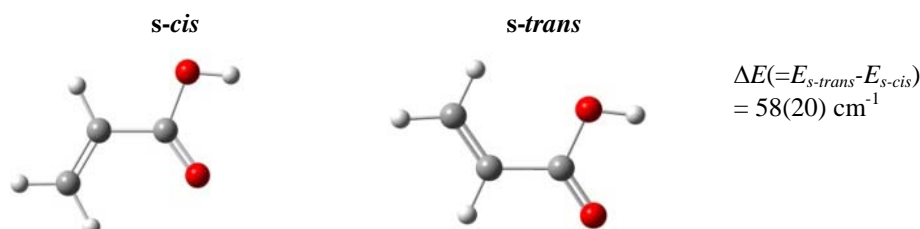


Figure 4.2 The two stable conformers of acrylic acid.

In this chapter, the case (iii) is considered, in relation to the dimer of acrylic acid (AA). AA has been investigated by MW spectroscopy, and the rotational spectra of two almost isoenergetic forms, shown in **Figure 4.2**, have been assigned.^[20] The dimerization of acrylic acid produces four different bi-molecules, as shown in **Figure 4.3**. They can be divided in two pairs, where the two forms are converted each other through a double proton exchange. The pair *cis*···*cis*/*trans*···*trans* is made of two different non-polar conformers, with different energies. The pair *cis*···*trans*/*trans*···*cis* is made of two equivalent polar conformers, with the same energies. For this form it is then possible to measure the rotational spectrum and tunnelling effects are expected.

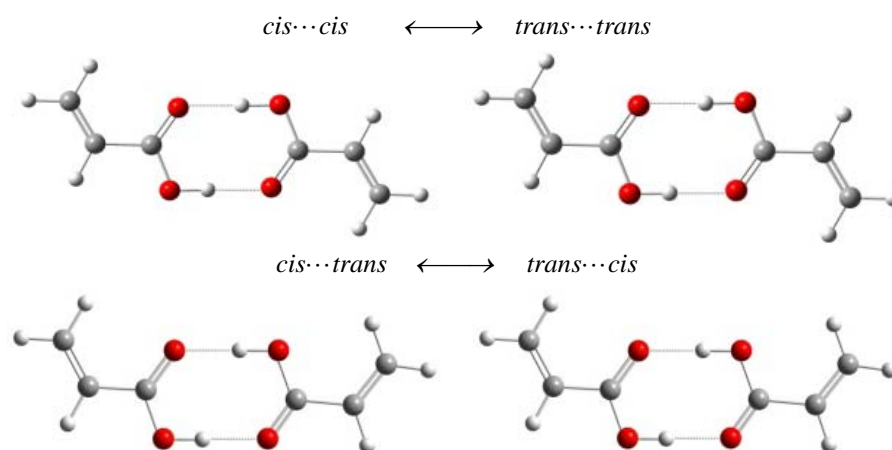


Figure 4.3 Homo-conformational dimers of AA (*s-cis*...*s-cis*, *s-trans*...*s-trans*) are non-polar, while hetero-conformational dimers (*s-cis*...*s-trans*, *s-trans*...*s-cis*) are polar molecules.

4.2 Experimental details

The spectra were recorded with the Fourier transform Bologna spectrometer (6–18.5 GHz), described detail in reference [21] and also in chapter 2.

A commercial sample of acrylic acid was supplied by Aldrich and used without further purification. A gas mixture of approximately 2% of acrylic acid in Helium at a total pressure of 3×10^5 Pa was expanded through the solenoid valve (General Valve, Series 9, nozzle diameter 0.5 mm) into the Fabry-Pérot cavity.

4.3 Theoretical calculations

Before searching for the spectrum, we performed B3LYP/6-311++G(d, p) theoretical calculations^[22] to estimate the relative energies of the dimers and of the transition state and to predict the values of the spectroscopic parameters. The shapes of the four conformers are shown in **Figure 4.3**, while the numerical results are reported in **Table 4.1**. There, ΔE and ΔE_0 , are the energies relative to the more stable adduct, with

and without zero point energy corrections. D_e and D_0 are the corresponding dissociation energies, while B_2 is the barrier to the proton transfer.

Table 4.1 Calculated (B3LYP/6-311++G(d, p)) values of relative energies, dissociation energies, spectroscopic constants and dipole moment components of the three conformations of the AA dimer.

	<i>cis</i> ··· <i>cis</i>	<i>trans</i> ··· <i>trans</i>	<i>cis</i> ··· <i>trans</i>
$\Delta E/\text{kJmol}^{-1}$	0 ^a	2.13	1.09
$\Delta E_0/\text{kJmol}^{-1}$	0 ^b	1.81	1.02
D_e/kJmol^{-1}	67.2	68.0	67.5
D_0/kJmol^{-1}	62.0	63.1	62.4
B_2/kJmol^{-1}	29.5	27.4	27.9
A/MHz	4508	4888	4260
B/MHz	498	489	502
C/MHz	448	445	449
D_J/kHz	0.02	0.02	0.02
D_{JK}/kHz	0.00	-0.02	-0.05
D_K/kHz	2.26	1.95	2.73
d_1/kHz	-2.07	-1.84	-2.47
d_2/kHz	-0.14	-0.10	-0.17
μ_a/D	0	0	-0.02
μ_b/D	0	0	0.90

^a Absolute value: $-534.532034 E_h$. ^b Absolute value: $-534.395795 E_h$.

Geometry optimization and harmonic frequencies calculations were also run using the counterpoise method which takes into account for the basis-set superposition error (BSSE) correction.^[23] Whereas the resulting structural changes are negligible, the zero point energy corrected dissociation energy values lower to $D_0=58.6, 59.6, 59.0 \text{ kJmol}^{-1}$ for the *cis*···*cis*, *trans*···*trans*, *cis*···*trans* conformers respectively. It is worthwhile noting that the *cis*···*cis* and *trans*···*trans* species have a C_{2h} symmetry, while the *cis*···*trans* form belongs to the C_s group. However feasible operation like the internal proton transfer will increase the symmetry of the bi-molecules, that, in the case of a low barrier to proton transfer will effectively be C_{2v} for the *cis*···*trans* conformer.

The geometries of the optimized structures of the minima were collected in **Table 4.2** and the structure of the transition state for proton transfer was collected in **Table 4.3**.

Table 4.2 Optimized geometries of *cis*...*trans* conformer.

Bond lengths/Å		Valence angles/Deg.		Dihedral angles/Deg.	
H2H1	2.4498				
C3H1	1.9142	C3H1H2	72.1		
C4H2	1.9156	C4H2H1	71.9	C4H2H1C3	180.0
O5H1	0.9990	O5H1H2	112.5	O5H1H2C4	180.0
O6C4	1.2286	O6C4H2	94.6	O6C4H2H1	0.0
O7C3	1.2296	O7C3O5	123.7	O7C3O5H1	0.0
O8H2	0.9992	O8H2O7	178.8	O8H2O7C3	0.0
C9C3	1.4793	C9C3O5	115.3	C9C3O5H1	180.0
C10C4	1.4817	C10C4O6	123.4	C10C4O6H1	180.0
C11C9	1.3326	C11C9C3	123.7	C11C9C3O5	0.0
C12C10	1.3318	C12C10C4	121.4	C12C10C4O6	0.0
H13C9	1.0835	H13C9C3	114.1	H13C9C3O5	180.0
H14C10	1.0836	H14C10C4	116.2	H14C10C4O6	180.0
H15C11	1.0839	H15C11C9	121.0	H15C11C9C3	180.0
H16C12	1.0834	H16C12C10	121.4	H16C12C10C4	180.0
H17C11	1.0834	H17C11C9	121.2	H17C11C9C3	0.0
H18C12	2.4498	H18C12C10	120.6	H18C12C10C4	0.0

The polar species is drawn again in **Figure 4.4**, in order to introduce some labels used through the text. First of all, with respect to the general case of Figure 4.3, the two hydroxyl hydrogens are different from each other. They are labeled as *zusammen* (*Z*) or *entgegen* (*E*) the one close and the one far away from the two allyl groups, respectively.

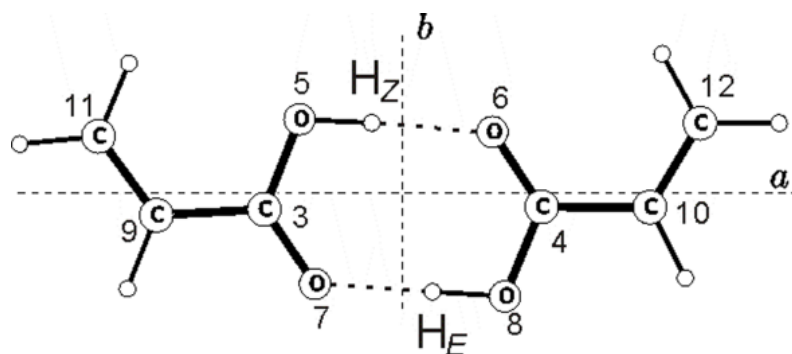


Figure 4.4 Atom labeling of the polar form of the (AA)₂.

Table 4.3 Optimized geometries of transition state of the double proton transfer connecting *cis*...*trans*/*trans*...*cis*.

Bond lengths/Å		Valence angles/Deg.		Dihedral angles/Deg.	
H2H1	2.1945				
C3H1	2.1075	C3H1H2	58.7		
C4H2	2.1075	C4H2H1	117.3	C4H2H1C3	0.0
O5H1	1.2706	O5H1H2	30.8	O5H1H2C4	180.0
O6C4	1.2055	O6C4H2	177.5	O6C4H2H1	180.0
O7C3	1.2069	O7C3O5	91.2	O7C3O5H1	0.0
O8H2	1.2069	O8H2O7	177.5	O8H2O7C3	180.0
C9C3	1.4800	C9C3O5	119.1	C9C3O5H1	180.0
C10C4	1.4800	C10C4O6	119.1	C10C4O6H1	180.0
C11C9	1.3322	C11C9C3	122.5	C11C9C3O5	0.0
C12C10	1.3322	C12C10C4	122.5	C12C10C4O6	0.0
H13C9	1.0835	H13C9C3	115.1	H13C9C3O5	180.0
H14C10	1.0835	H14C10C4	115.1	H14C10C4O6	180.0
H15C11	1.0836	H15C11C9	121.2	H15C11C9C3	180.0
H16C12	1.0836	H16C12C10	121.2	H16C12C10C4	180.0
H17C11	1.0838	H17C11C9	120.8	H17C11C9C3	0.0
H18C12	1.0838	H18C12C10	120.8	H18C12C10C4	0.0

4.4 Results and discussion

4.4.1 Rotational spectra

The rotational spectra of the most abundant species (normal species), and of the OD mono- and bi-deuterated species, prepared by mixing the sample with D₂O were collected. For simplicity, the normal and deuterated species were labeled as HH, DH, HD and DD, where the first and second positions of the capital letter indicate the isotopic (H or D) nature of the *Z* and *E* hydrogens, respectively.

The normal species was investigated first. This bi-molecule has a predominant μ_b dipole component, so that the search of its μ_b type transitions was targeted. Transitions of the type $(J+1)_{1,(J+1)} \leftarrow J_{0,J}$ transitions with *J* from 3 to 7 were observed and assigned first. Each transition was split into two lines due to the proton tunneling and each of them appeared as a doublet according to Doppler effect. The tunneling splitting of the $6_{16} \leftarrow 5_{05}$ transition of the parent, mono deuterated and bi-deuterated species were shown in **Figure 4.5**. Then some $K_a = 2 \leftarrow 1$ transitions and some *Q*-branch transitions were also measured. All transitions have been fitted simultaneously with a coupled Hamiltonian using the Pickett set of programs,^[24] with the following expressions:

$$H = \sum_i H_i^R + H^{CD} + H^{\text{int}}, \text{ with } i = 0, 1 \quad (4.1)$$

and

$$H^{\text{int}} = \Delta E_{01} + F_{\text{ab}} \times (P_a P_b + P_b P_a) \quad (4.2)$$

where H_i^R represents the rotational Hamiltonian for the state *i*. H^{CD} accounts for the centrifugal distortion corrections, corresponding to the I^r -representation of Watson's "S" reduced Hamiltonian,^[25] assumed to be the same for both states. ΔE_{01} is the energy difference between the $\nu = 0$ and $\nu = 1$ tunneling states. F_{ab} is the rotation-vibration coupling parameter between the two states. The spectroscopic constants obtained are reported in the first column of data of **Table 4.4**. A statistical weight of about 9/7 was

observed in favor of the transitions with the starting rotational level having an odd value (K_a+K_c) for $v = 0$, and vice versa for $v = 1$.

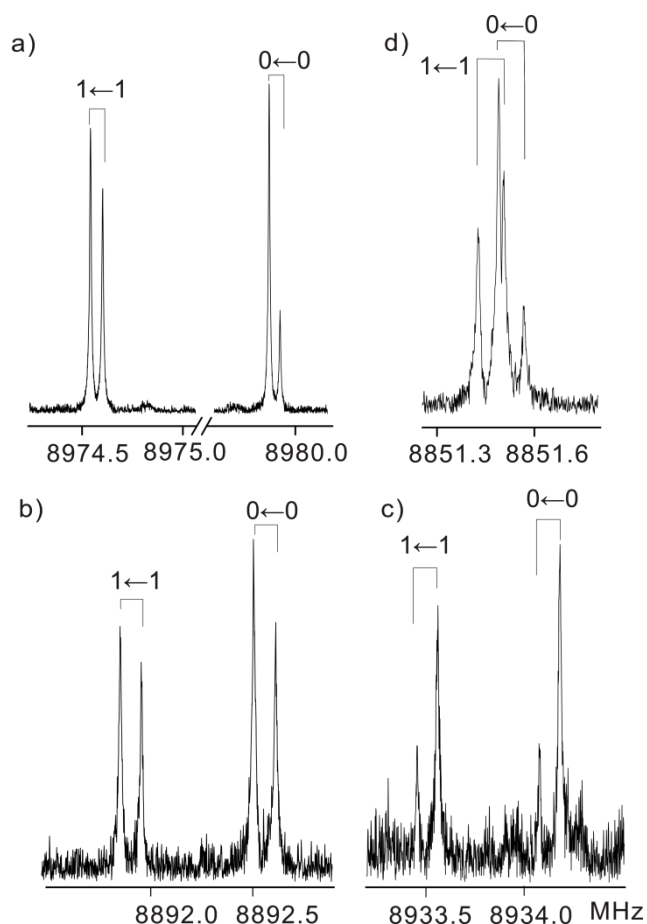


Figure 4.5 Observed the $6_{16} \leftarrow 5_{05}$ transition of a) HH, b) HD, c) DH and d) DD species.

Then the DH, HD and DD species were investigated. Since their ΔE_{01} splittings were quite smaller than that of the HH species, it was difficult to fit simultaneously the ΔE_{01} and the F_{ab} parameters. However, according to Pickett,^[26] These values could be calculated from the rotation of the principal axes system to the reduced Eckart axes system.^[27] The calculated F_{ab} values was slightly decreasing for the deuterated species with respect to the normal species. So, in the fits the F_{ab} parameters were fixed to the values scaled according to these indications. The results of the three fits (including scaled F_{ab} values) are also given in **Table 4.4**. In the case of the deuterated species, the hyperfine structure due to the quadrupole coupling constants of deuterium ($I = 1$) has been partially resolved. The obtained quadrupole coupling constants are also reported in **Table 4.4**. They are in good agreement with the *ab initio* values, $\chi_{aa} = 0.20$, $\chi_{bb} = -0.09$ and $\chi_{cc} = -0.11$ MHz, respectively, for both D_Z and D_E atoms.

In spite of the fact that the direct interstate transitions were not observed, one could determine the ΔE_{01} values for all isotopologues with good precision, may be rare to attain with other techniques.

Table 4.4 Experimental spectroscopic constants of the observed isotopologues of (AA)₂ (S-reduction, I^f representation)

	HH	DH	HD	DD
A_0/MHz	4235.871(2) ^a	4207.2469(2)	4171.29706(9)	4142.9926(2)
A_1/MHz	4235.850(2)	4207.2450(2)	4171.29347(9)	4142.9921(2)
B_0/MHz	508.874(1)	507.8477(3)	507.95476(7)	507.0070(1)
B_1/MHz	508.866(1)	507.8568(3)	507.95412(7)	507.0072(1)
C_0/MHz	454.2853(2)	453.1437(3)	452.8074(1)	451.7206(8)
C_1/MHz	454.2793(2)	453.1420(3)	452.80468(7)	451.7253(7)
D_J/kHz	0.0194(4)	[0.0194] ^b	[0.0194]	[0.0194]
D_{JK}/kHz	-0.051(3)	[-0.0517]	[-0.0517]	[-0.0517]
D_K/kHz	2.2(3)	[2.215]	[2.215]	[2.215]
d_1/kHz	-0.0014(2)	[-0.00142]	[-0.00142]	[-0.00142]
$\Delta E_{01}/\text{MHz}$	880.6(9)	117.0(9)	117.1(9)	30(4)
F_{ab}/MHz	-47.43(6)	{47.03} ^c	{46.73}	{46.43}
$\chi_{aa}(Z)/\text{MHz}$		0.177(2)		0.182(5)
$\chi_{aa}(E)/\text{MHz}$	-	-	0.175(2)	0.182(5)
$\chi(E)^d/\text{MHz}$	-	-	0.22(2)	
σ/kHz^e	2.2	3.0	3.3	3.4
N^f	82	94	92	100

^a Error in parentheses in units of the last digit. ^b Values in brackets have been kept fixed to the corresponding values of the HH species. ^c Values in braces fixed at the scaled values, see text. ^d $\chi = \chi_{bb} - \chi_{cc}$. ^e Root-mean-square deviation of the fit. ^f Number of lines in the fit.

In principle, from the rotational constants of the deuterated species, one could locate the r_s positions^[28] of the two hydroxyl hydrogens. However, both the fact that these two atoms undergo a large amplitude motions and that the Ubbelohde effect^[29, 30] produces a shrinkage of the O...O distances between the two oxygen atoms involved in each hydrogen bond, lead to meaningless values.

4.4.2 Model calculations for proton transfer

From the measured tunneling splittings it is in principle possible to determine the barrier to the concerted double proton transfer.

The situation is much more complex, however, than for the familiar determination of a barrier hindering the internal rotation of a methyl group. In this latter case the motion in question is well described by rigid frame – rigid top model, as its vibration is usually at the lowest frequency and therefore well separated from the other molecular vibrations. By contrast, proton transfer is a fast motion at high energy that involves breaking and forming strong bonds, and it depends on the cooperative rearrangement of slowly vibrating modes of heavy nuclei. A well-known example is the proton transfer in malonaldehyde. For this system it has so far not been possible to derive the barrier height directly from the experimental data, but a large amount of properties obtained *ab initio* on a grid along the minimum energy path (MEP) have been needed to devise a full dimensional model able to reproduce a set of observed properties.^[31]

Nevertheless, a simpler treatment of the most relevant molecular motions still seems to be desirable for the interpretation of spectroscopic data. We therefore tried to restrict the *ab initio* results to the stationary points of the potential energy surface and to use the structural changes obtained when going from the saddle point to either equilibrium configuration to define two modes of motion that are expected to be coupled most with the proton transfer. The simultaneous transfer of the proton pair is described by the displacement along the line connecting the carboxylic carbons from their midpoint. After dividing by the displacement at equilibrium one obtains the more useful reduced variable x . We note that the structure of the *cis-trans* acrylic acid dimer at the saddle point ($x = 0$) has C_{2v} symmetry, and that upon reaching equilibrium at $x = \pm 1$, the structural parameters (bond lengths and angles) change by amounts $S_i(\pm 1)$ that are predicted *ab initio*. S_i involves a component $[S_i(1) - S_i(-1)]/2$ of symmetry species B_1 and a component $[S_i(1) + S_i(-1)]/2$ of species A_1 . We associate these components with reduced variables y_1 and y_2 that are assumed to follow the MEP if $y_1 = x$ and $y_2 = x^2$. More generally the variables (x, y_1, y_2) refer to a planar 3D system^[32] where the deviations from the MEP, $y_1 - x$ and $y_2 - x^2$, are displacements of the virtual modes that are used as representatives for the larger set of vibrations interacting with the proton

transfer. The variable y_1 describes the B_1 type heavy atom motions, which are dominated by changes of CO bond lengths and C-CO₂ rocking angles, while the variable y_2 combines a large change of the distance between the two monomer units with several smaller A_1 type displacements. The potential surface assumed as

$$V(x, y_1, y_2) = s(x) \{B_2 (1-x^2)^2 + [f_1/s(1)] (y_1-x)^2 + [f_2/s(1)] (y_2-x^2)^2\} \quad (4.3)$$

involves a shape function $s(x)$ that ensures an asymptotic approach, along the MEP, to the dissociation energy D_0 and allows one to modify the barrier width by a factor w_b .

$$s(x) = 1/[1+w_b (B_2/D_0)^{1/2} x^2 + (B_2/D_0) x^4] \quad (4.4)$$

D_0 as well as the barrier B_2 can usually be obtained *ab initio* whereas the force constant factors $f_i = k_i/2$ ($i = 1, 2$) as well as the factor w_b are difficult to predict and should therefore rather be treated as parameters to be assumed or adjusted.

The proton motion in a deep double minimum potential involves high zero point vibrational energy and is hence much faster than the heavy atom modes. A study by Manz et al.^[33] for a prototype of coupled hydrogenic and heavy atom motion suggests an adiabatic approach, similar to the one applied to electronic and nuclear motion. Using methods developed for flexible molecules,^[34] therefore the energy levels of the proton motion (x) that depend parametrically on y_1 and y_2 were calculated in order to obtain the ‘protonic’ contribution to the potential energy of the y_1 and y_2 vibrations. For a symmetric reference system ($y_1 = 0, y_2 = 1$) the levels are grouped into tunneling doublets E_{n+}, E_{n-} . Therefore we expect for each n two surfaces with avoided crossing that are to be converted into crossing surfaces by referring to a ‘left’ and ‘right’ localized basis [$\langle\phi_{nL}|, \langle\phi_{nR}|$]. In this representation we get $E_{nL} = E_{nR} = E_n$ and the interaction $W_n = (E_{n+} - E_{n-})/2$. For ($y_1 \neq 0, y_2 = 1$) the elements of the reference, $E_n |\phi_{nL}\rangle \langle\phi_{nL}|$, are to be complemented by the elements of the potential energy difference,

$$|\phi_{mL}\rangle \langle\phi_{mL}| V(x, y_1, 1) - V(x, 0, 1) |\phi_{nL}\rangle \langle\phi_{nL}| \quad (4.5)$$

in order to obtain, after diagonalization, the surface point $E_{1L}(y_1, 1)$ and the expansion coefficients $U_{nL,1L}$ for the lowest state $\phi_{1L}(x; y_1, 1)$ at $y_1 \neq 0$ with respect to the reference states $\phi_{nL}(x; 0, 1)$. The corresponding point on the R surface, $E_{1R}(y_1, 1)$ is found

similarly. Then the tunneling interaction for the lowest vibrational state of the transfer motion is obtained as $W(y_1, 1) = \sum_n U_{nL,1L} W_n(0, 1) U_{nR,1R}$. In the same way the y_2 -dependent functions $E_{1L}(0, y_2)$, $E_{1R}(0, y_2)$ and $W(0, y_2)$ are calculated. To simplify the computations the complete functions $F(y_1, y_2)$ defining the two potential energy surfaces and the tunnel interaction function ($F = E_{1L}, E_{1R}, W$) are approximated by the one-dimensional profiles as

$$F(y_1, y_2) = F(y_1, 1) + F(0, y_2) - F(0, 1) \quad (4.6)$$

This means that we neglect kinetic energy interactions between the coordinates x , y_1 and y_2 , and it makes it possible to calculate the 2D wavefunctions for the heavy atom motions as products of 1D factors such as, $\chi_L(y_1, y_2) = \chi^{(1)}_L(y_1) \chi^{(2)}_L(y_2)$, where $\chi^{(1)}_L$ is obtained as the lowest state of the y_1 motion with the potential energy profile $E_{1L}(y_1, 1)$ and $\chi^{(2)}_L$ as the lowest state of the y_2 motion with the potential energy profile $E_{1L}(0, y_2)$. The tunnel interaction in the vibrational ground state is then given by

$$W_{gs} = \langle \chi_L(y_1, y_2) | W(y_1, y_2) | \chi_R(y_1, y_2) \rangle \quad (4.7)$$

and the respective tunneling splitting by $\Delta E = -2W_{gs}$.

As equations (4.3) and (4.4) involve five parameters, it is clear that their values cannot be determined from the available experimental data alone. Therefore we have fixed the presumably least important one, $D_0 = 5216 \text{ cm}^{-1}$, at the B3LYP result. Then, with different choices of fixed values for f_1 and f_2 , the barrier B_2 and the barrier width parameter w_b were adjusted to fit the observed splittings for the HH, DH, HD, and DD species, while expecting the barrier to remain in the range of the *ab initio* values 2328 cm^{-1} (B3LYP) and 2723 cm^{-1} (MP2). The relation of the assumed different values of the f_1 and f_2 with the corresponding variations of the B_2 and w_b were collected in **Table 4.5**. The parameter w_b affects the width of the barrier, a property relevant to reproduce the ratio of the splittings of deuterated to the parent species. **Table 4.6** shows the results obtained with a set of parameters that could be a plausible interpretation of the data. The chosen values $f_1 = 220 \text{ cm}^{-1}$ and $f_2 = 60 \text{ cm}^{-1}$ yield fundamental frequencies of 125 cm^{-1} and 41 cm^{-1} for the representative y_1 and y_2 vibrations, respectively. As may be expected from **Eq. (4.3)**, an increase in f_1 and/or f_2 will draw the system closer to the MEP, and thus increase the effective mass of the resulting transfer motion. Therefore a lower

barrier will be needed to offset the shrinking of the tunneling splittings. This is shown in **Table 4.5** that also led us to estimate the uncertainty of the barrier to proton transfer at 150 cm^{-1} .

Table 4.5 Variations of the B_2 and w_b parameters upon assuming different values of the force constants f_1 and f_2 .

Parameters				Calculated tunneling splitting			
assumed		adjusted					
f_1/cm^{-1}	f_2/cm^{-1}	B_2/cm^{-1}	$w_b/1$	$\Delta E_{\text{HH}}/\text{MHz}$	$\Delta E_{\text{DH}}/\text{MHz}$	$\Delta E_{\text{HD}}/\text{MHz}$	$\Delta E_{\text{DD}}/\text{MHz}$
270	60	2390	0.20	879.83	118.53	115.01	21.23
220	60	2485	0.90	880.54	118.75	115.23	21.42
170	60	2658	2.10	881.36	118.80	115.31	21.48
220	80	2460	0.90	880.13	118.77	115.25	21.46
220	60	2485	0.90	880.54	118.75	115.23	21.42
220	40	2513	0.90	881.21	118.83	115.31	21.41

The barrier to proton transfer appears consistent with the *ab initio* value (see **Table 4.1**), but is quite lower than the tentative values calculated from the spectroscopic data in some cases (see **Table 4.7**). As to the value for the benzoic acid dimer, the authors give the $B_2 = 6224 \text{ cm}^{-1}$ and report in parenthesis (7.45 kJmol^{-1}), but it should be 74.5 kJmol^{-1} , exaggeratedly high.

Table 4.6 Results of the flexible model calculations.

Tunnelling Splittings	Obs	Calc
$\Delta E_{01}(\text{HH})/\text{MHz}$	880.6(6) ^a	880.5
$\Delta E_{01}(\text{DH})/\text{MHz}$	117.0(9)	118.8
$\Delta E_{01}(\text{HD})/\text{MHz}$	117.1(9)	115.2
$\Delta E_{01}(\text{DD})/\text{MHz}$	30(10)	21.4
Determined parameters		
	$B_2/\text{cm}^{-1} = 2485(150)$	$w_b = 0.90$ ^b
	$f_1 = 220/\text{cm}^{-1}$ ^c	$f_2 = 60/\text{cm}^{-1}$ ^c

^a Errors in parenthesis are expressed in units of the last digit. ^b Shape function parameter. ^c Assumed, see text.

Table 4.7 Barriers to proton tunneling as estimated from the experimental spectroscopic data for some carboxylic acid bi-molecules.

	$\Delta E_{01}/\text{MHz}$	B_2/cm^{-1}	Ref.
$(\text{C}_6\text{H}_5\text{COOH})_2$	1114.0(10) ^a	6224	2
$(\text{HCOOH})_2$	474(12)	2480-5450	6, 7, 9
$\text{HCOOH-HC}_2\text{COOH}$	291.428(5)	8000	16
$\text{HCOOH-CH}_3\text{COOH}$	250.44(1) ^b	8000	17
$(\text{AA})_2$	880.6(6)	2485(150)	This work

^aErrors in parenthesis are expressed in units of the last digit. ^bThis splitting is for the “A” state of the internal rotation. A meaningless value of -136.167(3) MHz is reported for the “E” state.

4.5 Conclusions

In summary, the rotational spectra of four isotopologues of the dimer of acrylic acid have been assigned. The most important results are: (i) it is possible to investigate by rotational spectroscopy homo dimers of carboxylic acids; (ii) it is possible to determine the barrier to the double proton exchange; (iii) however, the ratios between the tunnelling splittings measured for the various H/D species which are the key parameters which allow to estimate the dynamics of the skeletal structural relaxation; (iv) the reduced mass of the motion changes step by step, so that a flexible model which takes into account these changes is especially suitable for the evaluation of the barrier.

References

- [1] P. Gilli, V. Bertolasi, V. Ferretti, G. Gilli, *J. Am. Chem. Soc.* **2000**, *122*, 10405.
- [2] I. Kalkman, C. Vu, M. Schmitt, W. L. Meerts, *ChemPhysChem* **2008**, *9*, 1788.
- [3] V. V. Matyilitsky, C. Riehn, M. F. Gelin, B. Brutschy, *J. Chem. Phys.* **2003**, *119*, 10553.
- [4] R. Georges, M. Freytes, D. Hurtmans, I. Kleiner, J. V. Auwera, M. Herman, *Chem. Phys.* **2004**, *305*, 187.
- [5] Z. Xue, M. A. Suhm, *J. Chem. Phys.* **2009**, *131*, 054301.
- [6] F. Madeja, M. Havenith, *J. Chem. Phys.* **2002**, *117*, 7162.

- [7] M. Ortlieb, M. Havenith, *J. Phys. Chem. A* **2007**, *111*, 355.
- [8] A. Gutberlet, G. W. Schwaab, M. Havenith, *Chem. Phys.* **2008**, *343*, 158.
- [9] O. Birer, M. Havenith, *Ann. Rev. Phys. Chem.* **2009**, *60*, 263.
- [10] C. Riehn, V. V. Matylitsky, M. F. Gelin, B. Brutschy, *Mol. Phys.* **2005**, *103*, 1615.
- [11] See Ref. 37 in chapter 1.
- [12] E. M. Bellott, E. B. Wilson, Jr. *Tetrahedron* **1975**, *31*, 2896.
- [13] L. Martinache, W. Kresa, M. Wegener, U. Vonmont, A. Bauder, *Chem. Phys.* **1990**, *148*, 129.
- [14] S. Antolinez, H. Dreizler, V. Storm, D. H. Sutter, J. L. Alonso, *Z. Naturforsch.* **1997**, *52a*, 803.
- [15] A. M. Daly, P. R. Bunker, S. G. Kukolich, *J. Chem. Phys.* **2010**, *132*, 201101.
- [16] A. M. Daly, K. O. Douglass, L. C. Sarkozy, J. L. Neill, M. T. Muckle, D. P. Zaleski, B. H. Pate, S. G. Kukolich, *J. Chem. Phys.* **2011**, *135*, 154304.
- [17] M. C. D. Tayler, B. Ouyang, B. J. Howard, *J. Chem. Phys.* **2011**, *134*, 054316.
- [18] V. V. Ilyushin, E. A. Alekseev, Y. C. Chou, Y. C. Hsu, J. T. Hougen, F. J. Lovas, L. B. Picraux, *J. Mol. Spectrosc.* **2008**, *251*, 56.
- [19] M. Oldani, A. Bauder, *Chem. Phys. Lett.* **1984**, *108*, 7.
- [20] K. Bolton, D. G. Lister, J. Sheridan, *J. Chem. Soc. Faraday Trans. 2*, **1974**, *70*, 113.
- [21] See Ref. 73 in chapter 1.
- [22] See Ref. 13 in chapter 2.
- [23] See Ref. 12 in chapter 2.
- [24] H. M. Pickett, *J. Mol. Spectrosc.* **1991**, *148*, 371. Current versions are described and available from: <<http://spec.jpl.nasa.gov>>
- [25] See Ref. 6 in chapter 2.
- [26] H. M. Pickett, *J. Chem. Phys.* **1972**, *56*, 1715.
- [27] C. Eckart, *Phys. Rev.* **1935**, *47*, 552.
- [28] See Ref. 11 in chapter 2.
- [29] A. R. Ubbelohde, K. J. Gallagher, *Acta Crystallogr.* **1955**, *8*, 71.
- [30] See, Ref. 83 in chapter 1.
- [31] R. Meyer, T.-K. Ha, *Mol. Phys.* **2003**, *101*, 3263; **2005**, *103*, 2687.
- [32] A similar approach was chosen earlier for a 2D model for the benzoic acid dimer, see: R. Meyer, R. R. Ernst, *J. Chem. Phys.* **1990**, *93*, 5518; A. Stöckli, B.H. Meier, R. Kreis, R. Meyer, R. R. Ernst, *J. Chem. Phys.* **1990**, *93*, 1502.
- [33] J. Manz, R. Meyer, E. Pollak, J. Römel, *Chem. Phys. Lett.* **1982**, *93*, 184.
- [34] See Ref. 26 in chapter 3.

Chapter 5 Conformational equilibrium, structure, and isotopic effect in acrylic acid - formic acid bi-molecule

5.1 Introduction

Carboxylic acids tend to exist as dimers in solution or gas phase, forming an eight-membered ring which includes two relatively strong $\text{OH}\cdots\text{O}$ hydrogen bonds (HB). The combination of the two HBs with the electronic delocalization which can take place within the two carboxylic groups, leads to one of the strongest HB assemblies found within neutral species. Sometimes this kind of HB is called “resonance assisted” HB,^[1] and its bonding energy is more than 60 kJmol^{-1} .

This kind of adducts is also interesting because a double proton transfers takes easily place, connecting either two equivalent, or two non-equivalent molecular conformations. In the first case tunnelling effects are expected as what has been discussed in chapter 4, which can lead to the determination of the potential energy surface for the motion.^[2, 3] In the second case, a conformational equilibrium to characterize the molecular system was expected. No reports matching the second case are available, to the best of our knowledge, in the literature.

Moreover, already in the first MW study of the carboxylic acid bi-molecule,^[4] it was outlined that the $\text{H} \rightarrow \text{D}$ isotopic substitution of the hydrogen atoms involved in the HB was producing an increase of the $\text{O}\cdots\text{O}$ distances. This experimental evidence is well known, in solid state, as Ubbelohde effect.^[5] In gas phase, however, such an increase is observed only in carboxylic dimers, while for complexes with the two subunits held together by a single $\text{OH}\cdots\text{O}$ HB, a shrinking of the $\text{O}\cdots\text{O}$ distance is observed.^[6-8]

In this chapter, the pulsed jet FTMW spectrum of a hetero dimer of carboxylic acids, acrylic acid ($\text{CH}_2=\text{CH}-\text{COOH}$) - formic acid (AA-FA), is presented. This is the

first case in which the rotational spectra of two different conformers are observed for a carboxylic acid dimer. In addition, plenty of structural information leading to a precise measure of the above mentioned Ubbelohde effect will be provided.

5.2 Experimental details

Commercial samples of HCOOH, C₂H₃COOH, and DCOOH were purchased from Aldrich and used without further purification. The deuterated FA (HCOOD) and deuterated AA (C₂H₃COOD) were made by mixing the acid with D₂O. The rotational spectra in the 6-18.5 GHz frequency region were measured on a COBRA-type pulsed supersonic-jet Fourier-transform microwave (FTMW) spectrometer as described in chapter 2.

A carrier gas of He at a total pressure of 3 bar was streamed over the mixture of FA and AA at room temperature, and expanded through the solenoid valve (General Valve, Series 9, nozzle diameter 0.5 mm) into the Fabry-Pérot cavity. Each rotational transition displays an enhanced Doppler splitting that originates from the supersonic jet expanding coaxially along the resonator axes. The rest frequency was calculated as the arithmetic mean of the frequencies of the two Doppler components.

5.3 *Ab initio* calculations

Before collecting the rotational spectra, MP2/6-311++G(d, p) geometry optimization calculations were performed by using Gaussian 03 suite of programs.^[9] The complex can adopt two configurations, depending on the *cis* or *trans* shapes of AA. The *cis* form of AA-FA is calculated to be slightly more stable than the *trans* one, according to the stability order of the AA monomer.^[10] Both conformers have strong μ_a and weak μ_b dipole moment. B3LYP calculations with the same basis set were also performed, the resulting theoretical rotational constants, dipole moments and the dissociation energy of the two conformers are reported in **Table 5.1** together with those obtained with MP2 method.

The molecular sketches, principal axes and the relative energies are shown in **Figure 5.1**, together with the atomic numbering used in the structural analysis.

Table 5.1 MP2/6-311++G(d, p) and B3LYP /6-311++G(d, p) calculated spectroscopic parameters of AA-FA.

Parameters	<i>cis</i>		<i>trans</i>	
	B3LYP	MP2	B3LYP	MP2
A/MHz	5010	4960	5417	5394
B/MHz	953	952	934	929
C/MHz	800	798	796	792
D_J/kHz	0.064	0.059	0.0717	0.0434
D_{JK}/kHz	2.000	2.848	1.089	4.148
D_K/kHz	4.315	10.145	0.808	33.223
d_1/kHz	-0.00708	-0.00288	-0.0104	0.00494
d_2/kHz	-0.00357	-0.00427	-0.00227	-0.00379
$ \mu_a , \mu_b , \mu_c /D$	1.4, 0.4, 0.0	1.2, 0.3, 0.0	1.4, 0.2, 0.0	1.2, 0.2, 0.0
$D, D_{CP}^a/\text{kJmol}^{-1}$	66, 62	64, 51	66, 62	64, 52

^a D and D_{CP} are the dissociation energy and the corresponding BSSE corrected value.

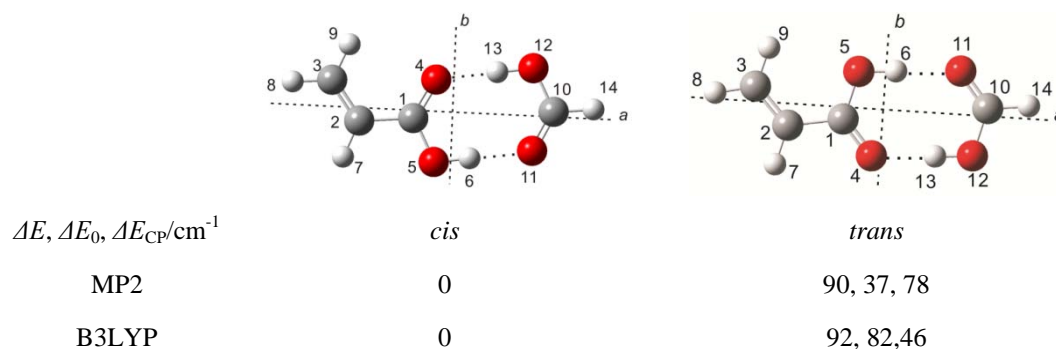


Figure 5.1 Molecular sketch, principal axes, atom numbering and relative energy of the *cis* and *trans* conformers of AA-FA. The absolute energies calculated at MP2/6-311++G(d, p) level are -455.928832, -455.825380, -455.923985 E_h for E, E_0 and E_{CP} , respectively. These values are -457.105941, -457.002686, -457.104403 E_h from B3LYP calculations.

Frequency calculations proved the two conformers to be real minima, and provided the resulted centrifugal distortion constants given in **Table 5.1**. Counterpoise

corrections^[11] were calculated in order to remove the well known basis set superposition error (BSSE).

In addition, the potential energy function to the double proton transfer, which interconverts the two conformers, has been calculated at the B3LYP level, and it is shown in **Figure 5.2**. In the left part of the graphic, corresponding to the most stable (*cis*) conformer, the potential energy is given as a function of the change of the r_{O5-H6} bond distance (see **Figure 5.1**) with respect to the transition state (top of the barrier) value, while in the right section it is given as a function of the $r_{O12-H13}$ bond length.

The value of the barrier to proton transfer (2453 cm^{-1}) is in a very good agreement with those, experimentally obtained, of the acrylic acid dimer^[2] and of the formic acid – benzoic acid^[3] bi-molecules. In the cases of these last two dimers, the experimental evaluation of the barrier to proton transfer has been made possible by measuring the tunnelling splittings, related to the symmetric double minimum potentials, of several isotopologues.

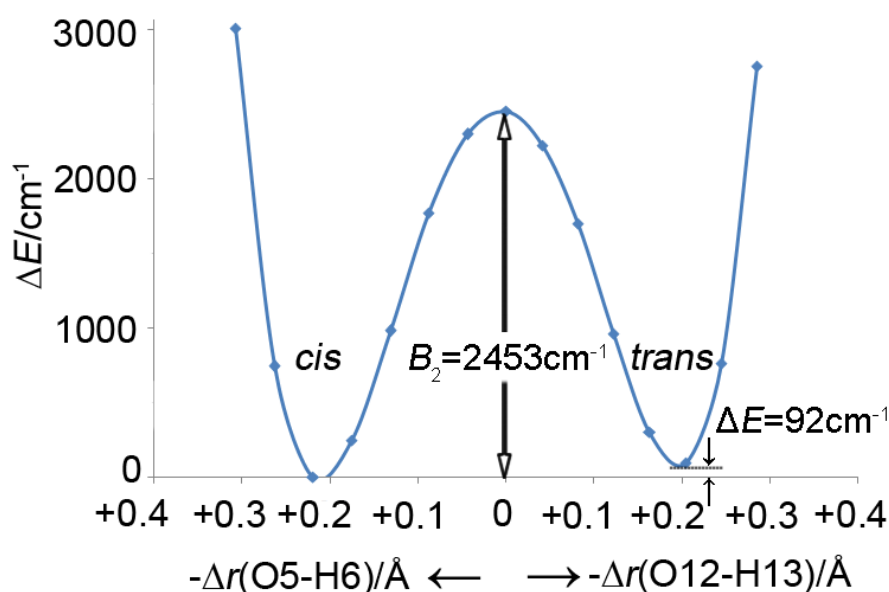


Figure 5.2 Potential energy surface of the double proton exchange motion in AA-FA.

5.4 Results and discussion

5.4.1 Rotational spectra

According to the indications of the *ab initio* calculations, the first search for the rotational transitions was focused on the μ_a -type transitions of the both *cis* and *trans* conformers. The observed lines were assigned to $J = 5 \leftarrow 4$ band, $K_a = 0, 1$ transitions of the two corresponding conformers, which were shown in **Figure 5.3**, each line appears as a doublet because of the Doppler effect. Then more μ_a -type transitions with J from 4 up to 10, K_a up to 3 were found and assigned. Several μ_b -type transitions were also measured and put into the fit.

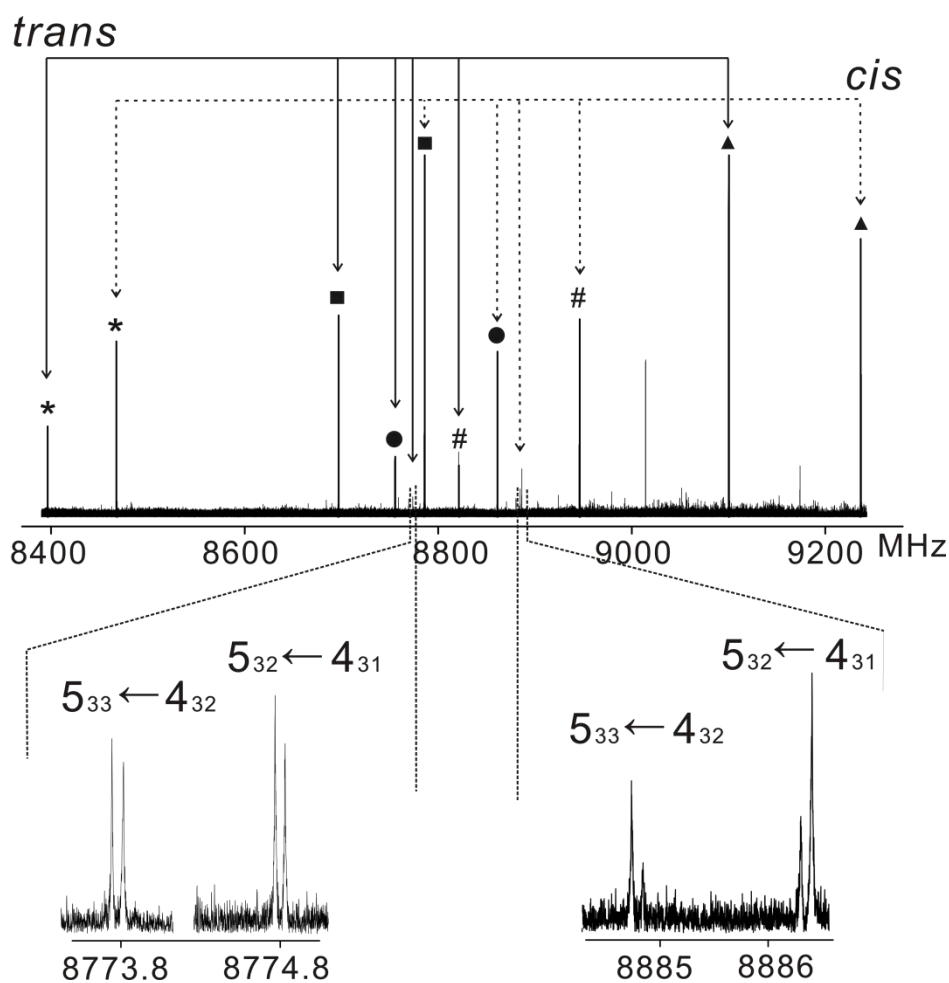


Figure 5.3 Frequencies and intensities of the $J = 5 \leftarrow 4$ μ_a -band of both *cis* and *trans* AA...FA. The single transitions are labeled in the Figure according to: * $5_{15} \leftarrow 4_{14}$, ■ $5_{05} \leftarrow 4_{04}$, ▲ $5_{14} \leftarrow 4_{13}$, ● $5_{24} \leftarrow 4_{23}$, # $5_{23} \leftarrow 4_{22}$.

The measured lines were fitted by using Pickett's SPFIT program,^[12] according to the Hamiltonian:

$$H = H_R + H_{CD} \quad (5.1)$$

where H_R and H_{CD} represents the rigid rotational part and the centrifugal distortion contributions, respectively of the Hamiltonian. The S reduction and I' representation have been used.^[13] The resulting values of the spectroscopic constants are collected in **Table 5.2** and **5.3** for the *cis* and *trans* conformers, respectively.

In order to obtain structural information on the two complexes, after the assignment of the most abundant species, the spectra of many isotopic species were measured. They include four deuterated isotopologues for each conformer, that is AA-DCOOH, AA-HCOOD, AA(OD)-FA, and AA(OD)-FA(OD). The corresponding rotational constants have been reported in the right columns of **Tables 5.2** and **5.3** for *cis* and *trans*, respectively. In addition, 8-14 transitions of the 4 isotopologues with one ^{13}C atom in natural abundance have been measured for both conformers. The obtained rotational constants are given in **Table 5.4**.

Finally, in order to obtain detailed information on the Ubbelohde effect (see the section below), the rotational spectra of some mixed ^{13}C and OD deuterated species were also measured. This was possible only for the most abundant conformer, *cis*. The obtained rotational constants are listed in **Table 5.5**.

Table 5.2 Spectroscopic parameters for *cis* AA-FA.

	Parent	D14	D13	D6	D6&D13
A/MHz^a	5039.6126(4) ^b	5036.694(1)	4974.441(5)	4961.220(5)	4896.813(5)
B/MHz	964.15536(4)	938.0629(4)	959.8600(5)	962.1740(5)	958.0517(6)
C/MHz	810.02227(4)	791.4872(4)	805.3080(6)	806.5813(6)	801.9792(7)
σ^c/kHz	0.6	4.0	4.2	4.3	3.3
N^d	46	25	13	13	11

^a First order centrifugal distortion constants have been determined for the parent species: D_J , D_{JK} , D_K , d_1 , $d_2 = 0.089(1)$, $0.348(2)$, $2.600(1)$, $-0.016(1)$, $-0.00229(1)$ kHz, respectively. This set of parameters has been fixed to the parent species values for the other isotopologues. ^b Error in parentheses in units of the last digit. ^c RMS error of the fit. ^d Number of lines in the fit.

Table 5.3 Spectroscopic parameters for *trans* AA-FA.

	Parent	D14	D13	D6	D6&D13
A/MHz^a	5376.748(4) ^b	5367.511(1)	5312.636(5)	5314.093(5)	5250.130(5)
B/MHz	946.7892(4)	921.7410(4)	941.1633(7)	944.8521(7)	939.4106(7)
C/MHz	805.8053(4)	787.4245(4)	800.2957(7)	802.9958(7)	797.6058(7)
σ^c/kHz	1.1	3.6	3.2	4.1	3.3
N^d	48	23	11	11	11

^a First order centrifugal distortion constants have been determined for the parent species: D_J , D_{JK} , D_K , d_1 , $d_2 = 0.088(1)$, $0.20(2)$, $2.7(9)$, $-0.015(1)$, $-0.0014(9)$ kHz, respectively. This set of parameters has been fixed to the parent species values for the other isotopologues. ^b Error in parentheses in units of the last digit. ^c RMS error of the fit. ^d Number of lines in the fit.

Table 5.4 Rotational constants of the ^{13}C species of AA-FA.^a

	$^{13}\text{C}10$	$^{13}\text{C}1$	$^{13}\text{C}2$	$^{13}\text{C}3$
<i>cis</i>				
A/MHz	5039.042(4) ^b	5037.273(4)	5032.408(4)	5016.638(5)
B/MHz	950.6067(5)	962.1708(4)	952.6111(4)	944.2989(5)
C/MHz	800.4296(6)	808.5659(3)	801.6836(6)	795.3920(6)
σ^c/kHz	4.1	3.7	3.4	3.3
N^d	14	13	13	13
<i>trans</i>				
A/MHz	5373.2(2)	5373.0(2)	5362.3(2)	5364.0(2)
B/MHz	933.7569(7)	944.9290(7)	935.9192(7)	926.8512(7)
C/MHz	796.2761(7)	804.3768(9)	797.6041(8)	791.0490(9)
σ^c/kHz	3.6	2.6	2.4	4.1
N^d	9	8	9	8

^a First order centrifugal distortion constants were fixed to the values of the parent species. ^b Error in parentheses in units of the last digit. ^c RMS error of the fit. ^d Number of lines in the fit.

Table 5.5 Rotational constants of the ^{13}C species of some deuterated isotopologues of *cis* AA-FA.^a

	C10	C1	C2	C3
1) D6				
<i>A</i> /MHz	4960.6(1) ^b		4954.5(1)	4938.7 (1)
<i>B</i> /MHz	948.7068(7)		950.6247(7)	942.3244(7)
<i>C</i> /MHz	797.0807(7)		798.2799(9)	792.0077(9)
σ^c /kHz	3.2		3.0	4.1
<i>N</i> ^d	9		8	8
2) D13				
<i>A</i> /MHz	4974.0(1)	4972.2(1)	4967.5(1)	4952.1(1)
<i>B</i> /MHz	946.4924(7)	957.8495(7)	948.3020(7)	940.0763(7)
<i>C</i> /MHz	795.8682(7)	803.8299(9)	796.9802(7)	790.7663(7)
σ /kHz	3.1	3.0	4.6	3.8
<i>N</i>	8	7	9	9
3) D6&D13				
<i>A</i> /MHz	4896.5(1)	4894.9(2)	4890.4(1)	4874.5(1)
<i>B</i> /MHz	944.7561(7)	956.0266(8)	946.4860(7)	938.2690(7)
<i>C</i> /MHz	792.6318(9)	800.5028(7)	793.6904(7)	787.4918(9)
σ /kHz	2.9	2.3	2.9	2.6
<i>N</i>	8	8	9	8

^a First order centrifugal distortion constants were fixed to the values of the parent species. ^b Error in parentheses in units of the last digit. ^c RMS error of the fit. ^d Number of lines in the fit.

5.4.2 Relative population of the two conformers in the jet

Relative intensity measurements of several nearby μ_a and μ_b -type transitions allowed to estimate the relative population of the two conformers in the supersonic expansion. It is not so obvious to obtain, from this data, the relative energy. This because, as outlined in other papers, when the one FA molecule meets the AA molecules, it is more probable that it meets a *cis*-AA molecule, which is more abundant. Then the rapid cooling freezes the system, without possibilities of reaching an equilibrium situation. If one would, however, try to calculate the relative energy,

assuming that the rotational energies of the initial states of the transitions involved in the relative intensity measurements are about the same, the following expression can be used:^[14]

$$\Delta(\Delta G^0) = \Delta G^0_{\text{T}} - \Delta G^0_{\text{C}} = k \cdot T_{\text{room}} \ln[(I_{\text{C}} \omega_{\text{T}} \mu_{\text{a,T}} \gamma_{\text{T}} \nu_{\text{T}}^2)/(I_{\text{T}} \omega_{\text{C}} \mu_{\text{a,C}} \gamma_{\text{C}} \nu_{\text{C}}^2)] \quad (5.2)$$

where I is the peak intensity, ω the conformational degeneracy (1 for both of the conformers), $\mu_{\text{a,g}}$ the dipole moment component, γ_{g} the line strength, ν_{g} the transition frequency. One would obtain the value $\Delta(\Delta G_0) = 170(50) \text{ cm}^{-1}$ which is practically the energy difference in the AA monomer.

5.4.3 Dissociation energy

A pseudodiatomic model was applied to calculate the dissociation energy (D) of the complex. An approximated value of the stretching force constant (k_{s}) can then be estimated:^[15]

$$k_{\text{s}} = 16\pi^4 (\mu R_{\text{CM}})^2 [4B^4 + 4C^4 - (B-C)^2 (B+C)^2]/(h D_{\text{j}}) \quad (5.3)$$

where μ is the pseudo-diatomic reduced mass and R_{CM} (= 3.828 Å and 3.852 Å for *cis* and *trans* conformer, respectively) is the distance between the centre of mass of the two subunits. The value $k_{\text{s}} = 43.0$ and 41.7 Nm^{-1} have been obtained, which corresponds to harmonic stretching frequencies of 161 and 158 cm^{-1} for the *cis* and *trans* complexes, respectively.

The assumption of a Lennard-Jones type potential relates the dissociation energy D to k_{s} :^[16]

$$D = 1/72 k_{\text{s}} R_{\text{CM}}^2 \quad (5.4)$$

The values $D \approx 53$ and 52 kJmol^{-1} has been obtained for *cis* and *trans*, respectively. These values are quite similar to those obtained when applying the BSSE corrections to the *ab initio* data.

5.4.4 Structures and Ubbelohde effect

Table 5.6 MP2/6-311++G(d, p) geometry of *cis* AA-FA.

Bond lengths/Å		Angles/°		Dihedral angle/°	
C2C1	1.4837				
C3C2	1.3412	C3C2C1	120.8		
O4C1	1.2287	O4C1C2	123.5	O4C1C2C3	0.0
O5C1	1.3275	O5C1C2	112.2	O5C1C2C3	180.0
H6O5	0.9891	H6O5C1	108.9	H6O5C1C2	180.0
H7C2	1.0848	H7C2C1	116.8	H7C2C1O4	180.0
H8C3	1.0845	H8C3C2	121.1	H8C3C2C1	180.0
H8C3	1.0855	H8C3C2	120.3	H8C3C2C1	0.0
C10C1	3.8496	C10C1C3	152.1	C10C1C3C2	180.0
O11C10	1.2218	O11C10C1	58.5	O11C10C1C3	180.0
O12C10	1.3176	O12C10O11	126.2	O12C10O11C1	0.0
H13O12	0.9934	H13O12C10	108.6	H13O12C10O11	0.0
H14C10	1.0956	H14C10O11	122.3	H14C10O11O12	180.0

Table 5.7 MP2/6-311++G(d, p) geometry of *trans* AA-FA.

Bond lengths/Å		Angles/°		Dihedral angle/°	
C2C1	1.4807				
C3C2	1.3420	C3C2C1	123.2		
O4C1	1.2304	O4C1C2	121.2	O4C1C2C3	180.0
O5C1	1.3268	O5C1C2	114.6	O5C1C2C3	0.0
H6O5	0.9886	H6O5C1	108.7	H6O5C1C2	180.0
H7C2	1.0849	H7C2C1	114.6	H7C2C1O5	180.0
H8C3	1.0850	H8C3C2	120.7	H8C3C2C1	180.0
H8C3	1.0846	H8C3C2	121.0	H8C3C2C1	0.0
C10C1	3.8498	C10C1C3	155.4	C10C1C3C2	180.0
O11C10	1.2219	O11C10C1	58.4	O11C10C1C3	0.0
O12C10	1.3174	O12C10O11	126.3	O12C10O11C1	0.0
H13O12	0.9934	H13O12C10	108.6	H13O12C10O11	0.0
H14C10	1.0955	H14C10O11	122.3	H14C10O11O12	180.0

ab initio calculations suggested that the two conformers have a plan of symmetry. The equilibrium structure of the two forms obtained with MP2/6-311++G(d, p) calculation was collected in **Tables 5.6** and **5.7**.

Table 5.8 r_s coordinates of the isotopically substituted 7 atoms of *cis* AA-FA. In parentheses the errors in units of the last digit.

	$a/\text{\AA}$		$b/\text{\AA}$	
	Exp.	Theor.	Exp.	Theor.
C10	$\pm 2.73979(3)$	-2.765	$\pm 0.095(1)$	0.115
C1	$\pm 1.04144(8)$	1.069	$\pm 0.2120(4)$	-0.229
C2	$\pm 2.52577(3)$	2.546	$\pm 0.3786(2)$	-0.363
C3	$\pm 3.32626(4)$	3.334	$\pm 0.6862(2)$	0.722
H14	$\pm 3.82063(3)$	-3.854	$\pm 0.2147(5)$	0.228
H13	$\pm 1.5297(1)$	-1.177	$\pm 1.1491(1)$	1.133
H6	$\pm 1.0425(1)$	-0.520	$\pm 1.2573(1)$	-1.262

Table 5.9 r_s coordinates of the isotopically substituted 7 atoms of *trans* AA-FA. In parentheses the errors in units of the last digit.

	$a/\text{\AA}$		$b/\text{\AA}$	
	Exp.	Theor.	Exp.	Theor.
C10	$\pm 2.7357(3)$	-2.762	$\pm 0.245(4)$	0.265
C1	$\pm 1.0270(9)$	1.049	$\pm 0.254(4)$	0.265
C2	$\pm 2.4951(4)$	2.507	$\pm 0.506(2)$	-0.526
C3	$\pm 3.3959(3)$	3.428	$\pm 0.476(2)$	-0.449
H14	$\pm 3.81043(4)$	-3.850	$\pm 0.3916(4)$	0.403
H13	$\pm 1.7849(1)$	-1.451	$\pm 1.0683(1)$	-1.090
H6	$\pm 1.0440(2)$	-0.268	$\pm 1.0532(2)$	1.093

The rotational constants are available for 7 isotopologues with a single atom isotopic substitution for each complex. It is then possible to determine the r_s substitution coordinates^[17] of the isotopically substituted atoms, 4 carbons, 1 alkyl and 2 carboxyl

hydrogen atoms. The obtained coordinates are reported in **Tables 5.8** and **5.9** for the *cis* and *trans* conformers, respectively, and there compared to the *ab initio* values. Since the complexes are planar, the *c*-coordinates have been fixed to zero.

One can see that the discrepancies between experimental and calculated values of the values of the *a*-coordinates of the carboxylic hydrogens are much larger than the remaining ones.

Such a kind of irregularity concerning the behavior of the OD deuterated species is confirmed by the differences between the model calculated and the observed positions of the rotational transitions of these isotopologues. **Figure 5.4** shown that the experimental (upper lines) and model calculated (with the r_0 structure of **Table 5.10**, lower lines) frequencies (intensities not to scale) of the 5_{05} - 4_{04} transition for all isotopologues of interest. One can see, indeed, that the model works well in predicting the frequency shifts for all ^{13}C and DCOOH species, but not for the carboxylic hydrogen's mono- or bi-deuterated species.

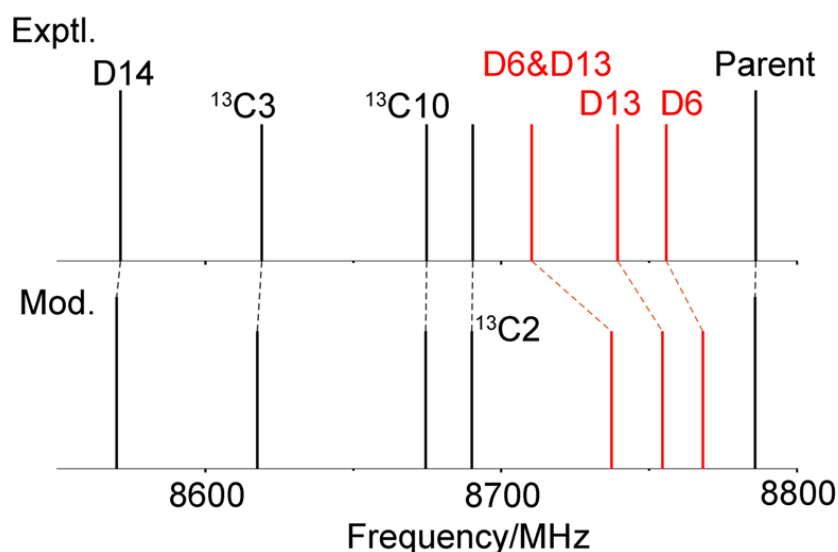


Figure 5.4 Experimental (upper lines) and model calculated (lower lines, see text) frequencies of the 5_{05} - 4_{04} transition for several isotopologues. The irregularities observed for the OD deuterated species (in red) underline the Ubbelohde effect.

It has been possible, however, for both conformers, to give partial r_s geometries for the structural parameters involving the other substituted atoms. In addition, a partial

refinements of the r_e (*ab initio*) structures have been performed in order to minimize the discrepancies between experimental and calculated values of all available rotational constants. The results are compared in **Table 5.10** to the *ab initio* values.

Table 5.10 Experimental (r_s and r_0) and theoretical (r_e , MP2/6-311++G(d, p)) structural parameters of AA-FA.

	Bond distances/Å			Valence angles/°			
	r_s	r_0	r_e		r_s	r_0	r_e
<i>cis</i>							
C1C10	3.7937(1) ^a	3.806(1)	3.850	O11C10C1		59.0(6)	58.5
C1C2	1.4936(1)	1.484 ^b	1.484	C10C1C3	153.89(2)	153.9(2)	152.1
C2C3	1.3321(2)	1.341	1.341	C1O4H13		124.9	127.8
H6O11		1.652	1.725	C10O11H6		123.6	125.7
H13O4		1.663	1.687	O4H13O12		179.1	179.2
H14C10	1.0874(1)	1.096	1.096	O11H6O5		177.5	179.2
				C1C2C3	120.53(2)	120.8	120.8
<i>trans</i>							
C1C10	3.796(1)	3.805(1)	3.850	O11C10C1		58.3(4)	58.4
C1C2	1.490(1)	1.481	1.481	C10C1C3	155.3(2)	154.6(3)	155.4
C2C3	1.333(2)	1.342	1.342	C1O4H13		127.1	128.0
H6O11		1.660	1.721	C10O11H6		125.3	125.7
H13O4		1.661	1.690	O4H13O12		179.0	178.9
H14C10	1.0847(6)	1.096	1.096	O11H6O5		179.2	179.6
				C1C2C3	122.8(2)	123.2	123.2

^aUncertainties (in parentheses) are expressed in units of the last digit. ^bDerived parameters.

Once again, the partial r_0 structure involving the carboxylic hydrogen displays discrepancies with respect to the *ab initio* values. The discrepancies relative to the unexpected changes in the rotational constants upon H → D substitution of the carboxylic hydrogens are removed if an increase the C2...C10 distance was taken into account, which is the considered deuteration cause the two subunits to move slightly apart. This increase can be calculated from the r_s coordinates of two carbon atoms, one belonging to one subunit, and the other to the second subunit. The r_s data are available

only for the *cis* conformer (combining the data from Tables 2, 4 and 5), which are shown in **Table 5.11**.

Alternatively, the r_0 increase of the C2...C10 distance required to match the frequencies of the upper red lines with those of the lower red lines of **Figure 5.4** was calculated. Those shifts are attributable, indeed, to the Ubbelohde effect. This corresponds to change the C2...C10 distance ($r_{\text{C2}\dots\text{C10}}$) in such a way to minimize the difference between the observed and model calculated ($B+C$) values, according to:

$$\Delta(B+C)_{\text{obs}} - \Delta(B+C)_{\text{calc}} = [\partial(B+C)/\partial r_{\text{C2}\dots\text{C10}}]_{p_i=\text{cost}} \Delta r_{\text{C2}\dots\text{C10}}. \quad (5.5)$$

Table 5.11 r_s distances between the C2 and C10 carbon atoms in the parent and some OD deuterated species of *cis* AA-FA, and their shifts upon deuteration.

	$r_s/\text{\AA}$	$\Delta(r_s(\text{D})-r_s(\text{H}))/\text{m\AA}$
Parent	5.2868(3) ^a	
D6	5.2915(12)	+4.6(12)
D13	5.2937(14)	+6.9(14)
D6&D13	5.2961(15)	+10.3(15)

^aUncertainties (in parentheses) are expressed in units of the last digit.

Table 5.12 r_0 shifts (Δr_0) upon deuteration OD of the distances between the C2 and C10 carbon atoms of *cis* and *trans* AA-FA.

	$\Delta(r_0)/\text{m\AA}$	
	<i>cis</i>	<i>trans</i>
D6	+3.8(12) ^a	+4.4(10)
D13	+4.2(12)	+4.4(10)
D6&D13	+8.4(12)	+8.4(10)

^aUncertainties (in parentheses) are expressed in units of the last digit.

The required r_0 corrections upon deuteration are shown in **Table 5.12**.

From the data of **Tables 5.11** and **5.12** the Ubbelohde effect is exactly quantified. As expected, the r_s and r_0 increases are very similar, and the effects of the two single deuterations appear to be additive.

5.5 Conclusions

This is the first study concerning the investigation of the conformational equilibrium, with rotational spectroscopy, which occurs in dimers of carboxylic acids. In addition, the investigation of the rotational spectra of a high number of isotopologues provided accurate structural information. More specifically, the measure of the rotational spectra of the ^{13}C isotopologues of the parent and OD deuterated species allows to sizing the Ubbelohde effect, which for this kind of dimers corresponds to an increase of the distances between the heavy atoms of the two moieties. This effect is reversed with respect to that (some times called reversed Ubbelohde effect) observed in dimers of aliphatic alcohols, where the $\text{OH} \rightarrow \text{OD}$ substitution of the hydrogen involved in the hydrogen bond determine a decrease of $\sim 0.006 \text{ \AA}$ of the $\text{O}\cdots\text{O}$ distance. The different behavior is connected to the two minima (carboxylic acid dimers) or to the single minimum (alcohol dimers) which characterize the corresponding potential energy surfaces.

References

- [1] See Ref.1 in chapter 4.
- [2] G. Feng, L. B. Favero, A. Maris, A. Vigorito, W. Caminati, R. Meyer, *J. Am. Chem. Soc.* **2012**, *134*, 19281.
- [3] L. Evangelisti, P. Écija, E. J. Cocinero, F. Castaño, A. Lesarri, W. Caminati, R. Meyer. *J. Phys. Chem. Lett.* **2012**, *3*, 3770.
- [4] See Ref. 37 in chapter 1.
- [5] A. R. Ubbelohde, K. J. Gallagher, *Acta Crystallogr.* **1955**, *8*, 71.
- [6] R. E. Penn, R. J. Olsen, *J. Mol. Spectrosc.* **1976**, *62*, 423.
- [7] See Ref. 83 in chapter 1.
- [8] M. S. Snow, B. J. Howard, L. Evangelisti, W. Caminati, *J. Phys. Chem. A* **2011**, *115*, 47.

- [9] See Ref. 13 in chapter 2.
- [10] K. Bolton, D. G. Lister, J. Sheridan, *J. Chem. Soc. Faraday Trans. 2*, **1974**, 70, 113.
- [11] See Ref. 12 in chapter 2.
- [12] See Ref. 24 in chapter 4.
- [13] See Ref. 6 in chapter 2.
- [14] See Ref. 9b in chapter 1.
- [15] D. Millen, *Can. J. Chem.* **1985**, 63, 1477.
- [16] S. E. Novick, S. J. Harris, K. C. Janda, W. Klemperer, *Can. J. Phys.* **1975**, 53, 2007.
- [17] See Ref. 11 in chapter 2.

Chapter 6 Conformational equilibria in adducts of alcohols with ethers: the rotational spectrum of ethylalcohol- dimethylether

6.1 Introduction

Many hydrogen-bonded molecular complexes have been investigated by rotational spectroscopy, especially after the development of Fourier transform microwave (FTMW) spectroscopy^[1] Generally, the investigated systems contained a relatively large organic molecule interacting with a small solvent molecule, such as H₂O,^[2] NH₃^[3] or HX^[4] (where X is a halogen atom or a pseudo-halogen group). A wealth of information about their shapes and on the intermolecular interactions has been obtained. More recently, some larger hydrogen bonded molecular complexes, made of two relatively large moieties, have been investigated by FTMW spectroscopy combined with supersonic expansions. Some of these complexes were dimers of chiral alcohols and so related to the topic of molecular recognition. This was the case of butan-2-ol dimer, for which one heterochiral dimer was assigned.^[5] The rotational study of the dimers of glycidol lead to the observation of dimers arising from the combination of different conformers,^[6] so giving insight to the molecular recognition of chiral conformers. Subsequently, the rotational spectra of three conformers of induced chiral dimers of ethanol,^[7] and of 5 conformers of induced chiral dimers of isopropanol^[8] have been reported. From the study of the OD deuterated species of some conformers of the dimer of isopropanol^[8] and of the dimer of tertbutylalcohol,^[9] a quantitative description of the Ubbelohde effect,^[10] that is, a shortening of about 5-7 mÅ of the O...O distance upon H → D substitution has been given. However, no FTMW investigations are available, to date and to our knowledge, concerning adducts formed by the combination of relatively large molecules of alcohols and ethers. In order to obtain information on this class of molecular complexes, the adduct ethylalcohol- dimethylether (EA-DME) was investigated by using FTMW spectroscopy.

Isolated EA is characterized by three conformational minima, two of which (*gauche*) are equivalent, as illustrated in **Figure 6.1**, and correspond to H-C-O-H torsional angles of about 60° and -60° , respectively. The third minimum (*trans* conformation) corresponds to an H-C-O-H torsional angle of 180° . The *trans* species is slightly more stable than the *gauche* one, by 39.2 cm^{-1} ,^[11] but the latter one is slightly more abundant at room temperature. The two *gauche* conformations form an enantiomeric pair. In the monomer, these are rapidly interconverted by quantum mechanical tunneling which occurs at a frequency of around 97 GHz,^[11] constituting then a transient chirality system. However, in the complex, the reduced mass of the tunneling motion would be much larger and it could quench its tunneling effects. Then, assuming that EA will act as a proton donor in forming the O-H \cdots O linkage, the related interesting problematics are: 1) will EA be in its *trans* or *gauche* configuration in the complex, or can both conformers be observed? 2) How will the relative energies of *trans* and *gauche* configurations change upon complexation with DME? 3) in the case EA adopts a *gauche* configuration, what will it happen to its transient chirality? 4) will the Ubbelohde effect produce sizable features in the rotational spectra?

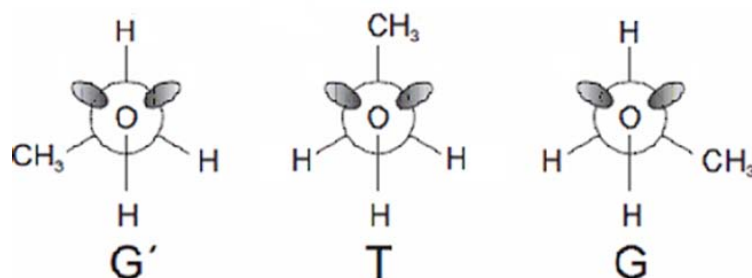


Figure 6.1 The three stable conformations of ethylalcohol (*G* and *G'* are equivalent).

6.2 Experimental section

Commercial samples of EA and DME were used without further purification. A mixture of 1% of DME in Helium at a pressure of ~ 2 bar was flown over EA at room temperature, and expanded through the solenoid valve (General Valve, Series 9, nozzle diameter 0.5 mm) into the Fabry-Pérot cavity to generate the expansion. OD

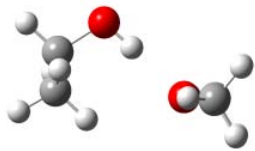
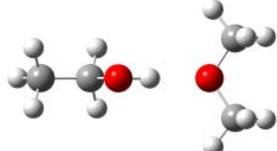
monodeuterated species were observed when flowing DME in Helium over a mixture of EA and D₂O.

6.3 Results and discussion

6.3.1 *Ab initio* calculation

Before collecting the rotational spectra, *ab initio* calculations were performed first using the Gaussian 03 package of programs,^[12] in order to estimate the plausible conformations of the complex and the values of its electric dipole moment components. The geometry of EA-DME is determined by the O-H...O hydrogen bond. The hydrogen bridge length estimated at MP2/6-311++G(d, p) level, for the *gauche* conformer, is 2.828 Å, the OH and O...H are 0.969 and 1.859 Å respectively. Instead, for the *trans* conformer, the hydrogen bridge length is 2.820 Å, the OH and O...H are 0.969, 1.851 Å. The results and the shapes of the two most stable conformers of the complex are shown in **Table 6.1**.

Table 6.1 MP2/6-311++G(d, p) calculated structures, energies and spectroscopic constants of the 2 most stable conformers of EA-DME.

	<i>EA-gauche</i>	<i>EA-trans</i>
		
$\Delta E/\text{cm}^{-1}$	0.0 ^a	108.0
A/MHz	4982.9	7367.5
B/MHz	1410.6	1063.2
C/MHz	1266.5	996.0
μ_a/D	2.6	2.9
μ_b/D	-1.1	0.0
μ_c/D	-1.3	-1.2

^a Absolute energy = -309.281305 E_h .

6.3.2 Rotational spectra and analysis

According to the theoretical values of the rotational constants, of the calculated dipole moment components and of the relative intensities of the predicted rotational transitions in the spectrometer frequency range, the first search has been targeted for the *gauche* conformer, which is expected to be the most stable species. The $J = 3 \leftarrow 2$ μ_a -R-band was observed first, and then the assignment was extended to higher J μ_a -R-lines, up to $J = 6$. Then, it was possible to measure some perpendicular μ_b - and μ_c -type transitions, for a total of 28 transitions. Subsequently, the spectrum of the *trans* conformer was searched, succeeding in observing μ_a -R-bands from $J: 4 \leftarrow 3$ up to $J = 9 \leftarrow 8$. Also some μ_c -type transitions have been measured, for a total of 30 transitions. The spectra were fitted with a Watson's type Hamiltonian (S reduction, F' representation),^[13] obtaining the spectroscopic constants reported in **Table 6.2**.

Table 6.2 Spectroscopic parameters (S -reduction, F' -representation) for the *gauche* and *trans* forms of $\text{CH}_3\text{CH}_2\text{OH}\cdots\text{DME}$ and $\text{CH}_3\text{CH}_2\text{OD}\cdots\text{DME}$.

	<i>Gauche</i>		<i>Trans</i>	
	OH-DME	OD-DME	OH-DME	OD-DME
A/MHz	5020.0468(2) ^a	4993.509(3)	7440.952(6)	7423.715(4)
B/MHz	1369.0730(7)	1370.8588(5)	1048.8480(7)	1050.8140(5)
C/MHz	1221.0046(5)	1222.5066(6)	978.1512(8)	980.2217(6)
D_J/kHz	1.993(8)	1.916(6)	0.668(3)	0.652(5)
D_{JK}/kHz	18.09(5)	18.0(2)	133.95(7)	130.7(2)
D_K/kHz	-108.8(6)	[-108.8] ^b	26(2)	[26]
d_1/kHz	-0.074(7)	[-0.074]	-0.065(6)	[-0.065]
d_2/kHz	-0.20(1)	[-0.20]	-0.038(1)	[-0.038]
σ^e/kHz	5	5	7	4
N^d	28	16	30	12
$P_{aa}/\text{u}\text{\AA}^2$	341.186	340.424	465.296	464.220
$P_{bb}/\text{u}\text{\AA}^2$	72.718	72.972	51.372	51.356
$P_{cc}/\text{u}\text{\AA}^2$	27.954	28.235	16.547	16.720

^a Error in parentheses in units of the last digit. ^b Data in brackets were fixed at the corresponding normal species values because they are not determined in the fit. ^c RMS error of the fit. ^d Number of lines in the

The rotational constants of the two species are so markedly different that the conformational assignment is immediate when comparing the experimental values to the theoretical data of **Table 6.1**.

After a refinement of the intermolecular parameters, the spectra of the OD deuterated species was predicted. All μ_a -R-type transitions were expected at lower frequencies with respect to those of the normal species, due to the decrease of the ($B + C$) rotational parameter. Bands similar to those of the normal species but, for both conformers, at higher frequencies than those of the normal species were observed. This frequency inversion is shown in **Figure 6.2**. However, apart from this effect, the spectra of the deuterated species could be fit with the same procedure used for the normal species, and the obtained spectroscopic parameters are also reported in **Table 6.2**. One can see from the values of the rotational constants given in **Table 6.2** that the H \rightarrow D replacement of the hydroxyl hydrogen participating in the hydrogen bond leads to an increase of these rotational constants. This effect is better outlined by the values of the P_{aa} ($=\sum m_i a_i^2$) planar moments of inertia, which represent the mass distribution along the a -axis. The P_{aa} values decrease, with respect to normal species, upon H \rightarrow D isotopic substitution. This shows unequivocally shrinkage of the complex along the a -axis. To reproduce the value P_{aa} expected in the case of a rigid system for a H \rightarrow D substitution a shortening of about 6 mÅ of the O \cdots O distance is required for both conformers.

6.3.3 Conformational equilibrium

Relative intensity measurements on some pairs of nearby μ_a -type lines of the two conformers allowed measuring the relative population of the two conformers. Because of the relaxation of the molecules in vibrational excited states to the vibrational ground state, $\Delta(\Delta G^0)$ rather than $\Delta E_{0,0}$ can be estimated. There, $\Delta(\Delta G^0)$ is a special kind of difference of free energy, which takes into account only the difference in vibrational state density below the interconversion barrier of the two conformers.

Assuming that the rotational energies of the initial states of the transitions involved in the relative intensity measurements are about the same, the following expression can be used [**Eq. (6.1)**]:^[1]

$$\Delta(\Delta G^0) = \Delta G_{\text{T}}^0 - \Delta G_{\text{G}}^0 = k \cdot T_{\text{room}} \ln[(I_{\text{G}} \omega_{\text{T}} \mu_{\text{a,T}} \gamma_{\text{T}} \nu_{\text{T}}^2) / (I_{\text{T}} \omega_{\text{G}} \mu_{\text{a,G}} \gamma_{\text{G}} \nu_{\text{G}}^2)] \quad (6.1)$$

where I is the peak intensity, ω the conformational degeneracy (2 for *gauche*, 1 for *trans*), $\mu_{\text{a,g}}$ the dipole moment component, γ_{g} the line strength, ν_{g} the transition frequency.

The value $\Delta(\Delta G^0) = 180(50) \text{ cm}^{-1}$ has been obtained. The complexation with DME reverses the conformational equilibrium, and the *gauche* form of ethyl alcohol, less stable in the monomer, becomes the global energy minimum in the adduct. This can be attributed to the secondary interaction between a hydrogen atom of the EA methyl group with the DME oxygen.

6.3.4 Structural analysis

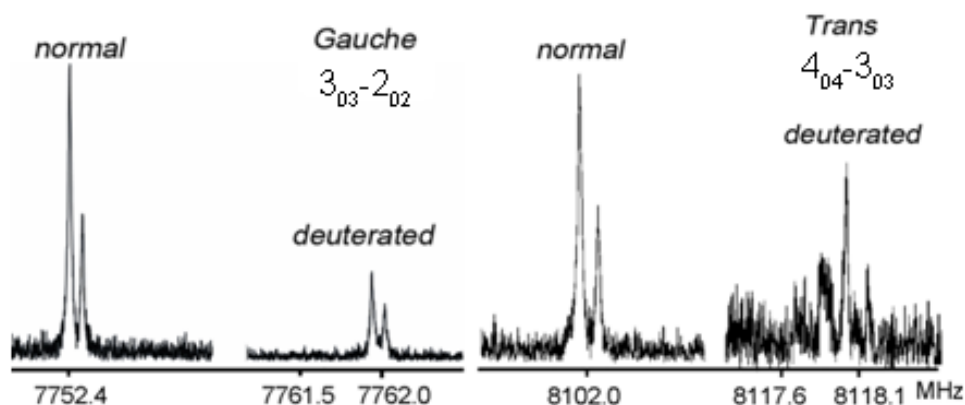


Figure 6.2 Left: The $3_{03} \leftarrow 2_{02}$ transition is shown for the *gauche* form of the $\text{C}_2\text{H}_5\text{OH}\cdots\text{DME}$ and $\text{C}_2\text{H}_5\text{OD}\cdots\text{DME}$ isotopologues; Right: the $4_{04} \leftarrow 3_{03}$ transition is shown for the *trans* species. In both cases, the Ubbelohde effect shifts the frequencies of the heavier isotopologue, $\text{C}_2\text{H}_5\text{OD}\cdots\text{DME}$, to values higher than those of the lighter one, $\text{C}_2\text{H}_5\text{OH}\cdots\text{DME}$.

Usual methods for the determination of the coordinates of the D atom of the hydroxyl group upon isotopic substitution do not work, of course, for the $\text{H} \rightarrow \text{D}$ substitution of the hydrogen involved in the H bond (atom 10 of **Figure 6.3**), because the effect due to the $\text{H} \rightarrow \text{D}$ mass change is overwhelmed by the shortening of the $\text{O}\cdots\text{O}$ distance. The differences between the experimental and theoretical values of the rotational constants (some tens of MHz) are however behind the discrepancies attributable to the different meanings (r_0 and r_e , respectively), so that we corrected two

structural parameters in order to reduce the discrepancies within 1-2 MHz. For both species the increase of H-bond length and the change one angle defining the orientation of DME with respect to the EA unit are required. The effective structures are shown in **Table 6.3** for both conformers. The parameters which needed an adjustment in order to give the experimental rotational constants were indicated in bold. The atom numbering is given in **Figure 6.3**.

Table 6.3 MP2/6-311++G(d, p) geometries of the two conformers of EA-DME. In bold, the parameters which have been adjusted to reproduce the experimental rotational constants

Bond length/Å		Valence angles/°		Dihedral angles/°	
<i>Gauche</i>					
C2O1	1.418				
C3O1	1.418	C3O1C2	111.5		
H4C3	1.090	H4C3O1	107.2	H4C3O1C2	-179.1
H5C3	1.098	H5C3O1	110.9	H5C3O1C2	-59.8
H6C3	1.098	H6C3O1	110.7	H6C3O1C2	61.6
H7C2	1.090	H7C2O1	107.2	H7C2O1C3	179.0
H8C2	1.098	H8C2O1	110.9	H8C2O1C3	59.7
H9C2	1.098	H9C2O1	110.7	H9C2O1C3	-61.7
O11O1	2.869^a	O11O1C2	113.5	O11O1C2C3	-136.9
C12O10	1.420	C12O10O1	105.6	C12H10O1C2	-112.3
C13C11	1.524	C13C11O10	112.2	C13C11O10O1	63.9
H10O11	0.969	H10O11C12	106.4	H10O11C12C13	59.4
H14C12	1.100	H14C12O11	110.8	H14C12O11O1	-64.8
H15C12	1.093	H15C12O11	106.1	H15C12O11O1	178.7
H16C13	1.095	H16C13C12	110.8	H16C13C12O11	177.9
H17C13	1.093	H17C13C12	110.1	H17C13C12O11	57.5
H18C13	1.094	H18C13C12	110.3	H18C13C12O11	-62.3
<i>Trans</i>					
C2O1	1.418				
C3O1	1.418	C3O1C2	111.5		
H4C3	1.090	H4C3O1	107.2	H4C3O1C2	-179.2
H5C3	1.098	H5C3O1	110.9	H5C3O1C2	-59.8
H6C3	1.098	H6C3O1	110.7	H6C3O1C2	61.5
H7C2	1.090	H7C2O1	107.2	H7C2O1C3	179.2
H8C2	1.098	H8C2O1	110.7	H8C2O1C3	-61.5
H9C2	1.098	H9C2O1	110.9	H8C2O1C3	59.8
H10O1	1.863	H10O1C2	116.1	H10O1C2H7	43.2
O11H10	0.969	O11H10O1	183.9	O11H10O1C2	-115.1
C12O11	1.420	C12O11H10	107.0	C12O11H10O1	1.9
C13C12	1.517	C13C12O10	108.2	C13C12O11H10	-179.9
H14C12	1.099	H14C12O11	110.7	H14C12O11H10	-59.6
H15C12	1.099	H15C12O11	110.7	H15C12O11H10	59.7
H16C13	1.094	H16C13C12	110.6	H16C13C12O11	-180.0
H17C13	1.093	H17C13C12	110.1	H17C13C12O11	-59.8
H18C13	1.093	H18C13C12	110.1	H18C13C12O11	59.8

^a The parameters in bold have been adjusted to reproduce the experimental values of the rotational constants. Their *ab initio* values are: a) *gauche*: O11O1=2.828 Å, C13C12O11O1=58.28°; b) *trans*:

$$\text{H10O1} = 1.851^\circ, \text{O11H10O1} = 179.08^\circ.$$

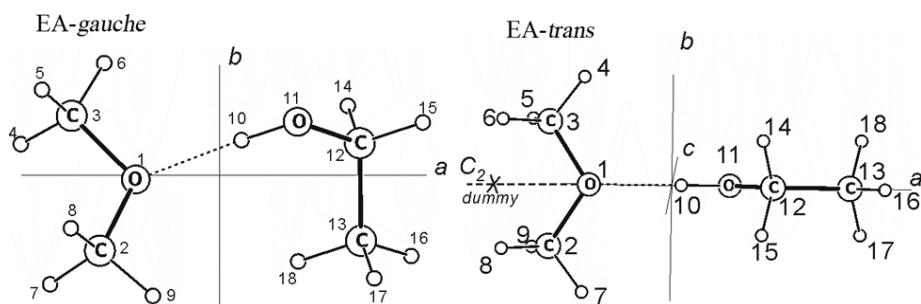


Figure 6.3 Sketch and atom numbering adopted for EA-DME.

6.3.5 Dissociation energy

The dissociation energies (E_B) of the two species of the complex can be calculated from the experimental values of the spectroscopic constants by using the pseudo-diatomic model. This model can supply some reliable, however approximate, values when the stretching motion leading to the dissociation takes place mainly along the a -axis. The stretching force constant (k_s) can be estimated with this approximation as [Eq. (6.2)]:^[14]

$$k_s = 16\pi^4 (\mu R)^2 [4B^4 + 4C^4 - (B-C)^2 (B+C)^2] / (h D_j) \quad (6.2)$$

where μ is the pseudo-diatomic reduced mass, D_j is the centrifugal distortion constant and R is the distance between the centers of mass of the monomers. The values $k_s = 5.2$ and 7.6 Nm^{-1} have been obtained for the *gauche* and *trans* species, respectively. The assumption of a Lennard–Jones-type potential relates the dissociation energy to k_s [Eq. (6.3)]:^[15]

$$E_B = 1/72 k_s R^2, \quad (6.3)$$

from which the values $E_B = 6$ and 11 kJmol^{-1} have been calculated for the *gauche* and *trans* conformers, respectively. Both E_B values appear too low for an O-H...O H-bond, for which values in the range $20\text{--}25 \text{ kJmol}^{-1}$ are expected. However, we can note that for the *trans* species, with the dissociation motion taking place almost along the a -axis, the obtained value is more in line with the bonding energies of this kind of H-

bond. Probably, it is the coupling of the stretching motion leading to the dissociation with the bending or internal rotation motions of one molecule with respect to the second one in the case of the *gauche* species, which make the pseudo-diatomic approximation inadequate.

6.4 Conclusions

The rotational spectrum observed for EA-DME describes two complexes with the two units held together by an O-H \cdots O H bond and which differ in the *gauche* or *trans* configuration of EA. The complexation of EA with DME produces a conformational switch, in the sense that the *gauche* form, less stable in isolated EA, becomes the absolute energy minimum in the complex. The *gauche* form, with a tunneling frequency of 97 GHz between the two equivalent minima in the monomer, becomes a chiral species in complex, in the sense that it does not display any tunneling splitting in the MW timescale. This is related to the higher inertial properties of the tunneling motion, once that the heavy DME group is attached to the hydroxyl hydrogen. Finally, the decrease of the measure of the O \cdots O distance upon H \rightarrow D substitution known as Ubbelohde effect was quantitatively determined.

References

- [1] See Ref. 9b in chapter 1.
- [2] See Ref. 51 in chapter 1.
- [3] See, for example, B. M. Giuliano, S. Melandri, A. Maris, L. B. Favero, W. Caminati, *Angew. Chem. Int. Ed.* **2009**, *48*, 1102 and references therein.
- [4] See, for example, S. Antolínez, J. C. Lépez, J. L. Alonso, *Angew. Chem. Int. Ed.* **1999**, *38*, 1772 and references therein.
- [5] A. K. King, B. J. Howard, *Chem. Phys. Lett.* **2001**, *348*, 343.
- [6] A. Maris, B. M. Giuliano, D. Bonazzi, W. Caminati, *J. Am. Chem. Soc.* **2008**, *130*, 13860.
- [7] J. P. I. Hearn, R. V. Copley, B. J. Howard, *J. Chem. Phys.* **2005**, *123*, 134324.
- [8] M. S. Snow, B. J. Howard, L. Evangelisti, W. Caminati, *J. Phys. Chem. A* **2011**, *115*, 47.
- [9] See Ref. 83 in chapter 1.

- [10] See Ref. 29 in chapter 4.
- [11] C. Pearson, K. V. L. N. Sastry, E. Herbst, F. C. De Lucia, *J. Mol. Spectrosc.* **1996**, 175, 246.
- [12] See Ref. 13 in chapter 2.
- [13] See Ref. 6 in chapter 2.
- [14] See Ref. 15 in chapter 5.
- [15] See Ref. 16 in chapter 5.

Chapter 7 On the weak H \cdots halogen hydrogen bond. A rotational study of CH₃CHClF \cdots H₂O complex

7.1 Introduction

Intra or intermolecular linkages or contacts such as C-H \cdots O, C-H \cdots F, CH \cdots S, C-H \cdots π are generally classified as weak hydrogen bonds (WHB) and represent a major topic in hydrogen-bond research.^[1] While “classical” hydrogen bonds like O-H \cdots O, O-H \cdots N, O-H \cdots S, and N-H \cdots O are characterized (for neutral species) by interactions energies in the range 15-25 kJmol⁻¹, the WHB interactions lie within a few kJmol⁻¹ and approach those of van der Waals forces. However, they have the same directional properties and electron density transfer similar to those of “classical” hydrogen bonds.^[2] A recent IUPAC meeting promotes a redefinition of “hydrogen bonding”,^[3] and it has been even suggested to consider these interactions as only being contacts, reflecting the fact that hydrogen atoms are generally in the external part of a molecular system.

Studies on such WHB have been mainly performed by X-ray diffraction^[4] and IR spectroscopy in rare gas solutions.^[5] Also rotational spectroscopy combined with supersonic expansions has been recently applied in order to study structural and energetic features of these weak interactions. The gas-phase investigations are free from solvent or crystal effects and can give more details on specific or local WHB interactions.^[6] C-H \cdots F,^[7] C-H \cdots O,^[8] CH \cdots S,^[9] C-H \cdots π ,^[10] and C-H \cdots N^[11] linkages have been recently structurally and energetically characterized with this technique.

In this chapter, rotational studies of one kind of WHB, the O-H \cdots Hal interaction (Hal = halogen) are presented. With reference to MW investigations, if we take into account a series of 1,3 substituted propanes, one can see that the rotational spectrum of 1,3 propanediol is formed by the signatures of five conformers, all of them stabilized by O-H \cdots O H-bonds,^[12] while in 3-fluoro-propane-1-ol, two conformers do not have any internal H-bond, and just one, the second in order of stability, is characterized by an

internal O-H···F H-bond.^[13] In the case of 3-chloro-propane-1-ol, two conformers have been observed, both without an internal H-bond.^[14] All these data suggest O-H···Hal (Hal = F, Cl) to be a weak interaction. This is confirmed by the investigations of adducts of water with freons. While in CH₂F₂-H₂O the two constituent molecules are held together by a weak (bonding energy, $E_B = 7.5 \text{ kJmol}^{-1}$) O-H···F bond,^[15] in CF₄-H₂O a halogen bond F···O is observed.^[16]

Naturally the interesting question arises: which of the O-H···Hal WHB is stronger? For example, what are the key interactions that make the O-H···Cl linkage stronger or weaker than the O-H···F one? A few years ago, following the MW study of the chlorofluoromethane (CFM)-water complex, where only the form with an O-H···Cl interaction was observed ($E_B = 8.5 \text{ kJmol}^{-1}$), the O-H···Cl was suggested to be stronger.^[17]

1-chloro-1-fluoroethane (Freon 151, from now CFE), has a structure similar as chlorofluoromethane, but with a hydrogen atom substituted by methyl group. The microwave spectrum of CFE has been first studied by Thomas *et al.*^[18] with a conventional Stark modulation spectroscopy and by Hinze *et al.*^[19] with Fourier transform microwave spectroscopy, but the complex of CFE with water is not reported. The information of intermolecular interaction between CFE and water will be helpful in understanding the behavior of CFE in atmosphere. Moreover, experimental results can prove which kind of interaction is preferred in the complex.

7.2 Experimental section

Commercial samples of CFE and deuterated water (98% enriched) were obtained from Aldrich and were used without further chemical treatment. Oxygen 18 water (98% enriched,) was obtained from CIL and used without further purification.

For searching for the rotational transitions of the complex of CFE/water, a gas mixture of 2% CFE in Helium at a total pressure of 3 bar was streamed over water at room temperature, and expanded through the solenoid valve (General Valve, Series 9, nozzle diameter 0.5 mm) into the Fabry-Pérot-type cavity.

Each rotational transition displays an enhanced Doppler splitting that originates from the supersonic jet expanding coaxially along the resonator axes. The rest frequency was calculated as the arithmetic mean of the frequencies of the two Doppler components. The estimated accuracy of the frequency measurements is better than 3 kHz, resolution is better than 7 kHz.

7.3 Results and discussion

7.3.1 Theoretical calculations

Before collecting the rotational spectra, full geometry optimization of the complexes were performed at the MP2/6-311++G(d, p) level theory with Gaussian 03 program.^[20]

Three stable conformers were found. Their shapes are shown in **Figure 7.1**, in order of stability. Their relative energies (ΔE), rotational and quadrupole coupling constants, and dipole moment components are reported in **Table 7.1**. Conformer I and conformer III display an O-H \cdots F interaction, whereas conformer II displays an O-H \cdots Cl interaction. The three forms of the complex are almost isoenergetic, their energies being within 160 cm⁻¹.

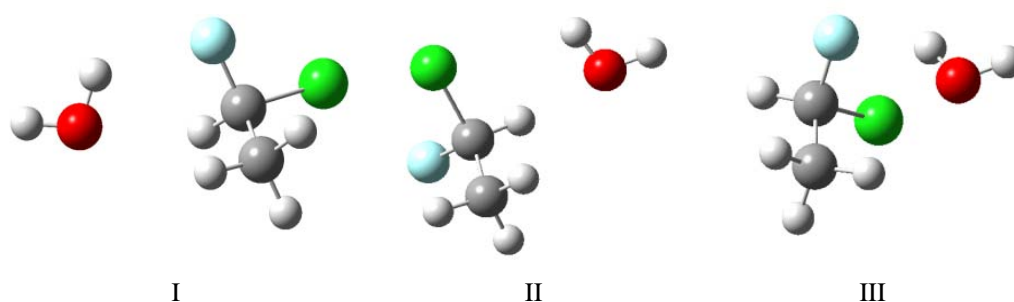


Figure 7.1 The three most plausible structures of the complex of water with CFE.

A counterpoise correction^[21] to the MP2/6-311++G(d, p) calculated energies (E_{BSSE}) was performed in order to remove the well known basis set superposition error (BSSE). The results shown the global minimum remains the same and the relative

energies of other conformers are in the same sequence but with the energy gaps slightly increasing.

Table 7.1 MP2/6-311++G(d, p) spectroscopic parameters of the plausible conformers of CFE-H₂O

	I	II	III
A/MHz	6541.6	3866.1	4131.3
B/MHz	1650.8	2230.3	1993.9
C/MHz	1503.1	1734.0	1802.9
χ_{aa}/MHz	-61.9	28.0	11.6
$(\chi_{bb}-\chi_{cc})/\text{MHz}$	-3.2	-85.9	-71.5
$ \mu_a /\text{D}$	2.0	3.2	0.8
$ \mu_b /\text{D}$	0.2	0.5	0.6
$ \mu_c /\text{D}$	0.3	0.2	0.2
$\Delta E/\text{cm}^{-1}$	0 ^a	58	156
$\Delta E_{\text{BSSSE}}/\text{cm}^{-1}$	0 ^b	123	188

^a Absolute energy: -284.981011 E_h . ^b Counterpoise corrected energy, absolute value is -713.990157

E_h .

7.3.2 Rotational spectra

According to the *ab initio* results, the first search for rotational transitions was focused on the μ_a -type transitions of conformers I and II. The first observed lines were assigned to $J = 3 \leftarrow 2$ band, $K_a = 0, 1$ transitions of conformer I, based on the considerably different expected quadrupole hyperfine structures between the two conformers. Only the rotational spectrum of conformer I was found and assigned. Each line was split into several components due to the nuclear quadrupole coupling of ³⁵Cl nucleus and appeared as a doublet because of the Doppler effect.

None of the observed transitions was split for internal rotation effects of the water moiety, suggesting that water should be quite “rigid” within the complex. **Figure 7.2** shows the quadrupole hyperfine structure of the $3_{0,3} \leftarrow 2_{0,2}$ transition.

The measured lines were used to determine the spectroscopic constants collected in **Table 7.2**. The fits were performed using Pickett's SPFIT program,^[22] according to the Hamiltonian:

$$H = H_R + H_{CD} + H_Q \quad (7.1)$$

where H_R represents the rigid rotational part of the Hamiltonian, H_{CD} represents the centrifugal distortion contributions and is analyzed using the S reduction in the F' representation,^[23] and H_Q represents the interaction of ^{35}Cl (or ^{37}Cl) nucleus quadrupole moment with the overall rotation.^[24]

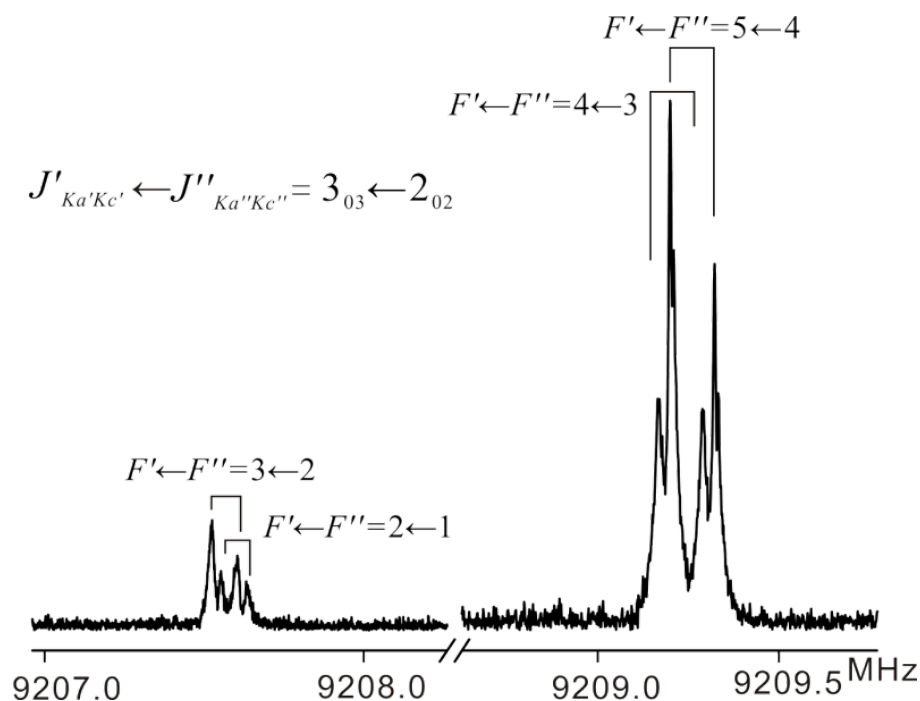


Figure 7.2 Recorded $3_{03} \leftarrow 2_{02}$ transition of the observed conformer of CFE- H_2O showing the ^{35}Cl hyperfine structure. Each line displays the Doppler doubling.

After the assignment of the spectrum of the normal species, the structure was adjusted successively to reflect the experimental rotational constants. Then the spectra of the ^{37}Cl , HOD, DOH, DOD and H_2^{18}O isotopologues were searched and assigned. These spectra were fitted with the same procedure described above for the normal one. The intensities of the rotational transitions of the CFE \cdots DOH species were about 50% stronger than those of the CFE \cdots HOD isotopologue, most likely because of zero-

vibrational energy contributions. The derived spectroscopic parameters are collected in the second and third data columns in **Table 7.2** for the ^{37}Cl and H_2^{18}O , and in **Table 7.3** for the deuterated species.

Table 7.2 Spectroscopic constants of three isotopomers of CFE-W (*S*-reduction, *I'* representation).

	Parent	$^{37}\text{Cl}(\text{CFE-H}_2\text{O})$	$\text{CFE-H}_2^{18}\text{O}$
A/MHz	6515.5 (1) ^a	6496.6 (5)	6477.8(1)
B/MHz	1609.0827 (3)	1575.4871(2)	1521.1690(2)
C/MHz	1465.4267 (3)	1437.5705(2)	1393.4850(2)
χ_{aa}/MHz	-63.467 (8)	-50.19 (1)	-94.71(3)
$(\chi_{bb}-\chi_{cc})/\text{MHz}$	-4.054 (9)	-3.12 (9)	-1.03(1)
χ_{ab}/MHz	-23.1(3)	-21.6 (5)	-22.8(6)
D_J/kHz^b	1.954 (3)	1.843 (8)	-1.827(3)
D_{JK}/kHz	16.91 (5)	17.55 (5)	16.9 (0)
d_1/Hz	5 (3)	[5] ^c	[5] ^c
d_2/Hz	22 (2)	[22] ^c	[22] ^c
N^d	54	41	29
σ^e/kHz	2.6	4.4	2.0

^a Errors in parenthesis are expressed in units of the last digit. ^b The omitted quartic centrifugal distortion constant, D_K , is undetermined from the fit and has been fixed to zero. ^c Values in brackets have been fixed to the values of the “normal” (i.e. most abundant) species. ^d Number of fitted lines. ^e Standard deviation of the fit.

Table 7.3 Spectroscopic constants of three H_2O deuterated species of CFE-W (*S*-reduction, *I'* representation).

	CFE-DOH	CFE-HOD	CFE-DOD
A/MHz	6500.4(1) ^a	6483.1(5)	6460.7(3)
B/MHz	1576.9202(2)	1538.1134(3)	1509.3648(3)
C/MHz	1435.0612(2)	1406.6168(3)	1379.3846(3)
χ_{aa}/MHz	-63.26(2)	-63.060(4)	-63.08(2)
$(\chi_{bb}-\chi_{cc})/\text{MHz}$	-3.97(1)	-3.78(1)	-4.13(1)
χ_{ab}/MHz	-28.4(5)	-27.0(6)	-24.3(5)
D_J/kHz^b	1.856(3)	1.867(4)	1.655(4)
D_{JK}/kHz	16.5(1)	18.4(2)	15.7(2)
N^c	37	26	28
σ^d/kHz	6.3	7.0	4.6

^a Errors in parenthesis are expressed in units of the last digit. ^b The omitted quartic centrifugal distortion constants, D_K , d_1 , d_2 are undetermined from the fit and have been fixed to zero. ^c Number of fitted lines. ^d Standard deviation of the fit.

7.3.3 Conformation and structure

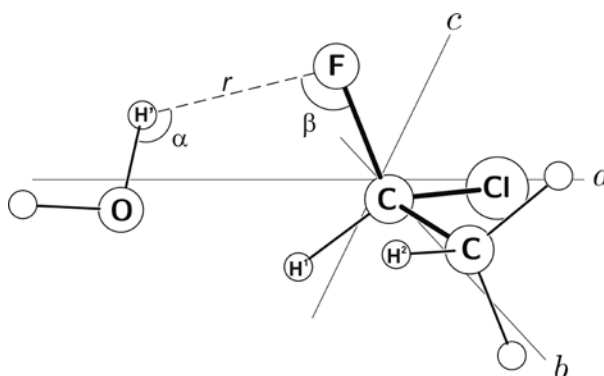


Figure 7.3 Some structural parameters used through the text are indicated in the sketch of the observed conformer of CFE-W.

Table 7.4 r_s coordinates of the isotopically substituted atoms of CFE/H₂O.

	$ a /\text{Å}$		$ b /\text{Å}$		$ c /\text{Å}$	
	exptl.	calc.	exptl	calc.	exptl	calc.
Cl	1.832(9) ^a	1.823	0.235(3)	0.233	0.251(7)	0.270
H _{W,Hbond}	2.604(6)	2.604	0.748(2)	0.759	0.610(2)	0.199
H _{W,Free}	3.781(4)	3.814	0.408(3)	0.520	0.495(3)	0.679
O	3.003(5)	2.945	0.168(8)	0.168	0.466(3)	0.478

^a Uncertainties (in parentheses) are expressed in units of the last digit.

Table 7.5 Partial r_0 geometry of CFE-W.

Fitted parameters:		Derived parameters:	
$r(\text{O}\cdots\text{F})/\text{Å}$	2.910(4) ^a	$r/\text{Å}$	2.140
$a(\text{O}\cdots\text{F}-\text{C})/^\circ$	87.4(1)	$a/^\circ$	98.7
$d(\text{O}\cdots\text{F}-\text{C}-\text{Cl})/^\circ$	156.6(9)	$\beta/^\circ$	136.2
$a(\text{H}^1-\text{O}\cdots\text{F})/^\circ$	30.6(1)	$r(\text{O}\cdots\text{H}^1\text{C})/\text{Å}$	2.753
$d(\text{H}^1-\text{O}\cdots\text{F}-\text{C})/^\circ$	-211.7(6)	$r(\text{O}\cdots\text{H}^2\text{C})/\text{Å}$	2.842
$d(\text{H}-\text{O}-\text{H}^1\cdots\text{F})/^\circ$	-149.3(4)	$R_{\text{CM}}/\text{Å}$	3.756

^a Uncertainties (in parentheses) are expressed in units of the last digit. Here, the distance R_{CM} is the separation between the centers of mass of the two constituent molecules (3.756 Å).

The values of rotational and Cl quadrupole coupling constants are in very good agreement with those calculated for form I, so that the conformational assignment is straightforward.

In addition, the r_s substitution coordinates^[25] of the isotopically substituted atoms, Cl, O, and H atoms of water, reported in **Table 7.4**, are in good accord with the *ab initio* values. The only remarkable discrepancy is the $|c|$ coordinate of the water hydrogen involved in the hydrogen bond, a quite frequent effect, related to the shrinkage of the H-bond upon H→D isotopic substitution.

A partial r_0 structure was calculated from the six sets of experimental rotational constants, with the geometry of water^[26] and CFE^[27] fixed to the structure of the isolated molecules. r_0 values of $r(\text{O}\cdots\text{F})$, $\angle(\text{O}\cdots\text{F}-\text{C})$, $\angle(\text{O}\cdots\text{F}-\text{C}-\text{Cl})$, $\angle(\text{H}'-\text{O}\cdots\text{F})$, $\angle(\text{H}'-\text{O}\cdots\text{F}-\text{C})$ and $\angle(\text{H}-\text{O}-\text{H}'\cdots\text{F})$ are calculated and reported in **Table 7.5**. The alternative H-bond parameters r , α , β , $r(\text{O}\cdots\text{H}^1)$ and $r(\text{O}\cdots\text{H}^2)$ and R_{CM} given with **Figure 7.3**, have been derived from the fitted parameters and reported in the right part of **Table 7.5**.

7.3.4 Dissociation Energy

The three translational motions and the three rotational degree of freedom of the isolated water molecule are replaced by six low-energy vibrations upon formation of the complex. One of them can be thought, in a first approximation, as the stretching between the two centers of mass of the two forming molecules. When this stretching motion takes place along the inertial a -axis of the complex, it is possible to roughly evaluate the dissociation energy with the approximate pseudiatomic molecule model. Within this approximation, the stretching force constant (k_s) can be estimated by considering the complex as made of two rigid parts, and using the following equation^[28]

$$k_s = 16\pi^4 (\mu R_{\text{CM}})^2 [4B^4 + 4C^4 - (B-C)^2 (B+C)^2] / (h D_J) \quad (7.2)$$

where μ is the pseudo-diatomic reduced mass, D_J is the centrifugal distortion constant and R_{CM} is the distance between the centers of mass of the monomers. The

value $k_s = 4.60 \text{ Nm}^{-1}$ was obtained, which corresponds to a harmonic stretching frequency of 73 cm^{-1} .

By assuming a Lennard-Jones-type potential the dissociation energy has been estimated by applying the approximate formula:^[29]

$$E_B = 1/72 k_s R_{CM}^2 \quad (7.3)$$

from which the value $E_B = 5.4 \text{ kJmol}^{-1}$ was obtained.

This value is similar to the dissociation energies determined for the related molecular complexes with a O-H...Hal linkage, difluoromethane-water^[15] and chlorofluoromethane-water.^[17] Their values are reported in **Table 7.6**.

All these dissociation energy values are smaller than typical E_B values underlying classical (O-H...O, O-H...N, O-H...S, and N-H...O) hydrogen bonds.

Table 7.6 Dissociation energies (E_B) for some molecular complexes with water linked to the partner molecule through a O-H...Hal WHB.

Complex	O-H...Hal	E_B/kJmol^{-1}	Ref.
CH ₂ F ₂ -W	O-H...F	7.5	15
CH ₂ ClF-W	O-H...Cl	8.5	17
CH ₃ CHClF-W	O-H...F	5.4	this work

7.4 Conclusions

The absolute minimum conformation and structure of the 1 : 1 adduct of CFE and water was established by investigating the rotational spectra of several isotopic species. A few years ago, according to the MW spectrum of CH₂ClF-H₂O, it was stated that the O-H...Cl hydrogen bond is stronger than the O-H...F one. Now, the MW spectrum of CFE-W seems to indicate the contrary. The two interactions have very similar energies

and it is the contribution of other effects, such as the stabilizing presence of secondary C–H \cdots O contacts and/or even small local dipole–dipole interactions, which steer and self-align the moieties into their preferred absolute configuration.

The dissociation energy of CFE–H₂O has been estimated to be 5.4 kJmol⁻¹, a value similar to that of other complexes with an O–H \cdots Hal linkage. This value suggests classification of this kind of interaction as a WHB. In CH₂F₂–H₂O and in CH₂ClF–H₂O the water unit was undergoing a feasible internal rotation around its symmetry axis, reflected by two tunneling component lines for each rotational transition. Rather unexpectedly, such a tunneling effect was not observed in CFE–H₂O: so water appears to be more weakly bound to the partner molecule, but its internal rotation is more hindered than in the two other cases. Probably, the secondary H-bonds between O and H¹C and H²C (see **Figure 7.3**) with O \cdots H¹C and O \cdots H²C distances of only ~2.7–2.8 Å (see **Table 7.5**) render the internal rotation of water more hindered than in other cases.

Despite the *ab initio* calculations suggesting two additional configurations of similar stability with energies only slightly higher than that of the observed one, their rotational lines could not be observed. This is rationalized by the fact that the different conformers are separated by only low interconversion barriers that allow for efficient relaxation into the global minimum. It has been shown, indeed, that for barriers smaller than $2kT$ (ca. 420 cm⁻¹ in our case), such a relaxation takes place.^[30] In addition, it is likely that the two molecular subunits experience repeated formation and dissociation in the jet expansion.^[31] Also this would lead to a strong preference for the most stable conformer in a jet expansion.

In this complex, two different halogens are involved with different diameters (and thus also size of the free electron pair) and different polarizabilities. Then the geometry of the organic frame sets constraints on the kind of directivity (which is supposed to be the characteristic feature of an H-bond compared to vdW or other mainly electrostatically driven interactions) that can be obtained if two interactions are present.

Finally, the spectroscopic findings in a situation that takes place at such a small energy scale represent evidence much stronger than quantum-chemical predictions at every available level.

References

- [1] See Ref. 45 in chapter 1.
- [2] P. L. A. Popelier, *J. Phys. Chem. A* **1998**, *102*, 1873.
- [3] http://www.iupac.org/web/nt/2010-10-25_hydrogen_bond.
- [4] See Ref. 46 in chapter 1.
- [5] S. N. Delanoye, W. A. Herrebout, B. J. van der Veken, *J. Am. Chem. Soc.* **2002**, *124*, 1154.
- [6] See Ref. 9b in chapter 1.
- [7] See, for example, W. Caminati, J. C. López, J. L. Alonso, J.-U. Grabow, *Angew. Chem. Int. Ed.* **2005**, *44*, 3840 and references therein.
- [8] See, for example, Y. Tatamitani, B. Liu, J. Shimada, T. Ogata, P. Ottaviani, A. Maris, W. Caminati, J. L. Alonso, *J. Am. Chem. Soc.* **2002**, *124*, 2739.
- [9] E. J. Cocinero, R. Sanchez, S. Blanco, A. Lesarri, J. C. López, J. L. Alonso, *Chem. Phys. Lett.* **2005**, *402*, 4.
- [10] J. C. López, J. L. Alonso, W. Caminati, *Angew. Chem. Int. Ed.* **2006**, *45*, 290.
- [11] L. B. Favero, B. M. Giuliano, A. Maris, S. Melandri, P. Ottaviani, B. Velino, W. Caminati, *Chem.–Eur. J.* **2010**, *16*, 1761.
- [12] W. Caminati, S. Melandri P. G. Favero, *J. Mol. Spectrosc.* **1995**, *171*, 394; D. F. Plusquellic, F. J. Lovas, B. H. Pate, J. L. Neill, M. T. Muckle, A. J. Remijan, *J. Phys. Chem. A* **2009**, *113*, 12911.
- [13] W. Caminati, *J. Mol. Spectrosc.* **1982**, *92*, 101.
- [14] M. J. Fuller, E. B. Wilson, Jr. W. Caminati, *J. Mol. Spectrosc.* **1982**, *96*, 131.
- [15] W. Caminati, S. Melandri, I. Rossi, P. G. Favero, *J. Am. Chem. Soc.* **1998**, *121*, 10098.
- [16] W. Caminati, A. Maris, A. Dell'Erba, P. G. Favero, *Angew. Chem. Int. Ed.* **2006**, *45*, 6711.
- [17] W. Caminati, S. Melandri, A. Maris, P. Ottaviani, *Angew. Chem. Int. Ed.* **2006**, *45*, 2438.
- [18] C. H. Thomas, K. D. Nisbet G. Graner, *J. Chem. Phys.* **1974**, *61*, 5072.
- [19] R. Hinze, A. Lesarri, J. C. López, J. L. Alonso, A. Guarnieri, *J. Chem. Phys.* **1996**, *104*, 9729.
- [20] See Ref. 13 in chapter 2.
- [21] See Ref. 12 in chapter 2.
- [22] See Ref. 24 in chapter 4.
- [23] See Ref. 6 in chapter 2.
- [24] J. K. Bragg, *Phys. Rev.* **1948**, *74*, 533.
- [25] See Ref. 11 in chapter 2.
- [26] F. C. Lucia, P. Helminger, W. Gordy, *Phys. Rev. A* **1973**, *8*, 2785.
- [27] W. Caminati, unpublished data.
- [28] See Ref. 15 in chapter 5.

- [29] See Ref. 16 in chapter 5.
- [30] R. S. Ruoff, T. D. Klots, T. Emilson, H. S. Gutowski, *J. Chem. Phys.* **1990**, *93*, 3142.
- [31] See for example, J. Thomas, F. X. Fumie, N. Nicole, Y. Xu, *Chem.–Eur. J.* **2011**, *17*, 4582.

Chapter 8 On the halogen bond. A rotational study of $\text{CF}_3\text{Cl}\cdots\text{H}_2\text{O}$ and $\text{CF}_3\text{Cl}\cdots\text{NH}_3$ complex

8.1 Introduction

Halogen bond (HaB) is one kind of non-covalent interaction that in some cases it has been found to be competitive or preferred to hydrogen bond (HB). Overviews on HaB are available,^[1] as well parallelisms with HB.^[2] Its importance in supermolecular chemistry and in crystal engineering has been outlined in several papers.^[3] Most of the investigations dedicated to HaB come from X-rays diffraction and are relative to the solid state.^[4]

Studies of small isolated complexes formed by two subunits held together by HaB interactions can give information on this interaction, neat of solvent effects or solid state linkages. Some studies in this sense have been performed by vibrational spectroscopy on HaB bonded complexes in cryo solutions by van der Veken and collaborators.^[5]

Accurate details on the nature of the HaB in the gas phase can be obtained by rotational spectroscopy of molecular complexes, as shown in some review or perspective articles by Legon.^[6, 7] There, FTMW spectroscopy studies of a series of $\text{B}\cdots\text{XY}$ complexes, where B is the electron donor and XY is the dihalogen molecule, are reviewed, to reveal some properties of the HaB interaction. For example, information on radial and angular geometry, on the intermolecular stretching forces and on the extent of charge redistribution upon formation of the HaB has been reported. These studies also proved that HaB is more linear than hydrogen bond, with $\text{B}\cdots\text{X-Y}$ angles close to 180° .

Freons seem to be ideal molecules for studying either weak hydrogen bonding interaction or halogen bonding interactions. Interesting results have been obtained by rotational spectroscopy in supersonic expansions of some Freon-water complexes.

Weak $F\cdots H-O$ hydrogen bonds have been found to play the main role in the formation of the CH_2F_2 -water^[8] and CH_3CHFCl -water^[9] complexes, while a $Cl\cdots H-O$ linkage is preferred in the CH_2FCl -water system.^[10] Vice versa, in CF_4 -water complex, it is a HaB interaction which plays a crucial role in forming the complex ($F\cdots O$).^[11]

An intriguing question is how a water molecule will interact with multihalogenated molecules, containing different halogen atoms, such as CF_3Cl (Freon-13).

In the CF_3Cl-H_2O complex, several configurations are possible and it appears difficult to state which one is the global minimum, that is, which one is the predominant interaction. Will the leading interaction in the complex be a hydrogen bond? And, in such a case, which halogen atom, chlorine or fluorine, will be involved in the H bond? Or, if a HaB is preferred, will it be an $O\cdots F$ or an $O\cdots Cl$ bond? The investigation of the high-resolution rotational spectrum of the CF_3Cl-H_2O complex should answer these questions.

Ammonia, similarly to water, can in principle act as a proton donor or a halogen acceptor when forming complexes with CF_3Cl . A theoretical study on the halogen bonds involved in adducts of ammonia with halofluoromethanes estimates the energy of this kind of interaction to be similar to that of a strong hydrogen bond, increasing from $X = Cl, Br$, to $X = I$.^[12] The complexes of trimethylamine with CF_3X , all of them with a $C-X\cdots N$ HaB, have been investigated by FTIR spectroscopy in cryogenic solutions.^[5] These $C-X\cdots N$ HaB appear similar to the $C-X\cdots O$ HaB.

No information on halogen bonds between freons and ammonia has been obtained, however, with high resolution rotational spectroscopy. For this reason, the rotational spectrum of the complex CF_3Cl-NH_3 was also investigated. The aim is to give an answer to the following questions: which kind of interaction, a halogen bond interaction or a hydrogen bond interaction, is preferred? And, if a HaB is formed, will it be a $F\cdots N$ or a $Cl\cdots N$ one?

8.2 Experimental section

A commercial sample of chlorotrifluoromethane, NH_3 , and ND_3 were purchased from Aldrich and used without further purification. While $^{15}\text{NH}_3$ (98% enriched) was purchased from ISOTECH. D_2O and H_2^{18}O water were used to measure the spectra of the deuterated and ^{18}O isotopologues.

For observing the rotational spectra of chlorotrifluoromethane/water, a gas mixture of ~1% chlorotrifluoromethane in Helium at a total pressure about 3 bar was flown over the water and expanded through in room temperature the solenoid valve (General Valve, Series 9, nozzle diameter 0.5 mm) into the Fabry-Pérot cavity.

For observing the rotational spectra of chlorotrifluoromethane/ammonia, a gas mixture of 2% CF_3Cl and ammonia in Helium at a total pressure of 3 bar was expanded through the solenoid valve (General Valve, Series 9, nozzle diameter 0.5 mm) into the Fabry-Pérot cavity.

Each rotational transition displays an enhanced Doppler splitting that originates from the supersonic jet expanding coaxially along the resonator axes. The rest frequency was calculated as the arithmetic mean of the frequencies of the two Doppler components. The estimated accuracy of the frequency measurements is better than 3 kHz, resolution is better than 7 kHz.

8.3 Chlorotrifluoromethane/water

8.3.1 Theoretical calculations

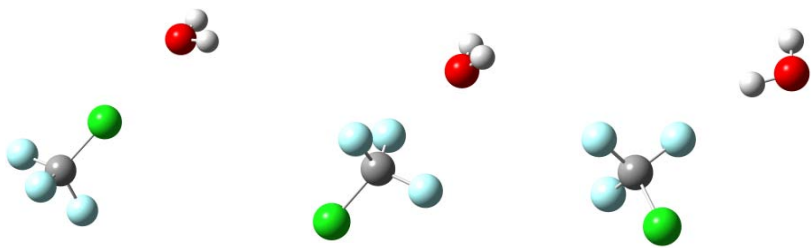
MP2/6-311++G(d, p) geometry optimization calculations were performed by using Gaussian 03 suite of programs^[13] before collecting the rotational spectra. The complex can be formed via either halogen bond interaction or HaB interaction. Three stable conformations have been obtained. The most stable conformer, as labeled as I in **Table 8.1** was formed via a $\text{Cl}\cdots\text{O}$ interaction. Conformer II and III were formed via $\text{F}\cdots\text{O}$

interaction and F \cdots H-O interaction, respectively. Theoretical rotational constants, dipole moments, quadrupole coupling constants and the dissociation energy of the three conformers are collected in **Table 8.1**.

The frequency calculations were conducted to obtain the zero point corrected energy, which also confirmed the three conformers were the real minimums. Counterpoise corrections^[14] were used to remove the well known basis set superposition error (BSSE).

Table 8.1 *Ab initio* (MP2/6-311++G(d, p)) values of spectroscopic constants of the three more stable conformers of the CF₃Cl–H₂O complex.

Parameter	I	II	III
Contact	O \cdots Cl	O \cdots F	O-H \cdots F
<i>A</i> /MHz	5638.6	5624.5	3499.9
<i>B</i> /MHz	1105.1	1436.8	1216.0
<i>C</i> /MHz	1102.6	1431.7	1071.6
μ_a /D	3.34	-1.77	-0.86
μ_b /D	0.03	0.04	-1.42
μ_c /D	0.00	-0.01	0.03
χ_{aa} /MHz ^a	-74.5	-72.3	20.4
χ_{bb} /MHz	37.5	36.2	-57.6
E_0 /cm ⁻¹	0 ^b	261	469
D_0 /kJmol ^{-1c}	11.1	7.9	5.4
D_{CP} /kJmol ⁻¹	6.5	0.7	1.7



^a μ_g and χ_{gg} (g=a,b,c) are the dipole-moment components and the ³⁵Cl quadrupole coupling constants, respectively, χ_{cc} is the completion to 0 of χ_{aa} and χ_{bb} . ^b E_0 is the ZPE corrected relative energy of each conformer. The absolute value of the MP2 energies is -872.960975 E_h . ^c D_0 and D_{CP} are the dissociation energies without and with counterpoise corrections, respectively.

8.3.2 Rotational spectra

According to the indication of *ab initio* calculations, the first searched was targeted for μ_a -type transitions of conformer I, II and III. Rather surprisingly, only a symmetric rotor spectrum could be identified, when all the predicted structures suggested asymmetric rotors. Some questions arise. Has the potential-energy surface be explored correctly and had any structure be missed? Was the theory wrong and was there a conformer, predicted to be an asymmetric rotor, which was effectively a symmetric rotor?

Indeed, it was found that compact sets of transitions evenly spaced by a quantity that is very close to the theoretical $(B + C)$ value (B and C are rotational constants) of the conformer predicted to be most stable. Following this conformational assignment, the rotational spectra of the isotopologues $\text{CF}_3^{37}\text{Cl-H}_2\text{O}$, $\text{CF}_3^{35}\text{Cl-H}_2^{18}\text{O}$, $\text{CF}_3^{35}\text{Cl-OHD}$, and $\text{CF}_3^{35}\text{Cl-D}_2\text{O}$ were easily predicted and assigned.

Although the rotational spectra have been observed readily, the data-fitting procedure was complicated mainly because of the overlap of various K -component lines (K is the quantum number of the projection of the rotational angular momentum along the axis of symmetry of the complex) of the corresponding hyperfine ^{35}Cl (or ^{37}Cl) quadrupole coupling structures. However, it was possible to obtain good fit functions by using Pickett's SPFIT program,^[15] according to the Hamiltonian:

$$H = H_R + H_{CD} + H_Q \quad (8.1)$$

where H_R represents the rigid rotational part of the Hamiltonian, H_{CD} represents the centrifugal distortion contributions and H_Q represents the interaction of ^{35}Cl (or ^{37}Cl) nucleus quadrupole moment with the overall rotation.^[16] As a consequence of the symmetric-top characteristic of the spectra, only one quadrupole coupling constants, χ_{aa} , was determined.

For the $\text{CF}_3^{35}\text{Cl-H}_2\text{O}$ and $\text{CF}_3^{37}\text{Cl-H}_2\text{O}$ complexes, transitions originating from $m = \pm 1$ and $K = 0$ were measured and fitted. The $K=1$ transitions were observed but were

not fitted because, similar to other cases, the data are affected by the odd powers of the angular momenta.^[11, 17, 18]

The relaxation process upon supersonic expansions of the metastable ($m = \pm 1$) state to the ground ($m = 0$) state is outlined^[19] to be nuclear-spin-forbidden for the “symmetric” species $\text{CF}_3\text{Cl-H}_2\text{O}$, $\text{CF}_3\text{Cl-D}_2\text{O}$, and $\text{CF}_3\text{Cl-H}_2^{18}\text{O}$. However, the spectrum of $m = \pm 1$ were measured for the most abundant species. The experimental spectroscopic constants are reported in **Table 8.2** for all isotopologues. A part of the spectrum corresponding to the $J: 4 \leftarrow 3$ transition of the $\text{CF}_3^{35}\text{Cl-H}_2\text{O}$ main isotopic species is shown in **Figure 8.1**.

Table 8.2 Experimental spectroscopic constants of the observed conformers of $\text{CF}_3\text{Cl-H}_2\text{O}$

$m = 0$	$\text{CF}_3^{35}\text{Cl-H}_2\text{O}$	$\text{CF}_3^{37}\text{Cl-H}_2\text{O}$	$\text{CF}_3\text{Cl-D}_2\text{O}$	$\text{CF}_3\text{Cl-HOD}$	$\text{CF}_3\text{Cl-H}_2^{18}\text{O}$
B/MHz	1094.0577 (3) ^a	1091.5176(3)	1014.4074(1)	1052.3865(6)	1031.5384(7)
χ/MHz	-78.42(7)	-61.82(6)	-78.35(1)	-78.40(6)	-78.46(7)
D_J/kHz	0.653 (5)	0.636(4)	0.578(2)	0.62(1)	0.55(2)
D_{JK}/kHz	10.33(5)	10.11	9.921(8)	10.45(5)	103.7(2)
σ^b/kHz	2	5	1	1	7
N^c	36	35	39	24	25
<hr/>					
$m = \pm 1$					
B/MHz	1093.6729(5)	1091.1357(8)			
χ/MHz	-78.39(1)	-61.87(8)			
D_J/kHz	0.450(1)	0.44(1)			
σ/kHz	1	1			
N	16	10			

^a Error in parentheses in units of the last digit. ^b Root-mean –square deviation of the fit. ^c Number of lines in the fit.

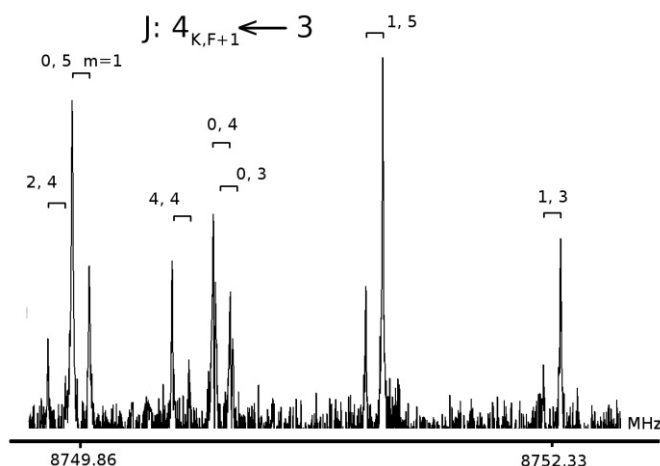


Figure 8.1 Portion of the rotational spectra of the $\text{CF}_3\text{Cl}\cdots\text{H}_2\text{O}$ which shows symmetric-top behavior and Cl hyperfine interaction of both $m = 1$ and $m = \pm 1$ states. Each line displays the Doppler doubling.

8.3.3 Molecular structure

$\text{CF}_3\text{Cl}\text{-H}_2\text{O}$ is an interesting quantum mechanical system. A symmetric-top molecule (CF_3Cl) is bound to an asymmetric planar-top molecule (H_2O) and therefore, the combined system should be an asymmetric top. However, the large-amplitude motions of water render the complex an effective symmetric top. This symmetric-top appearance of the rotational spectra of molecules that are predicted to be asymmetric-top complexes has been previously observed in $\text{CF}_4\cdots\text{H}_2\text{O}$ [11] and in benzene–water complexes.^[20, 21] In the structural analysis, the complex was described in the vibrationally averaged structure using at least the four coordinates shown in **Figure 8.2**.

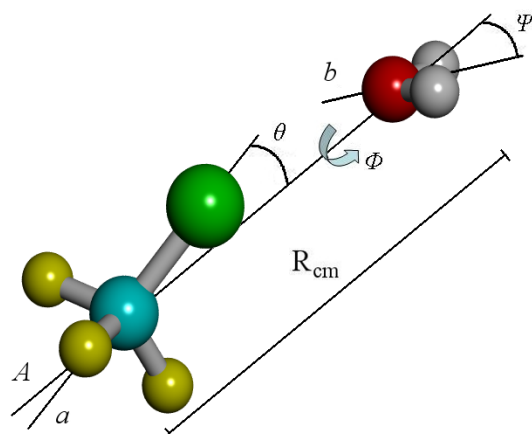


Figure 8.2 Molecular system with the coordinate used to discuss the structure and dynamics

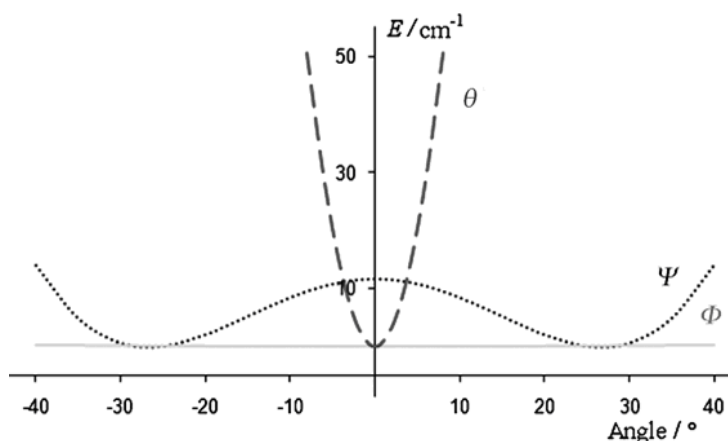


Figure 8.3 *Ab initio* potential-energy surface profiles along Ψ , Φ , and θ angles which are defined in figure 8.2.

There, R_{cm} is the distance between the two centers of mass of the two subunits. The two angles, Ψ and θ , measure the bending amplitudes of the two constituent molecules. The angle Φ describes the rotation of the two subunits with respect to each other. To estimate the potential curve for every structural parameter, an *ab initio* grid was calculated in steps of 28 over the full range of angles (and in steps of 18 close to the minima). While the dihedral angles were keeping fixed at every step, the rest of geometric parameters were reoptimized for each point along the path. The results are plotted in **Figure 8.3**.

Table 8.3 Relevant structural parameters of experimental and calculated substitution coordinates of the $\text{CF}_3\text{Cl}\cdots\text{H}_2\text{O}$ complex.

		Cl	O	H
$a/\text{\AA}$	<i>obs</i>	$\pm 0.740(2)$	$\pm 3.768(3)$	$\pm 4.280(8)$
	<i>calc</i>	+0.757	+3.738	+4.273

The obtained barriers can support some assertions: 1) the relative bending motion of CF_3Cl is at a single minimum, with the corresponding coordinate θ confined close to 0° , that is, the C-Cl \cdots O atoms are in a linear arrangement; 2) the bending of the water molecule with respect to CF_3Cl has two equivalent minima, $\Psi_e = \pm 27^\circ$ pointing to an asymmetric rotor with an interconversion barrier of about 14 cm^{-1} . This potential is similar to that reported for other systems;^[20, 22] 3) the V_6 potential (described by the Φ angle) is very flat, around 1 cm^{-1} . Such a flat potential-energy function and the

relatively light mass of the hydrogen atoms indicate that the water molecule is completely elocalized with respect to the C_3 -symmetric axis, allowing a free rotation. This is the key factor which makes the system an effectively symmetric top, with the water molecule rotating around CF_3Cl . Correspondingly, only the rotational constant B can be determined (for all isotopologues) from the MW spectrum. According to a rather approximate model, we can assume the symmetry axes of CF_3Cl and water to lie along the a -axis and their structure to not be altered upon formation of the complex, and then calculate the substitution coordinate of each substituted atom.^[23] The parameter r (the distance between the Cl and O atoms) was estimated to be 3.028(3)Å versus 2.982Å obtained by *ab initio* calculation. Moreover, because of the nearly free rotation of the subunits, one could assume that the C_{2v} symmetry of water is not perturbed upon full deuteration. The Chutjian method for multiple isotopic substitutions^[24] provides the coordinate of the hydrogen atoms $|a| = 4.280(5)$ Å, close to the calculated parameters (+4.273 Å). All r_s structural parameters are reported in **Table 8.3**.

8.3.4 Dissociation energy

The stretching force constant (k_s) is estimated from the distortion constants (D_J) because the halogen-bond-stretching motion lies almost parallel to the a -axis. For submolecules with large moments of inertia, **Eq. (8.2)** is used,^[24]

$$k_s = 128\pi^4 (\mu R_{cm})^2 B_0^4 / (h D_J) \quad (8.2)$$

where μ , R_{CM} and D_J are the diatomic reduced mass, the distance between the centers of mass and the first-order centrifugal distortion constants. A k_s value of 4.96 Nm^{-1} , which corresponding to a stretching frequency of 74 cm^{-1} , was obtained. By assuming a Lennard-Jones potential function and using the approximated equation:^[25]

$$E_D = 1/72 k_s R_{cm}^2 \quad (8.3)$$

The dissociation energy (E_D) was found to be 7.7 $kJmol^{-1}$. This value is in quite good agreement with the calculated value, once basis set superposition error (BSSE) corrections (see **Table 8.1**) are included. Moreover, this value is similar to the

dissociation energies determined for the related molecular complexes between CFCs and water, as shown in **Table 8.4**.

Table 8.4 Dissociation energies (E_D) for some molecular complexes with CFCs and water.

Complex	Interaction	E_D/kJmol^{-1}	Ref.
$\text{CH}_2\text{F}_2\text{-W}$	O-H...F	7.5	[8]
$\text{CH}_2\text{ClF-W}$	O-H...Cl	8.5	[10]
$\text{CH}_3\text{CClF-W}$	O-H...F	5.4	[9]
$\text{CF}_4\text{-W}$	Anti-H	5.0	[11]
$\text{CF}_3\text{Cl-W}$	Hal bond	7.7	This work

All of the complexes are weakly bound with interactions corresponding to dissociation energy values smaller than the E_D values characteristic of classical (O-H...O, O-H...N, O-H...S, and N-H...O) hydrogen bonds. However in the last two cases much remains to be learnt about the role of water.

During the formation of a HaB, CF_3Cl is an electron acceptor. The strength of the O...F interaction is intermediate with respect to the O...Cl and O-H...F interactions.

8.3.5 Conclusions

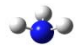
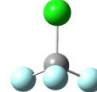
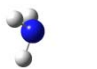
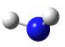
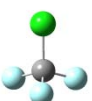
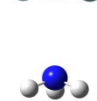

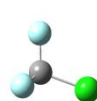
The electron-withdrawing group $-\text{CF}_3$ modifies the electrostatic potential and a positively charged region, centered in the direction of the C-Cl bond, is created. The so-called “ σ hole”^[7, 27] interacts favorably with the electron-rich part of a molecule, that is, the halogen bond. The σ hole is due to the special symmetry of CF_3Cl whereas it is inhibited by the T_d symmetry of CF_4 . Therefore, in the $\text{CF}_4\text{-H}_2\text{O}$ complex dipole-dipole interactions are dominant.

8.4 Chlorotrifluoromethane/ammonia

8.4.1 Theoretical calculations

Depending on the kind of intermolecular interactions, the complex can adopt several configurations. In order to obtain information on their geometries and relative energies, before collecting the rotational spectra, MP2/6-311++G(d, p) theoretical calculations were performed by using Gaussian 03 suite of programs,^[13] including geometry optimization. Four stable conformers were found, which relative energies, rotational constants, dipole moment components and quadrupole coupling constants are reported in **Table 8.5**. The shapes of the four conformers are shown at the bottom of **Table 8.5**. Conformer I, the global minimum, displays a C-Cl...N HaB. Conformer II, the second in order of stability, displays a tridentate CF₃...N HaB, while species IV is characterized by a single CF...N HaB. Only the third stable conformer (III) exhibits a CF...HN weak hydrogen bond. The obtained geometry of the most stable conformer is given in a subsequent section, while the geometries of conformers II-IV are collected in **Table 8.6**.

Table 8.5 MP2/6-311++G(d, p) spectroscopic parameters of the CF₃Cl...NH₃ complex.

	I	II	III	IV
$\Delta E/\text{cm}^{-1}$	0 ^a	489	737	897
$\Delta E_0/\text{cm}^{-1}$	0 ^b	372	597	742
A/MHz	5544.0	5529.2	3440.1	3558.3
B/MHz	1102.1	1367.9	1180.6	1179.3
C/MHz	1102.1	1367.9	1044.4	1054.2
$\chi_{aa}(\text{Cl})/\text{MHz}$	-74.9	-72.3	23.3	10.9
$(\chi_{bb}-\chi_{cc})(\text{Cl})/\text{MHz}$	0.0	0.0	-97.2	-83.6
$\chi_{aa}(\text{N})/\text{MHz}$	-4.1	-4.2	1.9	-4.2
$(\chi_{bb}-\chi_{cc})(\text{N})/\text{MHz}$	0.0	0.0	-6.05	0.0
$ \mu_a /\text{D}$	3.0	1.4	0.0	1.6
$ \mu_b /\text{D}$	0.0	0.0	1.0	0.7
$ \mu_c /\text{D}$	0.0	0.0	0.1	0.0
				
				

^a Absolute energy is -853.102276 E_h . ^b Relative zero point energy; absolute energy is -853.050897 E_h .

8.4.2 Rotational spectra

Table 8.6 MP2/6-311++G(d, p) optimized geometries for the conformer II-IV.

Conformer II					
Bond length/Å		Valence angle/°		Dihedral angle/°	
Cl2C1	1.758				
F3C1	1.326	F3C1Cl2	109.8		
F4C1	1.326	F4C1F3	109.1	F4C1F3Cl2	120.4
F5C1	1.326	F5C1F4	109.1	F5C1F4F3	-119.1
N6F3	3.231	N6F3C1	87.1	N6F3C1Cl2	-180.0
H7N6	1.014	H7N6F3	99.7	H7N6F3C1	125.5
H8N6	1.014	H8N6F3	99.7	H8N6F3C1	-125.5
H9N6	1.014	H9N6F3	134.8	H9N6F3C1	0.0
Conformer III					
Bond length/Å		Valence angle/°		Dihedral angle/°	
Cl2C1	1.743				
F3C1	1.330	F3C1Cl2	110.7		
F4C1	1.330	F4C1Cl2	110.7	F4C1Cl2F3	120.0
F5C1	1.333	F5C1F4	108.2	F5C1F4Cl2	-121.2
N6F5	3.356	N6F5C1	167.5	N6F5C1F3	-144.3
H7N6	1.013	H7N6F5	20.3	H7N6F5C1	-170.2
H8N6	1.013	H8N6F5	114.6	H8N6F5C1	-97.4
H9N6	1.013	H9N6F5	119.5	H9N6F5C1	133.0
Conformer IV					
Bond length/Å		Valence angle/°		Dihedral angle/°	
Cl2C1	1.750				
F3C1	1.332	F3C1Cl2	110.2		
F4C1	1.332	F4C1F3	108.2	F4C1F3F2	-120.5
F5C1	1.332	F5C1F3	108.8	F5C1F3F2	-118.0
N6F5	3.198	N6F5C1	179.6	N6F5C1F2	0.0
H7N6	1.014	H7N6F5	114.2	H7N6F5C1	-61.6
H8N6	1.014	H8N6F5	107.7	H8N6F5C1	-180.0
H9N6	1.014	H9N6F5	114.2	H9N6F5C1	61.6

According to the indications of the *ab initio* calculations, the first search on the μ_a -type transitions of conformer I was performed, which appears considerably more stable than the remaining ones. In addition, to simplify the spectrum, the spectra of the ^{15}N

enriched isotopologues were investigated first. This species have simpler spectra, with respect to those of the ^{14}N isotopologues, because, according to the nuclear spin quantum numbers [$I(^{15}\text{N})=1/2$, $I(^{14}\text{N})=1$], is free from quadrupole hyperfine structures. The observed spectrum is typical of a symmetric top, with bands evenly separated by $2B$. The first assignments were relative to the $K = 0, \pm 1$ transitions of the $J = 4 \leftarrow 3$ band. Each transition was split into several component lines, due to the nuclear quadrupole coupling of the Cl (^{35}Cl or ^{37}Cl) nucleus. In addition, a further doubling of the signals was originated by the Doppler effect (see the Experimental Section).

One can guess looking to the shape of conformer I of the complex that the NH_3 moiety, bound to the counterpart just by a nonbonding interaction undergoes an almost free internal rotation around to its symmetry axis. In this case several torsional states, each of them with its rotational spectrum are expected. Transitions belonging to the torsional ground state ($m = 0$) were mainly assigned and measured. The assigned lines were used to determine the spectroscopic constants collected in **Table 8.7**. The fit was performed using Pickett's SPFIT program,^[15] according to the Hamiltonian as shown in **Eq. (8.1)**.

Following the assignment of the ^{15}N species, the spectra of the ^{14}N isotopologues could be easily identified, while keeping the values of the ^{35}Cl or ^{37}Cl quadrupole coupling constants and of the centrifugal distortion constants fixed to those of the ^{15}N species. The observed transitions were further complicated by the splitting of the ^{14}N quadrupolar interaction. **Figure 8.4** shows the features of the $4_0 \leftarrow 3_0$ transition for both ^{15}N and ^{14}N species.

Table 8.7 Experimental spectroscopic parameters of the ^{15}N isotopomer.

	$^{35}\text{Cl}-^{15}\text{NH}_3$	$^{37}\text{Cl}-^{15}\text{NH}_3$
B/MHz	1066.8066(6) ^a	1064.466(5)
$\chi_{\text{aa}}(\text{Cl})/\text{MHz}$	-78.747(3)	-62.017(2)
D_J/kHz	0.540(6)	0.534(1)
D_{JK}/kHz	7.714(1)	7.657(3)
σ^b/kHz	3	2
N^c	114	56

^a Error in parentheses in units of the last digit; ^b Deviation of the fit; ^c Number of lines in the fit.

Table 8.8 Experimental spectroscopic parameters of the ^{14}N isotopomer and of the deuterated species.

	$^{35}\text{Cl}-^{14}\text{NH}_3$	$^{37}\text{Cl}-^{14}\text{NH}_3$	$^{35}\text{Cl}-^{14}\text{ND}_3$	$^{37}\text{Cl}-^{14}\text{ND}_3$
B/MHz	1100.8828(6) ^a	1098.163(2)	986.861(1)	985.233(2)
$\chi_{\text{aa}}(\text{Cl})/\text{MHz}$	-78.820(3)	-62.053(3)	-78.801(5)	-61.893(2)
$\chi_{\text{aa}}(\text{N})/\text{MHz}$	-3.10(2)	-3.07(2)	-3.390(3)	-3.385(1)
D_J/kHz	0.557(8)	0.551(1)	0.495(9)	0.499(2)
D_{JK}/kHz	8.338(4)	8.057(7)	7.046(6)	7.320(1)
σ^b/kHz	3	4	3	4
N^c	103	54	62	40

^a Error in parentheses in units of the last digit; ^b Deviation of the fit; ^c Number of lines in the fit.

Finally, the spectra of the isotopologues containing fully deuterated ammonia were investigated. To analyze these latter four spectra, a further term was added in the Hamiltonian of **Eq. (8.1)**, $H_Q(^{14}\text{N})$, which takes into account the ^{14}N quadrupolar contributions. The obtained spectroscopic parameters are collected in **Table 8.8**.

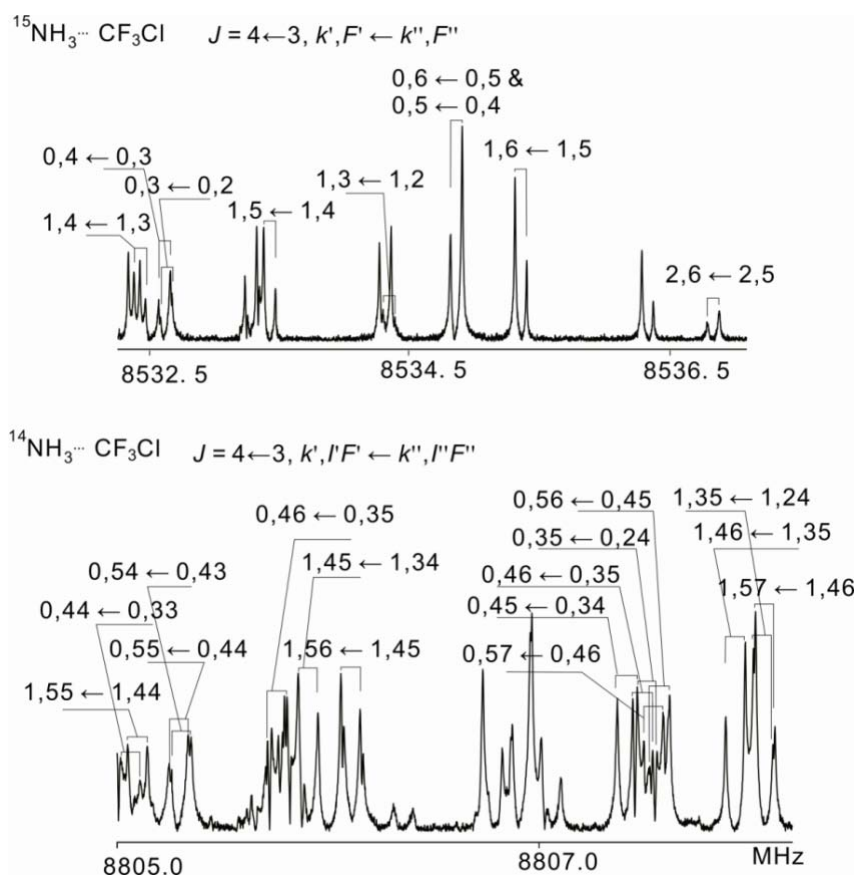


Figure 8.5 Top: the $4_0 \leftarrow 3_0$ transition is shown for the ^{15}N isotopomer of the $\text{CF}_3\text{Cl}\cdots\text{NH}_3$; bottom: the $4_0 \leftarrow 3_0$ transition of the ^{14}N species.

Because of the symmetrical properties of the complex, only one directional quadrupole coupling constant, χ_{aa} (N or Cl), can be determined experimentally. Other weaker lines have been observed for all isotopologues (but not involving the ND₃ species), presumably belonging to the $m = \pm 1$ state. Only the $K = 0$ lines could be reliably assigned as the reason already described in the complex of CF₃Cl-H₂O. The obtained spectroscopic parameters are reported in **Table 8.9**.

Table 8.9 Experimental spectroscopic parameters of the $|m|=1$ state.

	³⁵ Cl- ¹⁵ NH ₃	³⁷ Cl- ¹⁵ NH ₃	³⁵ Cl- ¹⁴ NH ₃	³⁷ Cl- ¹⁴ NH ₃
B/MHz	1066.604(6) ^a	1064.265(3)	1100.666(1)	1097.947(2)
$\chi_{aa}(\text{Cl})/\text{MHz}$	-78.748(1)	-61.917(1)	-78.785(5)	-62.040(3)
$\chi_{aa}(\text{N})/\text{MHz}$	-	-	-3.069(3)	-3.123(2)
D_j/kHz	0.539(6)	0.534(1)	0.560(2)	0.546(3)
σ^b/kHz	2.2	4.2	3.1	3.0
N^c	24	12	32	18

^a Error in parentheses in units of the last digit; ^b Deviation of the fit; ^c Number of lines in the fit.

8.4.3 Molecular structure and internal dynamics

Owing to the nature of the HaB interaction, the angle C-Cl...N was assumed to be very close to 180° in the equilibrium structure of the complex. However, the value of the χ_{aa} (N) quadrupole coupling constant (-3.10 MHz) is quite different with respect to the corresponding value in ammonia (-4.090 MHz).^[28] In the case of CF₃H-NH₃, Fraser *et al.* interpreted such a difference in terms of zero point angular oscillations of the NH₃ moiety relative to the a -axis of the complex.^[17] Assuming that the formation of the complex does not affect the electric field gradient at the nitrogen nucleus, the average value of the angle between the a -axis of the complex and the C₃ axis of ammonia (θ in **Figure 8.6**) can be estimated by comparing the observed ¹⁴N quadrupole coupling constant of the complex to that of free ammonia (χ_z) by:

$$\chi_{aa}({}^{14}\text{N}) = 0.5\chi_z (3\cos^2\theta - 1) \quad (8.4)$$

The value $\cos^2\theta = 0.83(8)$ was obtained which corresponds to an angle of 23.7° . The CF_3Cl bending vibration could likewise be treated as an oscillation about the CF_3Cl center of mass (ϕ in **Figure 8.6**), but in this case this method cannot be applied because $\chi_{\text{aa}}(^{35}\text{Cl})$ in the complex (-78.820 ± 0.003 MHz) is larger in magnitude than the reported $\chi_{\text{aa}}(^{35}\text{Cl})$ value in isolated CF_3Cl (-77.90 ± 0.03 MHz).^[29] Actually, such a magnitude decrease could be interpreted in terms of a small charge transfer from the nitrogen to the chlorine atom. This hypothesis matches also the small decrease in magnitude of $\chi_{\text{aa}}(^{14}\text{N})$. Then the value of the bending angle θ is an upper limit value, valid when there is no charge transfer.

The effective geometry of the complex, according to the rotational spectrum, is that of a symmetric top. The structural information reported and discussed below refers, then, to a C_{3v} symmetry of the complex. The corresponding *ab initio* geometry is shown in **Table 8.10**.

Table 8.10 Geometries of the observed $\text{CF}_3\text{Cl}\cdots\text{NH}_3$ complex obtained at MP2/6-311++G(d, p) level calculation.

Bond length/Å		Valence angle/°		Dihedral angle/°	
Cl2C1	1.740				
F3C1	1.334	F3C1Cl2	110.9		
F4C1	1.334	F4C1Cl2	110.9	F4C1Cl2F3	120.0
F5C1	1.334	F5C1Cl2	110.9	F5C1Cl2F3	-120.0
N6Cl2	3.080	N6Cl2C1	180.0	N6Cl2C1F3	0.0
H7N6	1.015	H7N6Cl2	112.2	H7N6Cl2C1	0.0
H8N6	1.015	H8N6Cl2	112.2	H8N6Cl2H7	120.0
H9N6	1.015	H9N6Cl2	112.2	H9N6Cl2H7	-120.0

To reproduce the six available B values of rotational constants, the halogen bond length needed to be increased by about 0.001 Å, resulting in a $\text{N}\cdots\text{Cl}$ distance of $3.081(1)$ Å. The sketch, principal axis, and atom numbering are given in **Figure 8.6**. On the average the ammonia is tilted with respect to the a -axis, but its precession with respect to the CF_3Cl symmetry axis makes the complex an effective symmetric top.

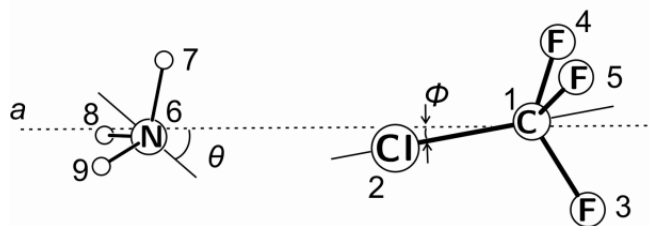


Figure 8.6 Sketch, principal axes and atom numbering adopted for $\text{CF}_3\text{Cl}\cdots\text{NH}_3$.

It was possible to calculate the substitution a -coordinate (see **Table 8.11**) of the Cl and N substituted atoms according to Kraitchman's equation.^[23] From the substitution coordinates of the Cl and N atoms, their r_s distance has been calculated to be 3.090(3), which is in agreement with the *ab initio* and r_0 data, 3.080, and 3.081(1) Å, respectively.

Table 8.11 Experimental substitution coordinates of the $\text{CF}_3\text{Cl}\cdots\text{NH}_3$ are compared to theoretical values

		Cl	N
$a/\text{Å}$	Exptl.	$\pm 0.761(2)^a$	$\pm 3.851(1)$
	Calc.	-0.774	-3.853

^a Error in parentheses in units of the last digit.

8.4.4 Dissociation energy

According to what have been already described above in 8.3.2 section, the stretching force constants (k_s) and dissociation energy (E_B) of the complex can be estimated from **Eq. (8.2)** and **(8.3)**. The value $k_s = 6.3 \text{ Nm}^{-1}$ has been obtained, which corresponds to a harmonic stretching frequency of 86 cm^{-1} . The dissociation energy has been calculated to be $\sim 11.0 \text{ kJmol}^{-1}$. This value is quite similar to the E_B values of weak hydrogen bonds (O-H \cdots F, O-H \cdots Cl, CH \cdots N). The stretching force constants and the dissociation energies of some C-Cl \cdots N bond and C-H \cdots N bond complexes are collected in **Table 8.12**. One can see that all E_B values of them fall in a small range, with values corresponding to about one half of those of strong hydrogen bonds.

Table 8.12 Comparison of C-Cl \cdots N bonding and C-H \cdots N bonding complexes

complex	Interaction	k_s/Nm^{-1}	E_B/kJmol^{-1}	Ref.
CH ₂ F ₂ \cdots H ₂ O	O-H \cdots F	7.7	7.5	[8]
CH ₂ FCl \cdots H ₂ O	O-H \cdots Cl	8.6	8.5	[10]
CF ₃ Cl \cdots OH ₂	C-Cl \cdots O	5.0	7.7	[30]
CF ₃ H \cdots NH ₃	C-H \cdots N	6.6	8.1	[17]
CF ₃ Cl \cdots NH ₃	C-Cl \cdots N	6.3	11.0	This work

8.4.5 Conclusion

The rotational spectra observed for six isotopologues of CF₃Cl \cdots NH₃ have a symmetric top behavior. The experimental configuration of the complex is characterized by a HaB interaction. From the fits of the experimental rotational constants, the r_0 structure of the complex was evaluated, which gives a 3.083 Å length of the Cl \cdots N halogen bond. The force constant, vibrational frequency and dissociation energy of the complex have been estimated. All these data have been obtained for the first time with a high resolution technique, such as pulsed jet FTMW spectroscopy, for a Cl \cdots N halogen bond. The energy of this kind of interaction is quite similar to that of weak hydrogen bonds and also that of Cl \cdots O HaB.

References

- [1] See Ref. 52 in chapter 1.
- [2] See Ref. 53 and 54 in chapter 1.
- [3] See, for example, P. Metrangolo, G. Resnati, T. Pilati, R. Liantonio, F. Meyer, *J. Polym. Sci., Part A: Polym. Chem.* **2007**, *45*, and references therein.
- [4] See, for example, D. Braga, G. R. Desiraju, J. S. Miller, A. G. Orpen, S. L. Price, *CrystEngComm* **2002**, *4*, 500. and references therein.
- [5] See Ref. 57 and 58 in chapter 1.
- [6] See Ref. 39 in chapter 1.
- [7] See Ref. 59 in chapter 1.
- [8] W. Caminati, S. Melandri, I. Rossi, P. G. Favero, *J. Am. Chem. Soc.* **1999**, *121*, 10098.
- [9] See Ref. 33 in chapter 7.

-
- [10] W. Caminati, S. Melandri, A. Maris, P. Ottaviani, *Angew. Chem. Int. Ed.* **2006**, *45*, 2438.
- [11] W. Caminati, A. Maris, A. Dell'Erba, P. G. Favero, *Angew. Chem. Int. Ed.* **2006**, *45*, 6711.
- [12] G. Valerio, G. Raos, S. V. Meille, P. Metrangolo, G. Resnati, *J. Phys. Chem. A* **2000**, *104*, 1617.
- [13] See Ref. 13 in chapter 2.
- [14] See Ref. 12 in chapter 2.
- [15] See Ref. 24 in chapter 4.
- [16] See Ref. 24 in chapter 7.
- [17] G. T. Fraser, F. J. Lovas, R. D. Suenram, D. D. Nelson Jr., W. Klemperer, *J. Chem. Phys.* **1986**, *84*, 5983.
- [18] W. H. Kirchhoff, D. R. Lide, Jr., *J. Chem. Phys.* **1965**, *43*, 2203.
- [19] A. W. Garrett, T. S. Zwier, *J. Chem. Phys.* **1992**, *96*, 3402.
- [20] S. Sukuki, P. G. Green, E. Bumgatner, S. Dasgupta, W. A. Goddard, G. A. Blake, *Science* **1992**, *257*, 942
- [21] H. S. Gutowsky, T. Emilsson, E. Arunan, *J. Chem. Phys.* **1993**, *99*, 4883.
- [22] B. R. Prasad, M. S. Krishnan, E. Arunan, *J. Mol. Spectrosc.* **2005**, *232*, 308.
- [23] See Ref. 11 in chapter 2.
- [24] A. Chutjian, *J. Mol. Spectrosc.* **1964**, *14*, 361.
- [25] See Ref. 15 in chapter 5.
- [26] See Ref. 16 in chapter 5.
- [27] See Ref. 52 in chapter 1.
- [28] M. D. Marshall, J. S. Muentner, *J. Mol. Spectrosc.* **1981**, *85*, 322.
- [29] J. H. Carpenter, J. D. Muse, C. E. Small, J. G. Smith, *J. Mol. Spectrosc.* **1982**, *93*, 286.
- [30] L. Evangelisti, G. Feng, P. Écija, E. J. Cocinero, F. Castaño, W. Caminati, *Angew. Chem. Int. Ed.* **2011**, *50*, 7807.

Appendices

A-Publication list

1. **Gang Feng**, Luca Evangelisti, Laura B. Favero, Jens-Uwe Grabow, Zhining Xia, Walther Caminati,
On the weak O–H···halogen hydrogen bond: a rotational study of CH₃CHClF···H₂O.
Phys. Chem. Chem. Phys. **2011**, *13*, 14092-14096.
2. Luca Evangelisti, **Gang Feng**, Patricia Écija, Emilio J. Cocinero, Fernando Castaño, Walther Caminati,
The Halogen Bond and Internal Dynamics in the Molecular Complex of CF₃Cl and H₂O.
Angew. Chem. Int. Ed. **2011**, *50*, 7807-7810.
3. Luca Evangelisti, **Gang Feng**, Roberto Rizzato, Walther Caminati,
Conformational Equilibria in Adducts of Alcohols with Ethers: The Rotational Spectrum of Ethylalcohol-Dimethylether.
ChemPhysChem **2011**, *12*, 1916-1920.
4. Vadim Ilyushin, Roberto Rizzato, Luca Evangelisti, **Gang Feng**, Assimo Maris, Sonia Melandri, Walther Caminati.
Almost free methyl top internal rotation: Rotational spectrum of 2-butynoic acid.
J. Mol. Spectrosc. **2011**, *267*, 186-190.
5. Laura B. Favero, Luca Evangelisti, **Gang Feng**, Lorenzo Spada, Walther Caminati,
Conformation and internal motions of dimethyl sulfate: a microwave spectroscopy study.
Chem. Phys. Lett. **2011**, *517*, 139-143.
6. Qian Gou, **Gang Feng**, Luca Evangelisti, Assimo Maris, Marianna Marchini, Biagio Velino, Walther Caminati,

- Rotational Spectrum and Internal Dynamics of Tetrahydrofuran-Krypton.
ChemPhysChem **2011**, *13*, 221-225.
7. **Gang Feng**, Luca Evangelisti, Nicola Gasparini, Walther Caminati,
On the Cl \cdots N halogen bond: a rotational study of CF₃Cl \cdots NH₃.
Chem. Eur. J. **2012**, *18*, 1364-1368.
 8. Luca Evangelisti, **Gang Feng**, Qian Gou, Walther Caminati,
Rotational spectrum of 2,5-Difluorobenzyl alcohol.
J. Mol. Struct. **2012**, *1023*, 15-17.
 9. **Gang Feng**, Laura B. Favero, Assimo Maris, Annalisa Vigorito, Walther
Caminati, Rolf Meyer,
Proton transfer in homodimers of carboxylic acids. The rotational spectrum of the
dimer of acrylic acid.
J. Am. Chem. Soc. **2012**, *134*, 19281-19286.
 10. Luca Evangelisti, **Gang Feng**, Qian Gou, Gloria Guidetti, Walther Caminati,
Orientation of the water moiety in CF₄-H₂O.
J. Mol. Spectrosc. **2012**, *282*, 39-41.
 11. **Gang Feng**, Qian Gou, Luca Evangelisti, Zhining Xia, Walther Caminati,
Conformational equilibria in carboxylic acid bimolecules: a rotational study of
acrylic acid-formic acid.
Phys. Chem. Chem. Phys. **2013**, *15*, 2917-2922.
 12. Luca Evangelisti, Qian Gou, Lorenzo Spada, **Gang Feng**, Walther Caminati,
Conformational Analysis of 1,4-Butanediol: A Microwave Spectroscopy Study.
Chem. Phys. Lett. **2013**, *556*, 55-58.
 13. Luca Evangelisti, Qian Gou, **Gang Feng**, Walther Caminati,
Effects of ring fluorination on the transient atropisomerism of benzylalcohol: the
rotational spectrum of 3,4-difluorobenzylalcohol.
Mol. Phys. Published (Online) 18 Mar 2013,
DOI:10.1080/00268976.2013.776713.
 14. Qian Gou, **Gang Feng**, Luca Evangelisti, Montserrat Vallejo López, Alberto

Lesarri, Emilio J. Cocinero, Walther Caminati,

Non bonding interactions and internal dynamics in $\text{CH}_2\text{F}_2 \cdots \text{H}_2\text{CO}$. A rotational and model calculations study.

Phys. Chem. Chem. Phys. Accepted.

B-Conferences**XXIV CONGRESSO NAZIONALE DELLA SOCIETA' CHIMICA ITALIANA
11-16 SETTEMBRE 2011, LECCE, ITALY.**

Poster FIS-PO-18: **Gang Feng**, Luca Evangelisti, Nicola Gasparini, Walther Caminati
On the Cl...N halogen bond: a rotational study of CF₃Cl...NH₃.

Poster FIS-PO-27: Qian Gou, **Gang Feng**, Luca Evangelisti, Assimo Maris, Marianna
Marchini, Biagio Velino
Rotational Spectrum and Internal Dynamics of Tetrahydrofuran-
Krypton.

**THE 22ND INTERNATIONAL CONFERENCE ON HIGH RESOLUTION
MOLECULAR SPECTROSCOPY, SEPTEMBER 4-8 2012, PRAGUE, CZECH
REPUBLIC.**

Poster H11: **Gang Feng**, Qian Gou, Luca Evangelisti, Walther Caminati
Structure, Ubbelohde effect, conformational equilibria and tunnelling
dynamics of carboxylic acid bi-molecules.

Poster H12: **Gang Feng**, Qian Gou, Luca Evangelisti, Geloria Guidetti, Walther
Caminati
Information on intermolecular interactions between water and other
molecules from the rotational spectra of the ¹⁷O water.

Poster D30: Luca Evangelisti, **Gang Feng**, Qian Gou, Walther Caminati
Effect of fluorine atom substitutions in benzyl alcohol derivatives.

Poster J15: Luca Evangelisti, **Gang Feng**, Qian Gou, Jens-Uwe Grabow, Walther
Caminati
Halogen bond and hindered motions in freons by microwave spectroscopy.

**THEORY, EXPERIMENTS AND MODELING OF CHEMICAL PROCESSES,
DYNAMICS AND MOLECULAR INTERACTIONS. NOVEMBER 29, 2012,
BOLOGNA.**

Flash talk YS10: Fourier transform microwave spectroscopic studies on the dimers of carboxylic acids.

XII GIORNATA DELLA CHIMICA DELL'EMILIA ROMAGNA, DECEMBER 17, 2012, FERRARA.

Poster: **Gang Feng**, Qian Gou, Luca Evangelisti, Laura B. Favero, Assimo Maris, Annalisa Vigorito, Walther Caminati, Rolf Meye, Zhining Xia
Chemical information on carboxylic acid bi-molecules from Fourier transform microwave spectroscopy.